2014

Exploration of Cell Cycle-Specific Essential Gene Functions in the Microbial Plant Chlamydomonas Reinhardtii

Frej Tulin

EXPLORATION OF CELL CYCLE-SPECIFIC ESSENTIAL GENE FUNCTIONS IN THE MICROBIAL PLANT *CHLAMYDOMONAS REINHARDTII*

A Thesis Presented to the Faculty of

The Rockefeller University

in Partial Fulfillment of the Requirements for

the degree of Doctor of Philosophy

by

Frej Tulin

June 2014

EXPLORATION OF CELL CYCLE-SPECIFIC ESSENTIAL GENE FUNCTIONS IN THE MICROBIAL PLANT *CHLAMYDOMONAS REINHARDTII*

Frej Tulin, Ph.D.

The Rockefeller University 2014

The cell cycle encompasses all the steps required for cell proliferation, and is normally tightly coupled to growth and division in all organisms. Much research has resulted in a well-supported model of eukaryotic cell cycle control. However, since most of this research has been carried out in yeast and animals (opisthokonts), it could in principle apply poorly to early-diverging groups of organisms, such as the green plants. Plant cell cycle research has largely followed a candidate strategy based on reverse genetics. These studies have a provided insights into plant cell cycle control, but are generally dependent upon sequence conservation between plant and opisthokont genes.

This thesis presents work from an ongoing screen to identify critical components of the plant cell cycle by forward genetic methods that are independent of prior knowledge of specific mechanisms of cell cycle control. The screen was carried out in the unicellular green alga *Chlamydomonas*, a microbial member of the *Viridiplantae*, which has well-established experimental Mendelian genetics, and many features that might facilitate identification of loss-of-function mutations.

We have developed semi-automatic techniques for isolation of temperature-sensitive lethal mutants that are capable of cell growth at a near-wild-type rate, but that exhibit first-cycle failure of cell division (*div* phenotype). We developed efficient methods for identification of causative mutations by next-generation sequencing of bulked segregant

pools.

The normal cell division cycle in *Chlamydomonas* is characterized by a long period of G1 growth, followed by a series of rapidly alternating rounds of S phases and mitoses (S/M phase). Analysis of more than 50 *div* mutants identified two main phenotypic classes. One class showed somewhat reduced growth and arrested in a G1-like state. This class included genes with diverse molecular functions based on gene annotations, including transcription, translation, and membrane biogenesis. The other class exhibited wild-type cell growth rate, and entered the S/M program on time; mutant cells then developed various S/M-specific defects. This class included genes directly involved in DNA replication and chromosome segregation.

Other mutations identified genes likely involved in cell cycle control, including the cyclin-dependent kinases *CDKA* and *CDKB*, two anaphase-promoting complex subunits, and the mitotic kinases Aurora B and MPS1. The phenotype of the *cdka-1* mutant suggested a specific role for CDKA in the transition from cell growth to initiation of the S/M cell division program. CDKB, in contrast, functions specifically after DNA replication, in entry into the first mitosis.

Although most *DIV* genes had clear homologues involved in cell cycle progression in opisthokonts, some genes had clear homologues in *Viridiplantae* but not in opisthokonts, including the BSL1 phosphatase, which we demonstrate to have a role in mitotic entry similar to that of CDKB.

The *div* mutants isolated in this screen provide an opportunity to study the plant cell cycle in a simple microbial setting. Since a large majority of the mutants alter genes with clear Arabidopsis sequelogues, the results also suggest targeted candidates for cell cycle experiments in Angiosperms.

To Ossian, my Mom and Dad,

Eric, Maja

ACKNOWLEDGEMETNS

I wish to thank the people who have contributed to this project: Dr. Susan Dutcher for inviting me to learn the genetic techniques of *Chlamydomonas* in her laboratory, and Dr. James Umen for providing strains and advice. I wish to thank Kresti Pecani for tireless work with DNA preparations, Craig Atkins for his contribution to revertant isolation and helpful discussions, Andrej Ondracka and Jamal Rahi for discussions and a good atmosphere. I am grateful to have met many other people during my years in the Cross laboratory, including Nick Buchler, Jon Robbins, Lucy Bai, Jess Rosenberg, Stefano di Talia, Lea Schroeder, Catherine Oikonomou and Andrea Procko.

I want to thank all the members of my advisory committee for guiding me through this project, especially Dr. Nam-Hai Chua for his support and honest words of advice. Most of all I am indebted to my mentor, Fred Cross, for giving me the opportunity to learn from his experience, and for teaching me the practice of science by demonstration.

My wife Taeryn for her support and optimism.

TABLE OF CONTENTS

LIST OF FIGURES

LIST OF TABLES

Chapter 1 Introduction

Organization of the thesis

This work was done in collaboration with Dr. Fred Cross. In this thesis, we present the result of a comprehensive screen in the green alga *Chlamydomonas*, to identify essential components of the cell cycle. In chapter 1, relevant background information is presented, centering around genetic control of the cell cycle in yeast and animals, where it has been most extensively studied. Chapter 2 focuses on how temperature-sensitive lethal mutants were isolated by UV mutagenesis, and how candidates for a cell cycle specific function were identified. To identify the candidates, we essentially adopted the criterion used by Nurse and colleagues, of wild-type cell growth rate in mutant cells, combined with first-cycle failure of cell division. These phenotypes were assessed semi-quantitatively by light microscopy. The temperature-sensitive mutants that expressed this target phenotype at restrictive temperature were called *div* mutants (for *div*ision). Chapter 3 describes how we used whole genome sequencing and genetic mapping to definitively identify causative mutations in about 30 *div* mutants, and generate a highly probable best candidate in about 30 more. A brief discussion about the identified genes and their potential connection to the cell cycle, based on knowledge about other systems, is provided. The last three chapters explore the phenotypic consequences of conditional inactivation of various *DIV* genes. Chapter 4 presents a breakdown of the mutant phenotypes represented in the entire

collection of *div* mutants, with a focus on the nuclear cycle - DNA replication and segregation. The conclusions we can draw about the organization of the cell cycle in *Chlamydomonas* are presented. In chapter 5, we describe experiments involving mutants in the two main cyclin dependent kinases in *Chlamydomonas*, CDKA and CDKB, and their function in *Chlamydomonas* cell cycle. Finally, in chapter 6, we present transcriptome data, which shows strong cell cycle regulation of many genes in wild-type cells, and the dependence of regulated transcription on CDKA function. Chapter 7 summarizes the main points of the thesis.

Overview of eukaryotic cell cycle control

Growth and development of all organisms, from single celled yeast to plants and animals, are tightly linked to cell proliferation. In the unicellular budding yeast, this is shown through mechanisms for sensing the nutrient status of the environment, and preventing a new round of cell division if the available energy and nutrient supplies are too low. Mating in budding yeast is also tightly coupled to the cell proliferation. Only during the G1 phase, before synthesis of new DNA has started, are yeast cells capable of conjugating with cells of the opposite mating type. This ensures that conjugation only happens between two cells with the same, haploid DNA content (McKinney et al., 1993).

In multicellular plants and animals, cell proliferation is under additional temporal and spatial constraints. This is illustrated by the tight coordination of cell division with

development in flowering plants. The male gametophyte undergoes two mitotic divisions to produce the two sperm nuclei necessary for the double fertilization event that is typical of flowering plants. When these sperm nuclei enter the female gametophyte, one will fertilize the egg cell to make the diploid embryo, and the other the central cell to make the triploid endosperm (Ma and Sundaresan, 2010). After fertilization, divisions in the embryo follow a strict spatial pattern to set up the body plan of the plant (Grossniklaus and Schneitz, 1998) (Jenik et al., 2007). In contrast, in the endosperm, nuclear divisions initially proceed rapidly, without cytokinesis, leading to a syncytium with hundreds of nuclei (Sabelli and Larkins, 2009). These nuclei become cellularized later in development and switch to an endoreduplication program, where the nuclear DNA is amplified, but not segregated into separate nuclei through mitosis. Modification of the cell-cycle program to leave out mitosis during specific stages of development is not restricted to plants. Endoreduplication is widespread among multicellular organisms (Edgar et al., 2014), most notably perhaps, in the development of the fruit fly *Drosophila* (Lee and Orr-Weaver, 2003). After germination, cell division in plants is largely restricted to defined meristematic regions in the root and shoot. Cells within these regions divide mitotically to produce all the cells of the adult plant (Bäurle and Laux, 2003). As newly generated cells leave the meristems, they typically stop dividing and begin differentiating into specific cell types. This differentiation is sometimes accompanied by a mitotic-to-endocycle switch, producing highly polyploid differentiated cell types (De Veylder et al., 2011).

Cell proliferation first requires cell growth (biomass accumulation), and second, dedicated machinery to regulate and execute the cell division cycle, often referred to as ‘cell cycle control machinery’. Based on the examples above, it is clear that this machinery must be both precise in the execution of cell cycle events, and flexible to be able to respond to developmental and environmental cues. To achieve these roles, the cell cycle control machinery has evolved into a complex network of proteins regulating the progression through the cell cycle. This progression has traditionally been divided into the four phases, G1, S, G2 and M. S phase (for Synthesis) is the period during which the genomic DNA is duplicated, and M phase (Mitosis) the time when the duplicated DNA is segregated into two daughter cells. The gap phases G1 and G2 separate these events. The emphasis on the S and M phases highlights the fact that accurate duplication and segregation of the nuclear DNA is the most critical objective of the cell cycle machinery. The ‘gap’ phases (in particular G1, in most organisms) are important for cell growth; this is especially true in *Chlamydomonas* due to its unusual ‘multiple fission’ mode of proliferation (see below). Coordination of cell growth and division is an important regulatory process to maintain size homeostasis (Jorgensen and Tyers, 2004).

Cell cycle studies in yeast model systems

The ease of genetic analysis by means of controlled crosses, vegetative haploid growth, and rapid and stereotyped cell divisions in budding yeast, made it ideal for studying the

genetic program controlling progression through the cell cycle. Budding yeast has an unusual type of cell division where a bud, the incipient daughter cell, appears on the mother cell wall early in the cell cycle. Because cell cycle progression is accompanied by progressive enlarging of the bud, the size of the bud relative to the mother cell provided an easily scorable marker for cell cycle progression. To identify genes with essential functions in cell division, Hartwell and colleagues looked for temperature-sensitive mutants that would bring an initially heterogeneous population of cells to an arrest with a uniform (and potentially abnormal) bud morphology. It was reasoned that a gene that functioned at a particular step in the cell cycle would result in such an arrest when mutated. This line of research generated a large collection of *cdc* mutants (cell division cycle) that arrested with different (but uniform within the population) bud morphologies, indicating that cell division was blocked at a specific stage. Further analysis of these *cdc* mutants identified genes necessary for several landmark events during the cell cycle, including DNA replication, bud emergence, nuclear division and cytokinesis (Hartwell et al., 1970)(Hartwell et al., 1973). It was discovered that these events were organized into three separate pathways of dependent events. One pathway included the steps of initiation of DNA replication, DNA replication and nuclear division, another bud-emergence and cytokinesis, and a third spindle-pole body duplication and spindle assembly. Each successive step in this pathway was dependent on successful completion of the previous step. For example, blocking bud emergence by the appropriate mutation also prevented

nuclear migration, but did not prevent execution of the events in the other pathways. Joining these pathways together, at the beginning of the cell cycle, was the event called START. Passage through the START step was necessary to initiate all of the other events of a normal cell cycle.

These studies in budding yeast raised the question of how successive events in the cell cycle could be organized with respect to one another. One possible way of ordering events is a substrate-product type mechanism, where the product of an early event serves as the substrate of a later event; a block of the early event leads to a block of the late event because the substrate is absent. Alternatively, events in the cell cycle could be ordered, not by intrinsic dependency like in the substrate-product model, but by extrinsic control. That is, a late cell cycle event could become dependent on an early event due to a control system that actively prevents the late event until the early event has been successfully completed. The correct order of many cell cycle events seemed to be ensured by this kind of control mechanism, referred to as a checkpoint (Hartwell and Weinert, 1989). Evidence in favor for checkpoints in the budding yeast cell cycle came from loss-of-function mutants that relieved the dependency of mitosis on successful completion of DNA replication (Weinert and Hartwell, 1988). In a similar fashion, mutations that relieved dependency of budding on successful completion of the previous mitosis were isolated (Hoyt et al., 1991)(Li and Murray, 1991). Normally, budding yeast delays exit from mitosis in the presence of drugs that interfere with microtubule function, which

prevents formation of a functional mitotic spindle. These mutants (mad1,2,3 and bub1,3), however, continued to re-bud in the presence of microtubule poisons, indicating that the checkpoint that normally maintains the mitotic state had been disrupted.

It is interesting to note that many of the *cdc* mutants isolated in the budding yeast screen were found precisely because the checkpoint system ensured a cell cycle block at a specific stage. For example, the Cdc9 gene encodes a DNA ligase, which is required during S phase. Without Cdc9, errors accumulate during DNA replication, which activate the DNA damage checkpoint, mediated by the Rad9 protein. This leads to the uniform arrest that was detected by Hartwell and colleagues (Weinert and Hartwell, 1988).

Genetic screens to identify cell cycle genes were also carried out, independently, in fission yeast (Bonatti et al., 1972) (Nurse et al., 1976). Fission yeast is cylinder-shaped and grows by extension at the tips of the cylinder. Cell division happens when the cell has reached a characteristic and rather well defined length. These mutant screens relied on the initial observation that fission yeast cells grew abnormally long when treated with drugs that inhibited DNA synthesis. It was thus reasoned that mutations that affected DNA replication, and possibly other steps in the cell cycle, would result in a similar "growth without division" phenotype. This morphological criterion would distinguish such cell-cycle mutants from mutants with defects in other essential functions, like basic metabolism, assuming that metabolic blocks would prevent cell growth. This screen also generated a set of *cdc* mutants that, when analyzed in detail, turned out to arrest cell-cycle

progression at specific steps.

The mutants isolated in the budding and fission yeast screens were a critical part in understanding the principles of eukaryotic cell-cycle control.

Identification of cyclin-dependent kinase (CDK) as a main driver of cell-cycle progression

Once molecular techniques made it possible to identify the mutations responsible for the *cdc* phenotypes, it became clear that there was a significant overlap between the genes controlling the cell cycle in budding and fission yeast. In particular, the budding yeast Cdc28 mutant and the fission yeast cdc2 mutant identified almost identical Ser/Thr protein kinases (Beach et al., 1982). In budding yeast Cdc28 was required to complete the START step (Hartwell et al., 1973); temperature-sensitive Cdc28 cells mostly arrested in G1. In fission yeast, cdc2 was found to be critically important for entry into mitosis, and $cdc2^{ts}$ mutants arrested with 2C DNA content but failed to complete nuclear division (Nurse et al., 1976). Later, using an allele of Cdc28 that could be specifically inhibited by addition of a drug, Shokat and colleagues demonstrated that Cdc28 catalytic activity was necessary to promote mitosis in budding yeast as well (Bishop et al., 2000).

Conservation of the cdc2 gene was not limited to budding and fission yeast. In fact, it was even shown, through isolation of cDNA from human cells, that human cells contained a protein kinase that could rescue fission yeast $cdc2^{ts}$ mutant from lethality,

demonstrating broad cross-species complementation of the cdc2-kinase (Lee and Nurse, 1987). In humans, and other animals, the homologue of cdc2 is called Cdk1. Thus, cdc2, Cdc28 and Cdk1 are homologous proteins. In a parallel line of research, a biochemical activity called MPF (maturation promoting factor) was discovered, which could induce mitosis in eukaryotic cells (Murray and Kirschner, 1989). This biochemical activity was shown to contain Cdc2, in complex with a protein called cyclin B (Nurse, 1990).

The cdc2 kinase needed the cyclin molecule for enzymatic activity. Cyclin was named after its cyclical appearance and destruction during the early divisions in the sea urchin embryo, where it was first identified (Evans et al., 1983). The main cyclin required for the mitotic function of cdc2 in fission yeast, cdc13, was identified in the original screen by Nurse and colleagues, and had the same pre-mitotic arrest phenotype as cdc2 (Nurse et al., 1976). Because of the requirement for a cyclin partner, the cdc2 kinase, and its homologues, are referred to as cyclin-dependent kinases, CDKs.

The activity of the cdc2 enzyme is controlled by multiple mechanisms, in addition to cyclin binding. Activating phosphorylation on a specific threonine residue in the T-loop is carried out by CDK activating kinases (CAKs) (Harper and Elledge, 1998). Residues at the N-terminus, close to the ATP binding site are the targets of inhibitory phosphorylation by the Wee1 kinase. Fission yeast cells in which the target of the Wee1 kinase, Tyr15, had been rendered unphosphorylatable, advanced prematurely into mitosis (Gould and Nurse, 1989). The phosphatase Cdc25 opposes Wee1 by removing the inhibitory Tyr15

phosphate. Together, the cdc2-wee1-cdc25 system is central for the decision to enter mitosis in both fission yeast and animal cell cycles (Nurse, 1990). The activity of the CDK complex is further controlled by stoichiometric inhibitors that bind to and inhibit the catalytic activity (Sherr and Roberts, 1999). In contrast to Cdc2/Cdk1, CDK inhibitors (CKIs) from different organisms generally have little sequence similarity. For example, the main CKI in budding yeast, Sic1 appears unrelated to the animal p27/Kip1 protein. Interestingly, land plants have CKIs that, although highly diverged, are likely related to p27/Kip1 (Torres Acosta et al., 2011), as well as another family of CKIs, Siamese (Walker et al., 2000), that appear unrelated to opisthokont inhibitors.

The eukaryotic CDK-driven cell-cycle oscillator

As will be described below for DNA replication, rising and falling activity of the cyclin-CDK complex is essential for ordering cell cycle events. How are these oscillations generated and sustained? A fundamental mechanism for generating oscillations in CDK activity is a negative feedback relationship between the CDK and its most important antagonist, the anaphase-promoting complex (APC). The APC is a large ubiquitin ligase protein complex that associates with two different co-activators during the cell cycle: Cdc20 and Cdh1. The APC^{Cdc20} and APC^{Cdh1} complexes ubiquitylate specific substrates and thereby target them for degradation by the proteasome (Pines, 2011). The negative feedback is established because CDK activates APC^{Cdc20} in mitosis (Rudner and Murray,

2000), and the APC^{Cdc20}, in turn, inactivates CDK by promoting degradation of its cyclin partner. At the end of mitosis and through G1, CDK activity is kept low by the action of APC^{Cdh1}. Thus, activation of the CDK enzyme drives cells into mitosis. Once in mitosis, CDK promotes activation of the APC, which degrades the cyclin, and thereby promotes exit from mitosis and re-establishment of the low CDK G1 phase (Fang et al., 1999). Since the APC^{Cdh1} is inhibited by CDK, when CDK activity drops at the exit from mitosis the APC^{Cdh1} becomes active and helps keep cyclin levels down during G1.

Although important for the cyclical activation and inactivation of CDK observed in the cell cycle, this simple CDK-APC^{Cdc20} negative feedback loop, on its own, is not sufficient to generate sustained oscillations in CDK activity. Without additional network components, the simple negative feedback system settles in a steady state. By adding positive feedback, the negative feedback network can be converted into a robust oscillator (Tyson et al., 2003). Two positive feedback mechanisms operating in the cell cycle of fission yeast and frog embryos involve the kinase Wee1 and the phosphatase Cdc25. Wee1 inactivates the cyclin-CDK complex, whereas Cdc25 activates it. Because cyclin-CDK activity itself inhibits Wee1 and activates Cdc25, this system sets up two positive feedback loops: one (Wee1 -| CDK -| Wee1) that stabilizes the state of low CDK activity, and the other (Cdc25 -> CDK -> Cdc25), which stabilizes the state of high CDK activity. An important consequence of this wiring is that it has the potential for creating a bi-stable switch between low and high CDK activity (Tyson et al., 2003). On its own, such a bi-

stable system would be indefinitely stable in either the low or the high state. However, as described above, when CDK activity is high, the APC^{Cdc20} negative feedback kicks in, degrades the cyclin, and brings the CDK activity down to the low state. The low state, in turn, could be gradually destabilized through production of new cyclin molecules, until the system switches to the high CDK activity state. This type of biochemical oscillator, driven largely by cyclin synthesis and periodic activation of the APC^{Cdc20}, is thought to play a central role in the rapid cleavage divisions observed in the frog embryo (Trunnell et al., 2011) (Pomerening et al., 2003). In somatic cells of all animals, and in yeast, the APC^{Cdh1} complex takes over at the end of mitosis, and keeps the cyclin concentration low through G1. Reciprocal inhibition between APC-Cdh1 and cyclin-Cdk creates another positive feedback loop stabilizing G1 (Cross, 2003).

The CDK oscillator controls once per cycle DNA replication

As noted above, it is essential that the DNA content of the cell is copied only once per cell cycle. How does the CDK oscillator ensure once per cycle execution of S phase? DNA replication is separated into two steps: assembly of prereplicative complexes (pre-RCs) onto DNA, followed by conversion of pre-RCs into preinitiation complexes and initiation of DNA replication.

The first part, assembly of pre-RC, can only take place when CDK activity is low. Pre-RC assembly involves the six-subunit origin recognition complex (ORC), and the

Cdc6 and Cdt1 proteins. Assembly of these components onto origins loads the main replicative helicase Mcm2-7 in an inactive form. Once the Mcm2-7 complex has been loaded onto DNA, replication can be initiated by the combined actions of the CDK and Cdc7 kinases (Labib, 2010). Activation of origins involves recruitment of several additional replication factors, including the Cdc45 protein and GINS complex. Cdc45, GINS and Mcm2-7 make up the CMG complex that travels with the moving helicase fork during the elongation phase. In budding yeast, phosphorylation of Sld2 and Sld3 by CDK has been shown to be critical for assembling the CMG complex and activating the origins (Masumoto et al., 2002). Animals have been proposed to have counterparts to the initiation factors Sld2 and Sld3 in the RecQ4 and Treslin proteins (Mueller et al., 2011). The role of Cdc7 seems to be primarily in phosphorylating the Mcm complex itself (Labib, 2010). However, both kinases are essential to initiation of DNA replication in budding yeast.

High CDK activity directly prevents pre-RC formation by multiple mechanisms. Some of the important ones in budding yeast are export of Cdt1 and Mcm subunits from the nucleus, phosphorylation of ORC by CDK, and proteolytic degradation of Cdc6 (Nguyen et al., 2001). In addition, animal cells have a protein called Geminin that binds to and inhibits Cdt1, thereby preventing pre-RC assembly. Geminin is a direct target of the APC, so when the APC is active during late mitosis and G1, Cdt1 is released and can function in pre-RC assembly (McGarry and Kirschner, 1998). These mechanisms ensure

that each origin is used only once and that DNA replication does not re-initiate later in the cell cycle (Blow and Dutta, 2005).

Thus, rising and falling CDK activity is directly coupled to once per cell cycle replication of the genome. Most of the components of the pre-RC and the preinitiation complex are conserved among eukaryotic species.

Many organisms, including both plants and animals, deviate from the canonical G1-S-G2-M cell cycle in certain cell types, where repeated rounds of DNA replication take place, without intervening mitoses. This endoreduplication program leads to amplification of the cellular DNA and an increase in ploidy, without generation of new cells (Edgar et al., 2014). Even though mitosis is omitted, endoreduplication is still tied to oscillations in CDK activity to establish a window during which pre-RCs can form. In flies, rounds of endoreduplication are tied to oscillations in the S phase cyclin, cyclin E, whereas mitotic cyclins are turned off (Edgar and Orr-Weaver, 2001). In plants, endoreduplication is widespread in non-dividing tissues. Regulation of the plant B-type CDK by inhibitory KRP proteins may contribute to control of endoreduplication (De Veylder et al., 2011).

The spindle assembly checkpoint prevents anaphase until the mitotic spindle has formed

When the cell enters mitosis, the duplicated chromosomes are held together by the cohesin complex, forming a pair of sister chromatids. The objective of mitosis is to

achieve accurate segregation of the sister chromatids away from each other and into the two daughter cells. This is accomplished by the mitotic spindle, which consists of a bi-polar array of microtubules, originating from two spindle poles at opposite sides of the cell. During the first part of mitosis, the mitotic spindle assembles and captures each sister chromatid by attaching to large proteinaceous structures called kinetochores (Cheeseman and Desai, 2008). It is critical that both chromatids of each pair become attached to spindle microtubules originating from opposite spindle poles. When all sister chromatids have achieved this bi-polar attachment to spindle microtubules, the APC^{Cdc20} ubiquitin ligase becomes activated. Activated APC^{Cdc20} promotes degradation of securin, which liberates a protease called separase, responsible for severing the cohesin structures that hold the sister chromatids together. Once the cohesin is cleaved, the force generated by the mitotic spindle pulls each sister chromatid towards opposite ends of the cell. The APC^{Cdc20} also promotes degradation of mitotic cyclins, which leads to exit from mitosis and reestablishment of the low CDK G1 state in the daughter cells (Peters, 2002).

The spindle assembly checkpoint (SAC) system actively monitors microtubule attachment to the kinetochores, preventing activation of the APC^{Cdc20} complex while unattached kinetochores are present (Musacchio and Hardwick, 2002). Since the APC remains inactive during checkpoint mediated cell cycle arrest, CDK activity remains high. As described above, each round of DNA replication requires a period of low CDK activity to assemble pre-RCs. Thus, one important consequence of checkpoint activation is

prevention of the next round of DNA replication until completion of mitosis.

Several core components of the SAC (Bub1 and 3; Mad1, 2, 3) were identified in yeast. These proteins have been conserved through evolution and are found in yeast, animals and plants, including *Chlamydomonas.*

Cell cycle control in plants

The green plants, comprising all land plants as well as the green algae, likely diverged early from the opisthokonts (animals and fungi) (Rogozin et al., 2009). It is possible, therefore, that the cell-cycle model outlined above, which is based almost entirely on results from opisthokonts, could apply poorly to this large and important group of organisms. Research into the molecular mechanisms of plant cell cycle control has relied heavily on a candidate approach, where genes with an established role in the cell cycle machinery have been studied in plants through their deletion or overexpression phenotypes. This line of research has provided evidence that many conserved opisthokont cell-cycle genes play a role in plant cell division as well (De Veylder et al., 2007). Examples of this include the requirement for CDKA, the plant counterpart to the opisthokont Cdk1/cdc2 kinase, during both gametophytic (Iwakawa et al., 2006) and sporophytic cell division (Inzé and De Veylder, 2006), and an essential role for RBR, the *Arabidopsis* homologue of the retinoblastoma tumor suppressor protein, during female gametophyte development (Ebel et al., 2004). In animals, the retinoblastoma/Rb protein

plays an important role as a regulator of gene expression during the G1/S transition (Dyson, 1998).

However, any evolutionary innovations along the green plant lineage that do not have a counterpart in yeast or animals, identifiable by sequence similarity, would be invisible to this approach. There are two likely reasons why the candidate approach has been the most popular avenue for discovery in plant cell cycle research, as opposed to more plant-centered genetic screens that have proven successful in many other areas of plant biology (Page and Grossniklaus, 2002). First, the cell cycle is an essential process, so mutations in critical components of the cell cycle engine are likely to have severe defects during gametophyte development or embryogenesis, complicating the study of gene function. A second and perhaps more fundamental reason is the expansion of several core cell cycle-genes into large gene families, through ancient polyploidization events during land plant evolution (Adams and Wendel, 2005). This has led to a rich repertoire of cell cycle genes in most plants. For example, *Arabidopsis* has over 30 cyclin genes, 5 CDKs (1 A-type and 4 B-type) and 7 KRPs (CDK inhibitory proteins) (Vandepoele et al., 2002). This widespread genetic redundancy is a serious complication for forward genetic screening in plants, although successful examples exist (Churchman et al., 2006). It is worth pointing out, in the context of the present study, that the genetic screen by Churchman e*t. al.* identified a CDK inhibitor of the SIAMESE family, which helps regulate endoreduplication in *Arabidopsis*, and is not found in opisthokonts.

General features of the *Chlamydomonas* cell cycle

Chlamydomonas reinhardtii is a unicellular chlorophyte alga, roughly 10 um length, with two anterior cilia and a single chloroplast. It can be grown in liquid culture or on agar plates, is naturally haploid, and has well developed methods for Mendelian genetic analysis. The complete genome sequence has been published (Merchant et al., 2007), and is currently housed at 'phytozome.org'. For reviews on *Chlamydomonas* cell biology and genetics, see (Harris, 2001) and (Rochaix, 1995).

Chlamydomonas divides by a multiple fission mechanism, where cells can increase in size as much as 32-fold during a prolonged G1-phase. This period of growth is followed by a division phase, where the cell divides n times in rapid succession to produce 2^n daughter cells. The number of daughter cells produced during this 'S/M phase' depends on how much the mother cell grew during G1 (Craigie and Cavalier-Smith, 1982). The term 'S/M phase' is used here and elsewhere in the literature to describe the rapid divisions in *Chlamydomonas.* To what extent these divisions are similar to S-M cycles in other organisms, for example during early development of *Drosophila* (Lee and Orr-Weaver, 2003), is unclear. However, since *Chlamydomonas* can complete the S/M phase in the dark under photoautotrophic conditions (i.e. without energy input), there is no requirement for cell growth between successive S/M phase cell divisions.

Under favorable conditions the mother cell can increase as much as 32-fold in size during G1 and then divide 5 times to produce 32 small daughter cells. More typical

division numbers under most culture conditions, however, are between 4-16 daughters per S/M phase (Figure 1.1).

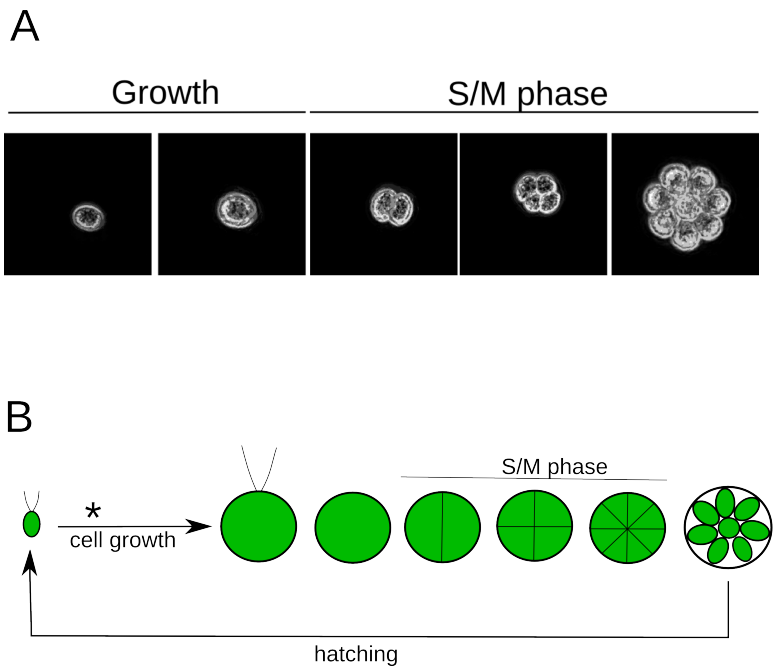

Figure 1.1: *Chlamydomonas* cell division cycle

(A) A *Chlamydomonas* cell growing on agar, imaged by time-lapse microscopy. A period of cell growth precedes the S/M phase, during which the cell divides several times in rapid succession to form a microcolony on the agar.

(B) Cartoon of *Chlamydomonas* cell cycle. Small newborn cells (far left) are slightly elongated and equipped with two flagella (or cilia). The cell cycle begins with a growth period. During this period of cell growth, the cell passes a 'commitment' point (asterisk). After passing the commitment point, the cell will complete an entire division cycle in the dark. The flagella are resorbed prior to the onset of the S/M phase (see chapter 3, vol. 3 in Harris, 2008). During the S/M phase the cell undergoes a series of rapid divisions without additional requirement for cell growth. The daughter cells remain inside the old mother cell wall until all divisions are completed, at which point they re-grow flagella and hatch.

It was shown that during the S/M phase, individual nuclei had either a 1C or 2C DNA content, leading to the conclusion that each S phase is followed by nuclear division (Coleman, 1982). EM studies also showed that nuclear division was followed by cytokinesis, separating the nuclei into two daughter cells, at least during the first division (Harper and John, 1986) (Johnson and Porter, 1968). Whether each division during the S/M phase is accompanied by complete separation of the cytoplasm is unknown. Once the S/M phase is complete, divided daughter cells remain inside the original mother cell wall until they hatch simultaneously as small G1 cells (Figure 1.1 B).

Under conditions of alternating light and dark, the growth phase roughly coincides with the light period and the divisions occur in the dark. Early work discovered a transition point in mid-G1 where cell-cycle progression in photo-autotrophic cultures (grown without an organic carbon source) becomes light independent (Spudich and Sager, 1980). That is, cells that are past this 'Commitment Point' (indicated by an asterisk in figure 1.1 B) will complete all the steps of the cell cycle in the dark, where they cannot photosynthesize. Under favorable growth conditions, cells can spend several hours continuing to increase in size after passing the commitment point, before the onset of the S/M phase. It is not known how the cells regulate the commitment step and entry into the S/M phase, but models based on a combination of sizers and timers (John, 1983) or on circadian control (Goto and Johnson, 1995) on cell cycle timing have been proposed. It has also been shown that blue light, but not red or far-red light can delay cell cycle

progression (Münzner and Voigt, 1992). This effect was observed in the presence of the photosystem II inhibitor DCMU, suggesting a photosynthesis independent effect of blue light on cell cycle progression. *Chlamydomonas* has an eyespot, a pigment-rich patch sandwiched between the chloroplast and plasma membranes that is used for phototaxis (Dieckmann, 2003). The phototactic response is sensitive to blue light with an action spectrum peak at 496 nm (Harris, 2008). Several eyespot mutants have been isolated, but whether any of these have altered cell cycle behavior in response to blue light is unknown.

During G1, the two flagella, or cilia, are anchored to two basal bodies at the anterior end of the cell. Four bundles of acetylated microtubules, two 2-membered and two 4-membered bundles, called rootlets, emanate from the basal bodies (LeDizet and Piperno, 1986) (Ringo, 1967). The flagellar apparatus, as well as the eyespot, occupy stereotyped positions inside the cell relative to the rootlets (Figure 1.2; G1 cell) (Holmes and Dutcher, 1989). At the onset of mitosis, the basal bodies lose the attachment to the flagellar apparatus and migrate away from each other. In metaphase, the basal bodies are found near the spindle poles. The 4-membered rootlets arch over the mitotic spindle and are thought to direct the formation of the cleavage furrow (Figure 1.2; mitotic cell) (Ehler and Dutcher, 1998).

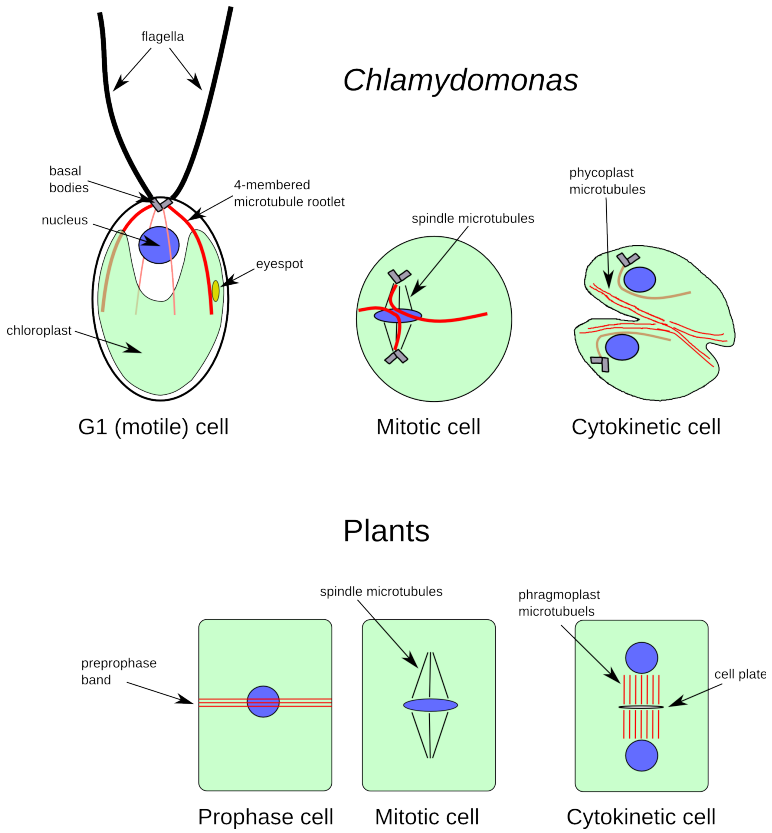

Figure 1.2: *Chlamydomonas* cells in G1 and mitosis

During G1 the flagella are anchored to the cell by two basal bodies. Four bundles of microtubule rootlets emanate from the basal bodies (two 2-membered and two 4-membered). When the cell enters mitosis, the flagella lose the connections to the basal bodies, which move away from each other and are found near the mitotic spindle poles. The 4-membered microtubule rootlets arch over the mitotic spindle and are thought to direct the formation of the cleavage furrow. In cytokinesis, the phycoplast forms along the cleavage furrow. For comparison, in plants the site of cell cleavage is determined in prophase by the preprophase band. The microtubules of the preprophase band dissappear in mitosis. In cytokinesis the phragmoplast microtubules direct formation of the cell plate (Guertin, 2002) (Müller et al., 2009).

It was suggested that cytokinesis operates largely independent of S phase and mitosis, since cells treated with drugs that inhibit DNA replication and nuclear division, still initiated cleavage furrows (Harper and John, 1986). This is different from the observation by Hartwell and colleagues in budding yeast, where cytokinesis is dependent on successful completion of mitosis. This might reflect a different organization of the *Chlamydomonas* and budding yeast cell cycles.

Genetic control over the *Chlamydomonas* cell cycle

Although there are numerous cytological studies on the structural and morphological changes that characterize progression through the *Chlamydomonas* cell cycle (Johnson and Porter, 1968)(Harper and John, 1986) (Salisbury et al., 1988), only limited work has been done to explore the genetic control over cell division. The *Chlamydomonas* genome does contain homologues of several genes involved in cell-cycle control in other systems, including A- and B-type CDKs, cyclins (Bisova et al., 2005) and components of the APC. The functional roles of these genes in *Chlamydomonas*, however, has not been explored so far due to the absence of mutants or an effective targeted method of conditional gene inactivation.

A size control mechanism normally couples growth in the mother cell to the number of divisions that take place during the S/M phase. Insight into this size control mechanism

came from the *mat3* mutant, which was shown to produce extremely small daughter cells, owing to an increased number of divisions during S/M phase (Umen and Goodenough, 2001). The *mat3* mutation inactivated the *Chlamydomonas* homologue of the Rb protein. In animals, Rb works as a negative regulator of gene expression at the G1/S transition by binding to the heterodimeric transcription factor E2F/DP1 (Classon and Harlow, 2002). Interestingly, the small size phenotype of the *mat3* null mutant in *Chlamydomonas* was suppressed by simultaneous deletion of the E2F or DP1 homologues, demonstrating a role for this pathway in size homeostasis (Fang et al., 2006). How the MAT3-E2F pathway helps coordinate cell size with cell-cycle progression, such that additional rounds of S phase and mitosis are initiated as long as the cells are above a certain size, remains an open question.

A connection between cytokinesis and flagellar maintenance has been suggested. Flagella are maintained through a process termed intraflagellar transport (IFT), which continuously shuttles cargo molecules up and down the flagellar axoneme (Kozminski et al., 1993). A number of IFT proteins, normally found in the flagella, re-localized to the cleavage furrow during cytokinesis (Wood et al., 2012), and knockdown of one of these, IFT27, resulted in cytokinetic defects (Qin et al., 2007).

Previous genetic screens for cell cycle mutants in *Chlamydomonas*

A number of previous studies have isolated conditional cell cycle mutants in

Chlamydomonas (Harper, 1999). Eleven mutants were generated by John and colleagues (Harper et al., 1995). They adopted the same "growth without division" strategy used to isolate *cdc* mutants in fission yeast (Nurse et al., 1976). The eleven mutants arrested with various terminal phenotypes with respect to nuclear DNA content, nuclear division, and tubulin distribution, while cell growth was largely unaffected, suggesting a block in cell-cycle progression. Analysis of these mutants confirmed earlier observations using inhibitors (Harper and John, 1986), that cytokinetic structures developed in cells that were unable to replicate DNA. Unfortunately, it was never determined how many genes these mutants defined, and these mutants themselves are no longer available. One mutant, *met1*, which was shown to arrest with assembled mitotic spindles (Harper et al., 2004), was available but unfortunately found to be recalcitrant to genetic analysis. We were unable to obtain viable progeny in crosses between *met1* to wild type, possibly due to diploidization of the original *met1* mutant.

Howell and Naliboff (Howell and Naliboff, 1973) also isolated a collection of proposed cell-cycle mutants; we obtained these mutants from the stock center, but these were found to have lost the original phenotype, probably owing to long periods of serial propagation.

Chapter 2 Isolation of cell-cycle mutants (*div* mutants) in *Chlamydomonas*

This chapter describes the process of isolating *div* mutants: temperature-sensitive *Chlamydomonas* mutants with a specific defect in cell division, but not in cell growth. Since the cell cycle is an essential process, we began our search for *div* mutants by isolating conditional temperature sensitive-lethal mutants (ts mutants). We used UV-light to induce random mutations in the DNA. UV light is thought to produce lesions in DNA, preferentially in adjacent pyrimidine bases (Sage, 1993), which can be converted to fixed mutations following errors during DNA repair. We reasoned that cell cycle-specific mutants would be found in any collection of temperature sensitive-lethal mutants.

Overview of mutant isolation pipeline

We developed an efficient pipeline for isolating ts mutants (Methods) and screening those ts mutants visually for phenotypes that might result from a cell cycle-specific defect (see below). To begin, cells were irradiated with UV light in liquid culture to about 5% survival, and then deposited on agar plates at permissive temperature (21^{o}C) to let colonies form. To get good use of the space on the agar plate we used a pinning tool with 384 pins and determined the density of viable cells in the irradiated culture such that each

pin, on average would contain a single viable, mutagenized cell. Using this pinning tool four times on one rectangular agar plate generated 1536 spots where, assuming a Poisson distribution, roughly one third of the spots were seeded with a single viable cell, giving rise to a clonal colony. In addition, one third of the spots would be empty (seeded with zero cells) and one third would contain more than 1 viable cell. The empty and multiply seeded spots were useless, but this procedure generated around 300 unique clonal colonies per plate. This method provided an enormous advantage compared to spreading liquid on Petri dishes and replica plating using velveteens.

Colonies were picked into 384-well plates filled with TAP medium by a robotic colony picker and incubated a second time at permissive temperature until the microcultures were sufficiently dense. At this point, the pinning tool was used again to make two replica plates that were incubated at permissive (21ºC) and restrictive (33ºC) temperature. After 6 days at permissive, and 3 days at restrictive temperature the replica plates were compared, either by eye or by computer-assisted image analysis, and spots with significantly reduced biomass formation at high temperature compared to low temperature were retained for further analysis: genetic characterization, phenotypic characterization and gene identification by whole-genome sequencing. The procedure is depicted in figure 2.1 and described more fully in the Methods section.

This study represents the screening of roughly 400,000 mutagenized colonies, with an average yield of 1%, resulting in about 4000 ts lethal mutants.

Figure 2.1: Screening pipeline

Wild-type *Chlamydomonas* cells were exposed to UV light to 5% viability. Following UV mutagenesis, the irradiated cells were incubated in the dark for 12 hours to fix the mutations. Next, irradiated cells were deposited on agar using a pinning tool and incubated at permissive temperature (21ºC) for 9 days to let colonies form. This generated agar plates containing on average 200-300 unique, clonal, mutagenized colonies per plate. Next, single colonies were picked robotically into 384-well plates filled with TAP medium. These plates were incubated at permissive temperature for another 7-8 days, until most wells had turned green. At this point, replica plates were prepared using the pinning tool. The replica plates (containing up to 768 unique mutants) were incubated at 33ºC for three days (restrictive), or at 21ºC (permissive) for six days. Cells that showed significant reduction in biomass accumulation at 33ºC compared to 21ºC (black arrowheads) were identified by eye or by computer-assisted image analysis, and isolated for further analysis by time-lapse microscopy. The time-lapse microscopy identified mutants that displayed the target phenotype of near wild-type growth accompanied by complete failure to undergo a normal division (explained in the text). These were considered candidate cell-cycle mutants. Candidate mutants were backcrossed to wild type to establish 2:2 segregation, and were then tested for allelism to other mutants. Selected mutants were then processed for phenotypic analysis and gene identification.

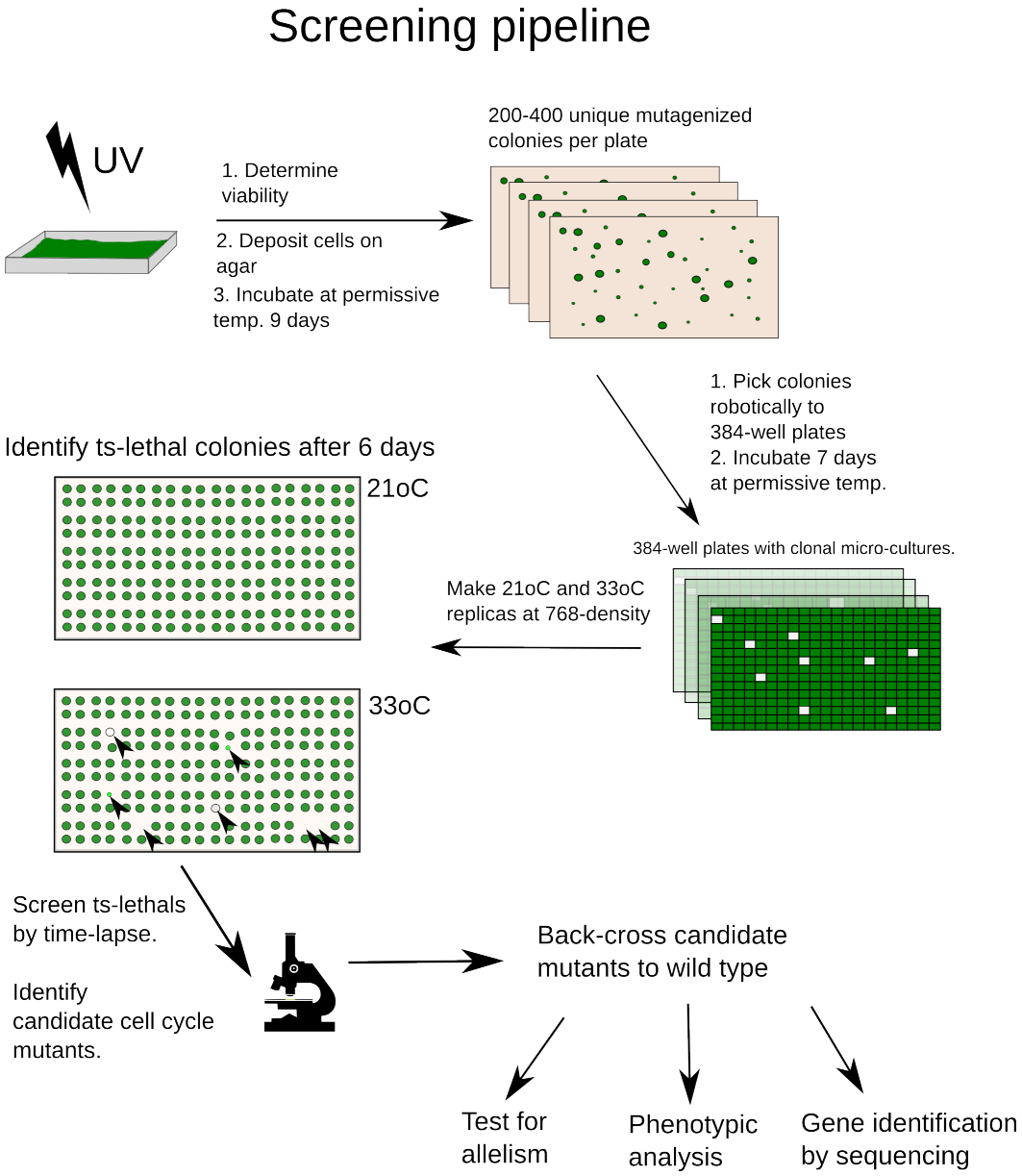

Figure 2.1: Screening pipeline

Time-lapse microscopy identified six main ts lethal phenotypes

We assumed that cell-cycle mutants in *Chlamydomonas* would exhibit a phenotype characterized by continued growth in the absence of cell division. This assumption was based on (i) the fact that both budding- and fission yeast *cdc* mutants continue to grow when cell cycle progression is blocked (Nurse et al., 1976)(Johnston et al., 1977), (ii) earlier studies in *Chlamydomonas* that reported mutants of this kind (Harper et al., 1995) and (iii) experiments with the microtubule inhibitor APM (James et al., 1993) that completely blocked cell division, but did not affect cell growth.

It should be pointed out here that the target phenotype of continued growth in the absence of cell division represents an assumption about how the cell cycle is organized in *Chlamydomonas*. While this behavior was observed in most *cdc* mutants in yeast, it does not automatically follow that *Chlamydomonas* should function the same way. For example, one obvious difference between yeast and *Chlamydomonas* is the large chloroplast that takes up almost half the cell volume. Thus, cell growth in C*hlamydomonas* reflects to a large extent growth of the chloroplast. One could imagine a mechanism that connects chloroplast growth or replication to the nuclear cycle. The screen presented in this thesis relies heavily on the Nurse criterion, with a focus on the nuclear DNA cycle, and it is clear that this was effective in identifying at least some definitive cell cycle-regulatory genes. In any case, with present technology and resources, the focus provided by the Nurse criterion was essential. It is an open question whether

there is a category of cell-cycle-specific genes that will be missed by this approach.

We imaged all ts lethal primary mutants by time-lapse microscopy to identify those exhibiting the "growth without division" phenotype. To obtain reproducible conditions for time-lapse imaging, we used a microscope equipped with a programmable stage and a temperature-control chamber. With this set-up we could image 96 strains growing in parallel on agar plates. Cells were pre-grown in liquid media to high density and deposited on agar just prior to the start of the time-lapse experiment, which was carried out under continuous illumination. Under these conditions, wild type started out as mostly small newborn cells at time zero, and then spent the first 8-10 hours at restrictive temperature growing in size without dividing. Between 8-12 hours, wild-type cells uniformly divided into microcolonies containing 8-16 daughter cells (Figure 2.2). Cytokinesis and cell wall synthesis produced clear separations between daughter cells; these daughters then each went through another long G1 and each underwent another ‘multiple fission’ event again, after another ~14 hrs. This allowed us to determine two quantitative measures that define the ‘growth without division’ criterion. These were: (i) a growth rate similar to wild type (as defined by increase in cell area [pixel number] in successive microscopic images) during the first 10 hours, combined with (ii-a) failure to complete a normal cell division (defined by failure of completion of septation into ~8-16 individual cells) or (ii-b) division appearing near-normal microscopically, but with the daughter cells failing to progress to a second division cycle. The first criterion would

allow us to differentiate against the large number of ts-lethal mutants expected to be defective in processes that are required for normal cell growth, and the second criterion guarantees a tight cell cycle block (ii-a), or a cell cycle sufficiently defective that ‘viable’ daughters were not produced.

Almost all ts-lethal mutants fell into one of six categories when imaged this way. These were: (1) near-complete failure of cell growth, (2) rapid cell lysis within 10 hours, (3) reduced growth rate compared to wild-type, usually accompanied by one seemingly normal division after (late) attainment of the wild-type division size, with little growth in the resulting daughter cells, (4) several cell divisions with progressively reduced viability, (5) a complete cell division failure, albeit with somewhat reduced growth rate during the first 10 hours, and (6) wild-type growth rate during the first 10 hours followed by complete cell lysis within 20 hours. These six phenotypes cover essentially all of the four thousand temperature-sensitive lethal mutants screened with this method (Figure 2.3 and 2.4).

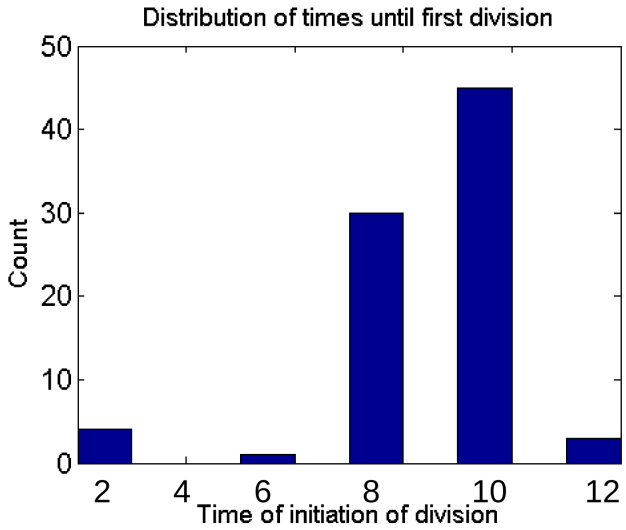

Figure 2.2: Distribution of times until initiation of division in wild type

Wild-type cells were spotted on agar and imaged every other hour at 33ºC. It was found that almost all wild-type cells initiated division, as scored by appearance of cleavage structures by light microscopy, between 8 and 10 hours. Nearly all cells had initiated (and completed) division by 12 hours, to form a microcolony of 8-16 daughter cells. This information was used to determine the most informative time to image mutant cells in order to score cell growth and cell division.

Figure 2.3: Non-*div* mutant phenotypes on agar

All ts-lethal mutants identified on the basis of reduced biomass accumulation were imaged by time-lapse microscopy after 0, 10, 20 and 40 hours at restrictive temperature. Under these conditions, parallel wild-type cells grow substantially in size during the first 10 hours, at which point they undergo several divisions to form a microcolony of 8-16 cells. Four morphological classes represented the majority (~90%) of phenotypes associated with ts lethality. Class 1: Near complete failure of cell growth. Class 2: Rapid lysis upon a shift to restrictive temperature. Class 3: Significant cell growth during the first 10 hours, followed by one apparently normal division, with no growth in the resulting daughters. Class 4: Several divisions with progressively reduced viability. These four classes were incompatible with the target phenotype of near wild-type growth rate accompanied by a tight cell-cycle block. Mutants exhibiting these phenotypes were not considered further.

Scale bar: 50 um

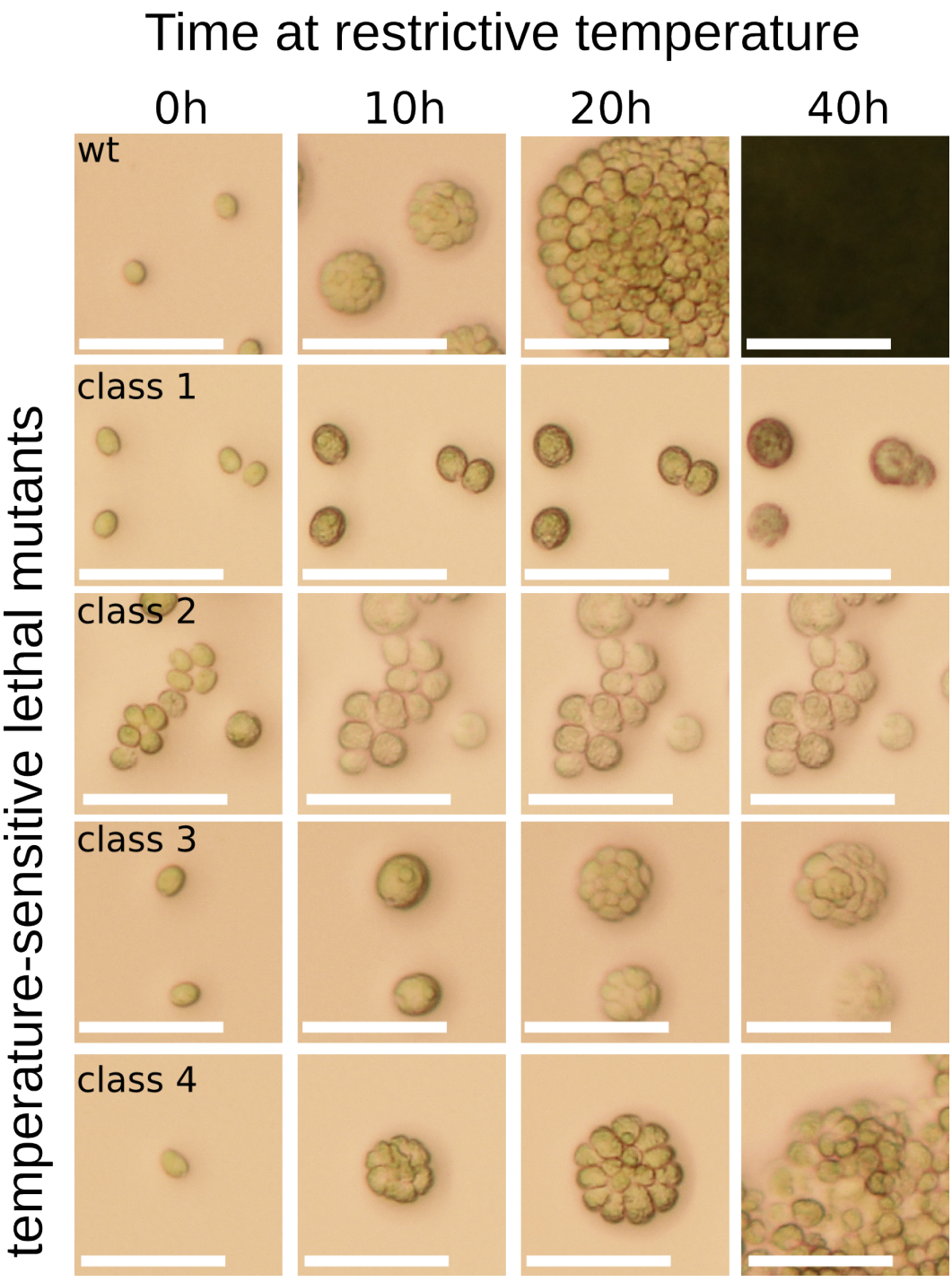

Figure 2.3: Non-*div* mutant phenotypes on agar

The first four phenotypes accounted for more than 90% of ts-lethal mutants isolated and fell outside the target phenotype of growth without division. It is expected that a large number of essential genes would be required for non-cell cycle stage specific functions. In budding yeast, the number of *cdc* genes was about 10% of essential genes (see discussion in Hartwell et al., 1973b). Our results point to a similar partitioning between putative cell cycle genes and other essential functions. The larger proportion of non-*cdc* essential genes in our study could be related to the growth of *Chlamydomonas* on minimal medium; thus, for example, any gene required for amino acid production would be essential in our screen, but not in the yeast screens carried out on rich medium.

Roughly 2.5% of ts mutants fell into class 5 (Figure 2.4), displaying a reduced growth rate compared to wild type during the first 10 hours at restrictive temperature, and a complete block in cell division. However, the growth in the class 5 mutants continued to a final size well above normal size of wild-type division. Within the class 5 mutants, two sub-groups were found: large round cells, and cells in which a separation of the green material inside the cell developed progressively after 10 hours, accompanied by an elongation of the cell body and resulting in an 'acorn'-like appearance. The class 5 mutants were distinct from class 1 mutants, which completely failed to grow, and from class 4 mutants, which did not have a tight cell division block.

Roughly 2.5% of ts mutants fell into class 6 (Figure 2.4). These mutants had no measurable growth defect during the first 10 hours, and exhibited complete lysis before

the 20-hour time-point. Three sub-groups within the class 6 mutants could be distinguished based on morphological changes that appeared around the time of normal wild-type division. Some remained round up until the time of lysis ('round'), some developed a single characteristic notch on the cell surface ('notch') and other seemed to produce several seemingly randomly placed invaginations across the cell surface ('popcorn'). The appearance of the notch and popcorn morphologies, at the expected time of wild-type division, suggested that these represented execution of some part of the cytokinetic program. It has been shown by others that cleavage furrows can form in cells chemically inhibited for DNA replication (Harper and John, 1986). The reason for the ultimate and complete cell lysis we observed in class 6 mutants is not clear. In a normal cell cycle, the old mother cell wall is degraded after the daughter cells have built their own cell walls. One possible, although speculative scenario to explain the cell lysis, is that cytokinesis can initiate in many class 6 mutants (leading to notch/popcorn morphologies) but the 'unfinished' daughter cells never assemble their own cells walls. If the old mother cells wall nevertheless breaks down, the unfinished (and likely structurally compromised) daughters inside might be unprotected from osmotic pressure, which causes the uniform lysis. The class 6 mutants were distinct from the class 2 mutants, which bleached promptly upon shift to restrictive temperature, without any noticeable morphological changes and before any significant cell growth.

We were surprised by the absence of some expected classes based on the budding

yeast and fission yeast *cdc* screens. Most of these *cdc* mutants exhibit continued cell growth without lysis for multiple generation times, and were generally reversible. The class 6 mutants grew well initially, but promptly lost viability upon cell lysis, shortly after the time of wild-type division; and most of the class 5 mutants tested were at best poorly reversible.

Despite this, the class 5 and class 6 mutants seemed like the most likely candidates for identifying cell-cycle-specific functions. Roughly 100 mutants each of class 5 and class 6 were isolated.

Figure 2.4: *div* mutant phenotypes on agar

Wild type along with class 5 and class 6 *div* mutants grown on agar and imaged at 0, 10, 20 and 40 hours at restrictive temperature. Class 5 and 6 represented approximately 5% of all ts-lethal mutants. **(A)** Wild-type cells reproducibly initiated division after 10 hours at restrictive temperature, after reaching a characteristic division size. Class 5 mutants showed a reduced growth rate compared to wild type over the first 10 hours, but ultimately exceeded wild-type division size by 20-40 hours without initiating division and without undergoing cell lysis. Significantly polarized growth that became apparent after 20 hours distinguished the "acorn" subgroup of class 5 mutants. Class 6 mutants were characterized by a wild-type growth rate during the first 10 hours at restrictive temperature and complete cell lysis within 20 hours. Three subgroups of class 6 mutants were distinguishable on the basis of morphology at the 10 hour time point: notch, popcorn and round. A single mutant, ts301, combined the rapid growth of class 6 mutants with the absence of cell lysis of the class 5 mutants. **(B)** Quantification of cell areas at the 10-hour time point shows that class 5 mutants in most cases failed to reach wild-type division size, whereas class 6 mutants generally exceeded it.

Scale bar: 50 um

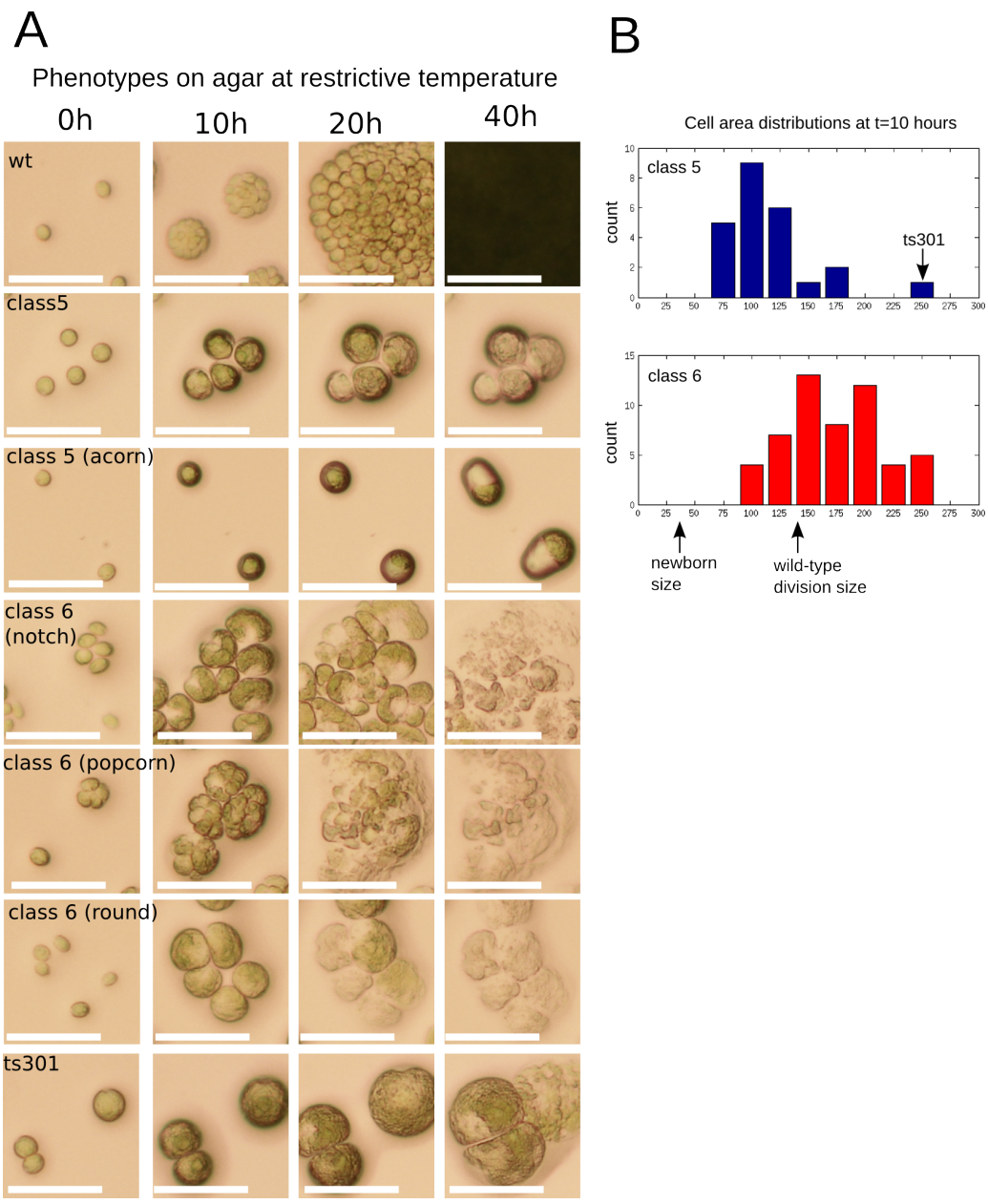

Figure 2.4: *div* mutant phenotypes on agar

Genetic analysis of class 5 and class 6 ts mutants: genetic mapping and test for allelism

All class 5 and class 6 mutants were backcrossed once to the isogenic parent wild-type strain. This established 2:2 segregation for ts lethality in more than 90% of mutants. However, as will be shown below, one mutant that deviated from 2:2 segregation but had a particularly interesting cell cycle phenotype was kept. The backcrossing program was also important for obtaining a mating type plus (mt+) and minus (mt-) of each class 5 and 6 mutant, as well as for making pools for bulked segregant genome sequencing. In addition, introgression into the parent strain helped clean up the genetic background.

We developed a method for assessing allelism between class 5 and 6 ts-mutants. Since *Chlamydomonas* does not mate efficiently on plates, crosses were done in liquid medium. Placing cells in nitrogen-free medium for several hours induces the gametogenic program, and cells are mated by mixing together the gametes of opposite mating type (Dutcher, 1995). It is believed that a majority of mated cells directly enter the meiotic program, with a minority ending up as vegetative diploid cells. Thus, a positive result in this test (that is, no growth coming from the mating mixture at high temperature) implies that the two genes are unlinked, or if on the same chromosome, at a sufficient distance from each other to recombine readily, and/or able to complement each other in doubly heterozygous diploids.

The large number of mutants isolated necessitated an efficient method for performing

parallel crosses and scoring failure to recombine to form TS+ progeny (Figure 2.5). We took advantage of a plate-filling robot to mix gametes directly into 96-well plates, allowing us to routinely perform 100-1000 crosses in parallel. The cells were allowed to mate in the 96-well plates and were then spotted on agar and incubated at restrictive temperature. A second plate was kept in the dark as a control for mating efficiency since microscopically distinct zygospores (mating products) form in the dark without undergoing meiosis. As the number of isolated mutants grew, we also divided up the mutants based on phenotype, reasoning that the class 5 and 6 phenotypes were unlikely to result from lesions in the same gene, given their very distinct appearance. Most mutant parents were completely inviable at restrictive temperature, as were self-crosses between opposite mating types carrying the identical *div* mutation (diagonal line in figure 2.5). In contrast, in crosses between any two random mutants, generally colonies at high temperature were observed, indicating that recombination/complementation had produced TS+ progeny. Two mutants were considered allelic only if both reciprocal crosses failed to reconstitute TS+ cells. That is, the crosses with mutant A (mt-) x mutant B (mt+), and mutant A (mt+) x mutant B (mt-), should give the same result. Examples of *div* mutants determined to be allelic by this method are indicated in Figure 2.5. In almost all cases the mutants determined to be allelic this way displayed very similar phenotypes**,** and were ultimately found to contain missense mutations in the same ORF (see below). The observation that allelic *div* mutants generally displayed very similar phenotypes further

indicated that the observed ts phenotype was due to a loss-of-function mutation in a given gene, rather that other 'passenger' mutations or due to particular features of the mutated alleles.

We expect the majority of *div* mutants to carry recessive loss-of-function alleles, since this is the typical result for temperature-sensitive mutations; almost all temperature-sensitive *cdc* mutants in budding- and fission yeast were recessive (Hartwell et al., 1973) (Nurse et al., 1976). However, putative dominant *div* alleles, that do not prevent meiosis, would not be identified by this method, since recombination in meiosis would produce Ts+ progeny. Dominant alleles that block mitotic divisions in vegetative diploid and also prevent meiosis would score as allelic to all other *div* mutants. In the minority of cases where this behavior was observed it appeared more likely to result from a failure to mate, either because no mating was observed by visual inspection, or because the same strain was crossed successfully to produce Ts+ progeny on other occasions.

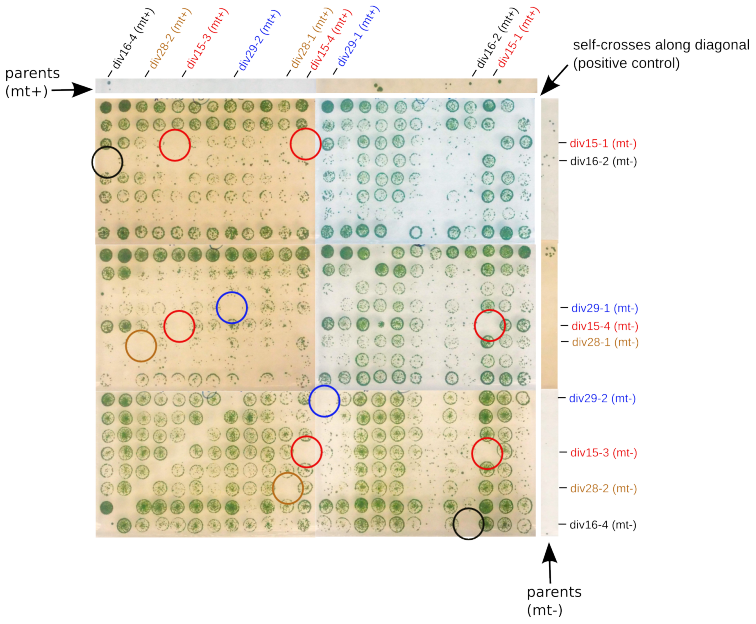

Figure 2.5: A test for allelism between *div* mutants

After backcrossing to the isogenic wild-type parent, an mt+ and mt- version of each *div* mutant was isolated and used to test for allelism between sets of *div* mutants (generally with the same phenotype). The mt+ and mt- parent were generally completely inviable at restrictive temperature (black arrows: parents). In contrast, in most crosses between any two *div* mutants, ts+ progeny was obtained, indicating recombination between the *div* genes, or complementation in vegetative diploids. Coloured circles indicate allelic div mutants identified through this method. As expected, self-crosses between *div* mutants in opposite mating type always failed to reconstitute ts+ progeny (black arrow: self-crosses).

Summary

The procedures described here were used to obtain a collection of *div* mutants: temperature-sensitive mutants that exhibit a tight cell cycle arrest, but a nearly wild type growth rate. A limited number of phenotypic classes were routinely observed in ts-lethal mutants. Two of these, class 5 and class 6, exhibited the target phenotype of continued growth in the absence of cell division. Class 5 mutants generally had a slightly reduced growth rate compared to wild type, but cell growth continued to a final cell size well above normal division size. Class 6 mutants had a wild-type growth rate during the first 10 hours at restrictive temperature, and usually lysed completely within 20 hours. The development of distinct morphological signatures around the 10 hours time point, coinciding with the timing of normal wild-type division, suggested that the lethality in class 6 mutants was cell-cycle dependent.

Most of these mutants are represented by a single allele, indicating that the screen is still far from saturation.

Chapter 3 Identification of causative mutations by sequencing

Identifying the causative *div* mutation is necessary in order to understand the molecular basis for the failure to divide. The use of UV light as a mutagen is expected to generate primarily point mutations or small genetic lesions (deletions or insertions) (Sage, 1993) ; this is consistent with our data. This chapter describes the use of whole genome re-sequencing, in combination with genetic mapping, to identify causative mutations.

Overview of the strategy to identify causative mutations

As described above, we had generated a collection of about 200 primary *div* mutants. In all cases, except for ts301 (see chapter 2), genetic analysis had clearly indicated that the *div* phenotype segregated as a single locus, and some mutants were known to be allelic based on the recombination/complementation test.

We backcrossed each *div* mutant to wild type and isolated roughly 10 *div* mutant segregants from five tetrads. These were grown up and pooled in equal proportions. DNA was extracted from the pool and sequenced at ~50x coverage (Methods). The advantage of this "bulked segregant" approach is that unlinked UV-induced SNPs will segregate randomly in the pool. Only the real causative mutation, and closely linked SNPs, will be reliably uniformly present in the DNA pool. That is, when sequencing the pool, most positions showing UV induced non-causative SNPs will also have a significant contribution of wild-type reads. This will be a clear signal that a SNP is unrelated to the *div* phenotype. In contrast, the causative SNP is expected to be uniformly non-wild type.

With 10 segregants in the pool, the probability that any given unlinked SNP will be uniformly present should be <1/1000. In most pools, we observed only one or a few regions of uniformly non-wild type SNPs; such regions typically extended 1-2 Mb, containing approximately 10 SNPs per Mb (mainly annotated as non-coding; see below).

The pipeline we used to identify SNP candidates, developed in collaboration with Dr. Cross, was based upon both open source software (bowtie2 (Langmead and Salzberg, 2012), mpileup (Li et al., 2009)) and custom-written scripts in MATLAB.

Multiple SNP candidates

Due to the density of UV-induced mutagenesis, many bulked segregant pools yielded a region of uniform SNPs containing more than one SNP that changed coding sequence (a 'functional' SNP) in a gene model from the annotated reference sequence ((Merchant et al., 2007); Phytozyme.org website). This presented us with the problem of deciding on the likely causative mutation, since we assume that only one mutation was causative and the rest passengers. To solve this problem, we employed two strategies. First, for a subset of *DIV* genes, we developed methods we considered would give 'definitive' identification. Then, we used properties of these definitive mutations combined with linkage mapping to develop a Bayesian calculation of probability that a given SNP candidate was causative.

'Definitive' identification of causative mutations

By the test for allelism described in chapter 2 (Figure 2.5), we sorted the independent *div*

mutants into 29 complementation groups, containing genes that were hit by a UV-induced mutation in more than one independent isolate. In 26 of these, whole-genome sequencing and SNP detection identified missense mutations in the same gene model, almost always in different residues, and with different repertoires of flanking SNPs.

We considered that identification of missense mutations in a common gene model in multiple allelic mutants represented strong and near-conclusive evidence that these were the causative mutations. We estimate that the probability that the same gene model is hit by mutation in two independent strains by chance, given the use of bulked segregant pools for each strain, is low enough that we expect no errors in the assignments of causative mutations based on multiple hits (Table 3.2) (Appendix A3).

In some cases where we had only a single *div* allele, but the bulked-segregant sequencing provided a strong candidate for causality, we were able to generate revertants, by mutagenizing with UV light, that changed the candidate SNP back to the wild-type sequence (exact revertant) or to some other sense sequence (pseudo revertant). We considered this to provide definitive evidence of the causative mutation, since it cannot give an incorrect answer unless the rate of back-mutation of a passenger mutation is >0.05 (since we never assayed more than ~20 revertants for changes in the SNP), which would be an extraordinarily high mutation rate, therefore extremely unlikely.

In total, we identified 29 *DIV* genes for which the causative mutation(s) were considered definitive based on multiple alleles or reversion.

Comparison between definitive SNPs and passenger SNPs

The 29 definitively identified *DIV* genes were used to generate two populations of mutations: 50 causative *div muta*tions, and 100 "passenger" mutations picked from the same 29 strains. We noted two differences between the *DIV* and passenger mutations: the *div* mutations were typically more severe (based on Blosum62 substitution scores, Henikoff and Henikoff, 1993) than the passengers, and the *div* mutations were more likely to fall in protein sequences conserved in *Arabidopsis* based on BLAST search. These are both plausible properties since the *div* mutations probably seriously perturb protein folding or function, and conservation of cell-cycle control makes sequence conservation between species highly likely. These properties could be combined to create eight categories (Table 3.1) for which *div* mutations and passenger mutations had very different likelihoods (Figure 3.1).

Table 3.1: Classification of candidate mutations based on BLAST/Blosum62 scores

	Severe mutation Blosum62 <= -1	Not severe mutation Blosum62 > -1
BLAST hit, conserved residue	1	2
BLAST hit, conserved region, not residue	3	4
BLAST hit, mutation not in conserved region	5	6
no BLAST hit	7	8

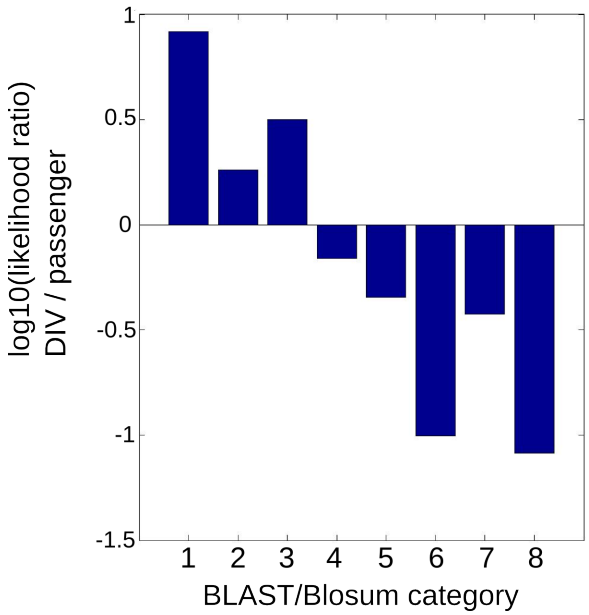

Figure 3.1: Log10 likelihood ratios for *div* mutations versus passenger mutations

div mutations and passenger mutations were categorized based on the severity of the amino acid substitution, and on conservation of the mutated gene between *Chlamydomonas* and *Arabidopsis*, into eight categories (Table 3.1). The log10 likelihood ratio for *div*/passenger was calculated for each category.

Linkage mapping

Bulked segregant sequencing typically generated one or a few small chromosomal segments containing uniform SNPs, frequently including one or a few missense mutations. If more than one region containing uniform SNPs was detected, we used linkage mapping to determine which region was linked to the *div* locus. Linkage crosses were done to high confidence SNPs: either definitive *div* mutations, or *div* loci that had been mapped relative to the definitive *div* mutations. Linkage was also established, in

some cases, by backcrossing the mutant to wild type and scoring co-segregation of the candidate SNP with the *div* phenotype. Evidence from linkage to other loci (L) or PCR markers (P) is indicated in Table 3.2. The distribution of *div* mutations on chromosomes 4 and 6 are shown in Figure 3.2A. The correlation between the chromosomal locations between pairs of candidate SNPs and the observed genetic distance conformed, on average, to the published value of 10 cM per Mb (Figure 3.2B) (Merchant et al., 2007a), supporting these assignments.

Bayesian probability that a given SNP is causative

It is likely that one of the observed functional SNPs in an interval of uniform SNPs will be causative, but there is a non-trivial chance that the true causative mutation was not detected, and consequently, that all the observed uniform SNPs are in fact passengers. Failure of detection could come about for multiple reasons. The genome assembly is incomplete, with both large segments of Ns (unspecified bases) and small missing segments in many gene models. Some sequences might be chemically incompatible with Illumina sequencing technology. Finally, a mutation might be difficult to align due to presence in repeated sequence, or due to complexity of the lesion (reconstructions indicate that deletions larger than ~20 bp are detected with very low efficiency by the bowtie2 aligner). We call such mutations ‘unsequenceable’. In several cases we have clear evidence for unsequenceability. For example, for *DIV14* and *DIV16*, we have bulked segregant sequence data for multiple alleles, in some cases with over 200X coverage.

These data yield clear map locations (positions of segments of uniform SNPs) on chrIVR and chrXR respectively (Appendix A2), but no overlapping gene model between alleles (and frequently, no functional SNPs at all in the region). We estimate the frequency of unsequenceability to be <=0.25.

Qualitatively, given two possible candidate mutations, the causative one is likely to be more 'severe', and likely to lie in a region of strong evolutionary conservation (Figure 3.2); it is also more likely to lie in a physical position mapping close to the estimated map position of the *DIV* gene. We systematized these qualitative considerations in a Bayesian calculation based on the BLAST/Blosum properties of the mutations, compared to the 'training set' of causative and passenger mutations, integrated with relative likelihoods of the SNPs based on linkage mapping to known physical markers. This approach is explained in detail in Appendix A1. The calculation yielded probability estimates for each SNP being causative (as well as for 'unsequenceability'). These values are reported in Table 3.2.

Importantly, this calculation is independent of prior qualitative information or knowledge about gene function – it is entirely based on statistical properties of the sequences, and on linkage mapping.

In the following discussion, we will assume that these assignments are correct, although we recognize that there is likely at least one error among the assignments. The most important assignments for future chapters (such as *cdka-1* and *cdkb-1*, discussed in detail in chapters 5 and 6) have high Bayesian probability (>0.97 for the *cdk* mutations),

and these are almost surely correct.

Figure 3.2: Linkage mapping of *div* mutants
(A) The positions of *DIV* genes (thick arrows: 'definitively' causal, thin arrows: 'probably' causal) are shown for chromosome 4 and 6. Genetic distances (cM) between *DIV* genes are indicated above the arrows. Tickmarks indicate megabases. *DIV* genes are assigned locations on the physical map based on the following requirements:

1. From bulked segregant sequence analysis, a region of uniform SNPs (functional, i.e. cds-changing, or not) that is either the only one in the library, or that is shown to be the only one consistent with other genetic linkage data.
2. At least one independent cross showing co-segregation of this uniform region with other markers on the same chromosome, with physical distances approximately consistent with location of the region and the marker, assuming an average 10 cM/Mb (Merchant et al., 2007a).

DIV genes are assigned a specific gene model based on a SNP within the uniform region changing the gene model, where the SNP is either:

1. 'Definitively causal' based on multiple non-complementing alleles with cds-changing uniform mutations in the same gene model;
2. 'Definitively causal' based on isolation of intragenic revertants that are true or pseudo-revertants at the site of the original mutation;
3. Probably causal based on Bayesian analysis (see text and Appendix A1), with a cutoff of Bayesian probability >=0.7. (This cutoff was arbitrary, and most gene models indicated have probability > 0.9; Table 3.2).
4. In some cases, no candidate is proposed (e.g. *DIV14* on chr IV). This is either because the *div* mutation is apparently 'unsequenceable' (see text), or

because there are multiple candidate SNPs in the interval that cannot be distinguished reliably by the Bayesian analysis (Table 3.2).

Linkage experiments were of two types. (1) Two different *div* mutants were mated, and segregation of ts lethality assessed (Ts+: Ts- ratios 2:2: PD; 1:3: T; 0:4: NPD; map distance in cM 50*(T+6 NPD)/(PD+T+NPD). Numbers of tetrads varied between experiments from ~20 - ~100. (2) A *div* mutant was mated to wild type, and co-segregation of Ts- with the SNP at the indicated physical location established by PCR/resequencing, typically of 10-20 segregants from 4-viable-spore tetrads. A single map distance from such an experiment (unless the distance is ~0, as in the PCR case) is ambiguous since the linkage can be in either direction. In all cases, we could rule out one direction based on the positions of the regions of uniform SNPs, and/or on crosses with other markers and requiring approximate consistency of distances.

(B) Observed correlation between physical distance between candidate mutation and genetic distance (cM) between ts-lethal mutations. The genome-wide average of 10 cM/Mb, as reported in (Merchant et al., 2007), is represented by the red line.

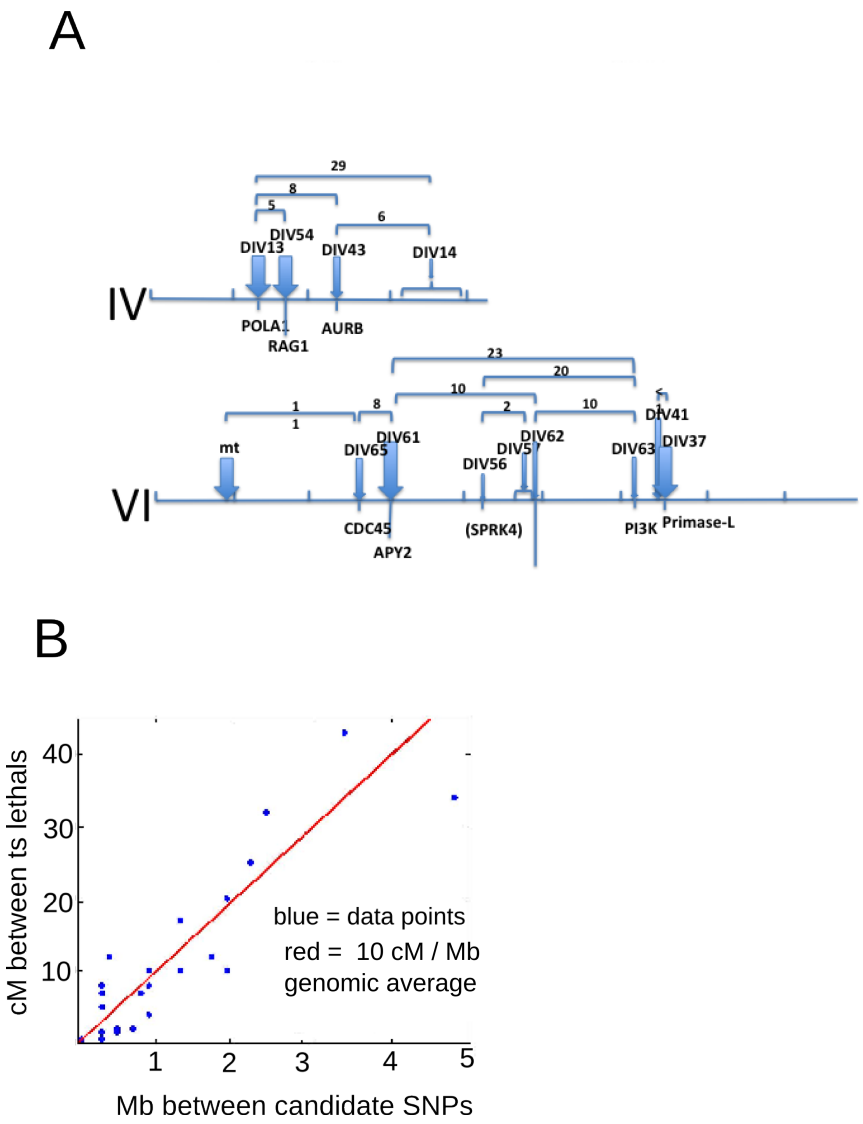

Figure 3.2: Linkage mapping of *div* mutants (see Appendix A2 for all chromosomes) **(A)** Physical position of *DIV* genes on chromosomes 4 and 6. Tickmarks: megabases, Numbers indicate cM between *DIV* genes obtained by mapping. Thick arrows: 'definitively' identified genes, thin arrows: 'most likely' identified genes (see main text). mt: mating type locus. *DIV14* has been mapped to a region of chromosome 4, but no candidate mutation was found. **(B)** Correlation between physical distance between candidate *DIV* genes and observed genetic distance (cM). Red line: genome-wide average of 10 cM/Mb.

Overview of mitotic (class 6) div-genes

The rest of this chapter provides a brief overview of the identified *DIV* genes. The genes are grouped according to cellular functions, based on similarity to genes in other organisms.

Six *div* mutations identify genes with a likely function in the core cell cycle machinery

As described in the introduction, a central theme of the cell cycle oscillator as defined in opisthokonts is rising and falling cyclin-CDK activity, and the negative feedback relationship between cyclin-CDK and the APC. We identified temperature-sensitive mutations in two components of the APC complex, as well as mutations in CDKA and CDKB, two CDKs closely related to opisthokont Cdc2/Cdk1, and probably the two main cell-cycle CDKs in plants (De Veylder et al., 2007). These mutants are likely to directly perturb the cell cycle oscillator in *Chlamydomonas* and offer a unique opportunity to explore both conserved and potentially plant-specific features of cell cycle control.

The *Chlamydomonas* genome also encodes other CDK proteins, more distantly related to Cdc2, called CDKC, CDKD, CDKE and CDKG (Bisova et al., 2005). One of these, CDKD/Cre09.g388000, is related to opisthokont Cdk7 and might function as a CDK-activating kinase (Takatsuka et al., 2009), and CDKC in *Arabidopsis* has been proposed to function in transcription (Cui et al., 2007). The functions of CDKE and CDKG are unclear.

We also isolated mutations in the kinases MPS1 (Liu and Winey, 2012) and Aurora B (Carmena and Earnshaw, 2003). Both proteins play multiple roles in cell cycle coordination in opisthokonts.

Six *div* mutations identify genes that are likely required for chromosome organization and microtubule function

Three *div* mutations identify genes likely to be required for proper chromosome organization: DIV35/SMC2 , DIV19/Topo2 and DIV30/ESP1. SMC2 is part of the condensin complex that condenses chromosomes prior to mitosis (Hirano, 2012), Topo2 is responsible for decatenation of intertwined DNA strands (Champoux, 2001), and ESP1/separase is responsible, at anaphase, for cleaving the cohesin links that hold sister chromatids together (Peters, 2002).

Three *DIV* genes were likely involved in microtubule function. These were the tubulin folding cofactors DIV24/TFC-E and DIV51/TFC-B (Szymanski, 2002), as well as DIV49/GCP2 (Murphy et al., 1998). The tubulin folding cofactors are conserved proteins that are important for the maturation of tubulin subunits to be incorporated into microtubule filaments. GCP2 is a component of the gamma tubulin ring complex that nucleates the minus end of microtubules (Wiese and Zheng, 2006).

Sixteen *div* mutations identify genes with a likely function in DNA replication

By sequence conservation, the DNA replication machinery is well conserved between plants and animals (Shultz et al., 2007).

DNA replication in yeast and animals is carried out by multi-protein complexes that are in general highly conserved, including in plants (Shultz et al., 2007) and *Chlamydomonas*. We obtained mutations in many of these genes (encoding all four subunits of Polα, two subunits of Polδ, Cdc45, and multiple enzymes required for dNTP synthesis (Table 3.2).

A critical regulatory step in initiation of DNA replication is the conversion of a replication origin loaded with ORC and MCM complexes ('pre-RC') to an incipient replication fork. This step is under positive control by cyclin-Cdk, which phosphorylates the yeast/animal proteins Sld2/RecQ4 and Sld3/Treslin, promoting their interaction with the BRCT-domain-protein Dpb11/Topbp1 (Boos et al., 2012). Unlike most enzymes involved in DNA replication, these three proteins are highly diverged comparing animals and yeast. *DIV20* and *DIV21* encode clear sequelogs of *RECQ4* and *TOPBP1* respectively, resembling the animal proteins much more than the yeast versions. *Chlamydomonas* and animal RecQ4 both share a weak region of N-terminal homology to Sld2, supporting this functional alignment (Figure 3.3). This pattern of higher conservation to animal proteins in plants than in yeast was noted previously for other proteins (Cross et al., 2011) and may reflect accelerated sequence evolution in yeast lineages, which can hide the more recent evolutionary divergence from animals.

Figure 3.3: DIV20 sequence alignment

Alignment (ClustalW) of *Chlamydomonas* DIV20 to Sld2 from *S. cerevisiae* and RecQ4 from *X. laevis* and *H. sapiens*. Conserved, or conservatively substituted residues indicated by black arrows.

We did not identify a mutation in any gene resembling Treslin/Sld3, nor could we detect a Treslin sequelog in the *Chlamydomonas* genome by BLAST searches.

All *Chlamydomonas* mutants blocking DNA replication shared a common microscopic phenotype: presence of a ‘notch’ (which we interpret as an incipient cytokinetic structure). The mutants all also share the property of near-quantitative cell lysis after a few hours of arrest that marks ‘class 6’ mutants. Both of these observations are odd given the existence in yeast and animals of replication checkpoints that block any mitotic events, and that can maintain cell viability for extended periods, in cells undergoing replication blockade. Differences in checkpoint control between plants and yeast/animals were noted previously on other grounds (Dissmeyer et al., 2009).

The mutants we have isolated should provide the opportunity to study the sequence of steps involved origin loading, origin activation and DNA replication in the plant superkingdom.

Mutations in genes with a possible connection to phosphoinositide and actin-related processes

We identified mutations in two genes with a likely connection to the actin cytoskeleton and perhaps cytokinesis: DIV31/PIP5K and DIV68/profilin. Profilin is a conserved eukaryotic actin-binding protein that plays a central role in actin polymerization (Witke, 2004). PIP5K (phosphatidylinositol phosphate 5-kinase) catalyzes the production of the phospholipid PtdIns(4,5)P_2 (Toker, 1998). PtdIns(4,5)P_2 plays multiple roles in eukaryotic membranes (Di Paolo and De Camilli, 2006), and has specifically been implicated in cytokinesis, by interacting with the actin cytoskeleton (Logan and Mandato, 2006). Interestingly, PtdIns(4,5)P_2 is thought to promote actin polymerization, in part, through direct interaction with profilin (Lassing and Lindberg, 1985). PtdIns(4,5)P_2 has also been implicated in tip-growing plant cells like pollen tubes and root hairs (Saavedra et al., 2012)(Kusano et al., 2008). Disruption of the pollen-expressed PIP5K4 kinase in *Arabidopsis* caused growth defects in the pollen tube, and reduced transmission through the male germline (Sousa et al., 2008).

Actin has been shown to localize to the cleavage furrow during cytokinesis in *Chlamydomonas* (Harper et al., 1992), possibly directed by the location of the four-membered microtubule rootlet (Ehler and Dutcher, 1998). Thus, it is possible that the *div31-1* and *div68-1* mutants identify essential components of the cytokinetic machinery in *Chlamydomonas*. The phenotypes of *div31-1*/PIP5K and *div68-1*/profilin were distinct. *div68-1* arrested as large round cells, whereas *div31-1* developed several apparent

cytokinetic structures on the cell surface.

The arrest phenotypes of *div31-1* and *div68-1* are not known beyond basic morphology. It will be interesting to determine if these mutants are, in fact, arrested at cytokinesis.

Other genes and pathways

The genes mentioned above have relatively well-established functions in the cell cycle in other systems, and high sequence similarity makes it probable that some aspect of this function is conserved in *Chlamydomonas*. However, a number of *div* mutants identified genes for which homology-based annotations provided much less information.

SGT1, mutated in *div42-1* (Bayesian probability 0.95), was identified in a yeast screen as a suppressor of a temperature sensitive allele of Skp1, a component of the SCF ubiquitin ligase complex (Kitagawa et al., 1999). In yeast, SGT1 has been found both at the kinetochore and associated with the SCF complex. In plants, SGT1 has been implicated in a variety of functions, including immunity (Meldau et al., 2011) and auxin response (Gray and Muskett, 2003), but not so far implicated in cell cycle progression.

Three GIF genes (GRF Interacting Factor) were identified in Arabidopsis. They were proposed to work as co-activators of gene expression together with GRF. Interestingly, reduction of GIF activity in Arabidopsis led to both cell proliferation and developmental defects (Lee et al., 2009). *Chlamydomonas* has a single GIF gene, which is mutated in *div47-1*, related to Arabidopsis GIF1-3. The mutation (with a Bayesian probability of

0.89) is a severe isoleucine to asparagine (Blosum score -3) substitution in the N-terminus of the protein, in a region that is highly conserved between DIV47 and *Atabidopsis* GIFs (Figure 3.4). In addition, DIV40 shares the features of a glutamine-rich C-terminus with all three GIFs from *Arabidopsis*, making is a plausible GIF homologue. However, BLAST searches could not identify any GRF protein in *Chlamydomonas*. This observation could suggest that GIF function is basal, with GRFs evolving in higher plant lineages to modulate GIF function.

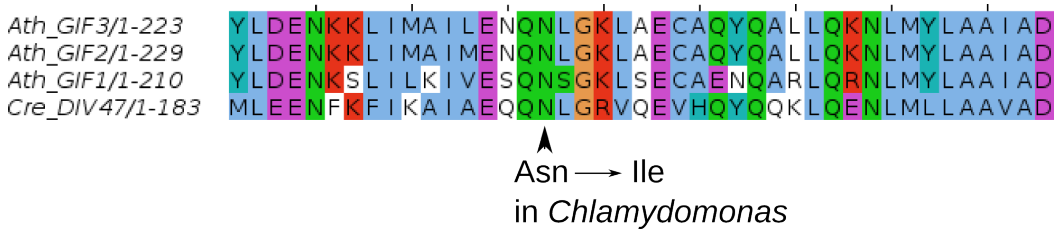

Figure 3.4: DIV47 sequence alignment

Alignment (ClustalW) of DIV47 from *Chlamydomonas* with GIF1, 2 and 3 from *Arabidopsis*. The Asn to Ile mutation is causative in *div47-1*.

The *div55-1* mutant (Bayesian probability 0.99) has a mutation in a protein kinase gene. It is annotated in Phytozyme as resembling a CDK activating kinase (CAK), but another gene model, Cre09.g388000, shows a much better alignment to known CAKs: human CAK/CDK7, as well as to Arabidopsis CAK/CDKD (Umeda et al., 2005).

div60-1 has a mutation in P450 reductase (Bayesian probability 0.87). *div70-1* has

mutation in a putative homologue of cactin (Bayesian probability 0.79), a nuclear protein required for embryogenesis in Arabidopsis (Baldwin et al., 2013). No cell-cycle roles for these proteins have been proposed.

The *div39-1* mutation identifies the *Chlamydomonas* sequelog of the *Arabidopsis* cell cycle regulator DUO3, which has diverse roles in male gametogenesis and embryogenesis in *Arabidopsis* (Brownfield et al., 2009).

The *DIV44* mutation identifies a member of the *BSL* phosphatase family. In *Arabidopsis*, there are three BSL (BSU1-like) proteins. BSU1 plays a role in brassinosteroid signaling, but it is likely that the BSL family has a more general, if still unidentified function for cell viability (Maselli et al., 2014). The *Chlamydomonas* genome lacks any BLAST-recognizable sequelogs of components upstream or downstream of BSU1 in brassinosteroid signaling, with the exception of the immediate downstream BSU1 target BIN2 (GSK2 kinase) (see Chapter 4). As with *DIV47/GIF3*, this could reflect the basal function of BSL phosphatases, brought under additional regulatory control by brassinosteroids in some plant lineages.

Overview of G1 (class 5) div genes identified in the screen

In contrast to most mitotic (class 6) *div* mutants, the mutations identified by the class 5 mutants showed no clear connection to control or execution of cell division. Based on annotation and similarity to genes in other organisms, the G1 *div* mutations were loosely

grouped into four categories: transcription/translation, protein folding/proteasome, membrane lipids and others.

Mutations in genes with a likely function in transcription/translation

The two alleles of *div2* carried STOP mutations in exons number 5 and 8, respectively, out of the 26 exons in TAF2. TAF2 is a conserved component of the TFIID complex, which is critical for initiating transcription at many promoters (Goodrich and Tjian, 2010). These stop mutations likely truncate TAF2 sufficiently to eliminate function. It is interesting that *div2* has only mild defects at permissive temperature, but is completely inviable at restrictive temperature. The requirement for TAF2 at high temperature could be due to decreased stability of the TFIID complex in the absence of TAF2. Alternatively, one could speculate about a more direct role for TAF2 in transcription of subsets of genes required at the high light / high temperature the cells experience under restrictive conditions. Notably, the *med6-1* mutant also has an early STOP mutation in a component of a major complex involved in transcription, the Mediator (Malik and Roeder, 2010). *med6-1* is viable at high temperature but displays a variety of morphological defects.

All four alleles of *div6* have either STOP or frameshift mutations in the g12333 gene model. g12333 has small segments of homology to MED27, a component of the Mediator complex (Malik and Roeder, 2010), from *Arabidopsis*, human and mouse. Since *Chlamydomonas* does not have another gene that is a better match to Med27, *DIV6* may be the *Chlamydomonas* homolog of Med27. These *div6-1* null mutants do not have

striking defects at permissive temperature.

DIV33 contains a helicase domain and a SNF2 domain, suggesting that DIV33 might play a role in chromatin remodeling (Knizewski et al., 2008). DIV26 is probably a homologue of Nop52, a nucleolar protein involved in processing of pre-rRNA (Savino et al., 1999), and the *div62-1* mutant has a mutation in an Aspartyl tRNA synthetase.

Mutations in genes with a likely function related to protein synthesis or degradation

DIV69 is an AAA^+ ATPase family protein with similarity to yeast and *Arabidopsis* Cdc48 proteins. The best BLAST hit to *DIV69*, however, is a yeast protein called Rix7, which may be required for ribosome biogenesis (Gadal et al., 2001). DIV27 is a homologue of the HSP70 heat shock protein (Kampinga and Craig, 2010), and DIV36/RPT5 is a component of the proteasome regulatory particle (Park et al., 2010).

Mutations in genes with a connection to intracellular trafficking

div63-1 has a mutation in a homologue of a protein called VPS15, a Ser/Thr protein kinase that regulates the PI3K (phosphatidylinositol 3-kinase) Vps34 (Stack et al., 1995). Reduced function of Vps15 and Vps34 led to defects in vacuolar protein sorting. In general PI3K activity has been associated with intracellular trafficking (Lindmo and Stenmark, 2006). In *Arabidopsis*, a mutant Vps34 allele could not be transmitted through the male germline, largely due to failure in germination and pollen tube growth (Lee et al., 2008). Interestingly, profilin (*DIV68*, above) has been proposed as a binding partner

of PI3K (Aparicio-Fabre et al., 2006). The *Chlamydomonas* VPS34 protein has PtdIns 3-kinase activity (Molendijk and Irvine, 1998). Thus, a possible role for DIV63/Vps15 might be in intracellular trafficking.

ORP3A is a conserved oxysterol binding protein, that may be involved in membrane trafficking (Raychaudhuri and Prinz, 201) (Saravanan et al., 2009). The *Chlamydomonas div5-1*/*orp3a* mutant developed a strong "acorn" phenotype, characteristic of a small subset of class 5 *div* mutants (Figure 2.4), where the cell develops a highly abnormal, elongated growth pattern.

The *div18-1* mutation also resulted in the acorn morphology. *DIV18* encodes a dynamin-related protein, related to *Arabidopsis* DRP2, which is essential for male and female gametophyte development and/or cell cycle (Backues et al., 2010). DIV18/DRP2 contains a pleckstrin homology domain (Taylor, 2011), which can interact with phospholipids (Lemmon, 2004), providing an additional possible link between membranes and the acorn morphology.

Mutations in other genes

DIV54 is homologous to *Arabidopsis* Kinase-Associated Protein Phosphatase/Root-attenuated growth (KAPP/RAG1), which functions as a negative regulator of plant receptor kinases (Tichtinsky et al., 2003), and may be involved in salt tolerance (Manabe et al., 2008).

div56-1 is a mutation in a largely uncharacterized kinase, related to *Arabidopsis* ‘Ser/Arg-rich protein kinase 4’ (NP_566977.1).

Table 3.2 *DIV* gene map positions and candidate genes. Columns:

1: *DIV* gene classification. Classes 6 and 5 are based on time-lapse microscopy; see text. Functional subdivisions are based on annotations, confirmed by experimental data in some cases; see text.

2: Gene name.

3: *DIV* physical map position based on mapping of co-segregating SNPs.

4: Most likely candidate gene model for the causative mutation. Entries of 'None' (*DIV14*, DIV16) reflect real absence of any overlapping candidate based on sequence of multiple bulked segregant pools from independent isolates (3 and 4 alleles respectively; see text). Entries of 'no clear candidates' reflect single alleles with defined map positions, for which no single SNP had calculated Bayes probability greater than 0.7. This category is expected to be a mix of cases where the causative SNP was detected in the sequence analysis but not clearly identified by the Bayesian procedure, and cases where the causative SNP is 'unsequenceable' (see text).

5: Evidence for this causative mutation: M: multiple alleles; R: intragenic (pseudo)-reversion; L: linkage between *div* mutants with linked candidate SNPs (Figure 3.2); P: cosegregation of ts lethality with the candidate SNP based on sequencing of PCR products from multiple (typically 10-20) segregants.

6: Number of alleles isolated based on complementation testing and identification of lesions in the same gene model following sequencing of bulked segregants.

7: Blosum62 scores for the SNPs in the most likely candidates (see Figure 3.1 for *div* and passenger Blosum scores).

8, 9,10: Identity and score of highest-scoring BLAST hit to Arabidopsis proteome (NA: no hit). @: while CDKD1;2 (probable Cdk-activating kinase) is the best *Arabidopsis* blast hit for DIV55, it is unlikely that DIV55 is a true CDKD homolog, since the homology is limited to a part of the kinase domain, and

there is a much better *Chlamydomonas* CDKD homolog than DIV55 (Bisova et al., 2005). #: this homology was only detectable through the Volvox carterii homolog to g12333 (BLAST score 230), which then detected Arabidopsis Med27 (BLAST score 45). There is no better alignment to Med27 in Volvox or *Chlamydomonas* than these, and the alignments have significant mutual overlap.

11: Blosum62 scores for Arabidopsis vs. *Chlamydomonas* at the aligned position where the candidate *div* mutation occurred (NA: either no BLAST hit, or the mutation falls in a non-aligned region).

12: A Bayesian probability was calculated for the probability that the indicated mutation was causative, based on statistical characteristics of definitive DIV mutations compared to control 'passenger' mutations: Blosum score, existence of an Arabidopsis BLAST hit (E<0.0001), and the location and sequence conservation of the mutated residue relative to the Arabidopsis alignments (see text). For definitive *DIV* alleles this probability was arbitrarily assigned a value of 0.99 (asterisk). #: One linked uniform SNP was ruled out before Bayesian analysis in this case: Cre12.g523050 XII 4.6: gene is FABIA. *div27-2* library contains null allele (stop codon at Q1790) in addition to definitive mutation in DIV27, therefore it is highly unlikely that FABIA mutation could cause *div50-1*.

13: Bayesian probability that the causative *div* mutation is 'unsequenceable' (that is, not on the list of candidate SNPs detected by sequence analysis of bulked segregant pools). For definitive DIV alleles this probability was arbitrarily set at 0.01 (asterisk). For the 'unsequenceable' multi-allelic DIV14 and DIV16 (see text), this probability was arbitrarily set at 0.99 (carat). DIV75 is a single isolate with high sequence coverage and only a single uniform region. This region is meiotically linked to the causative mutation, but contains no detectable functional SNPs (carat).

14,15: Number and summed Bayesian probability of linked uniform SNPs in the bulked segregant analysis, found along with the preferred candidate in column 4.

Table 3.2 DIV gene candidates and map positions

1	2	3	4	5	6	7	8	9	10	11	12	13	14	15
CLASS 6	GENE	Map pos.	Cre candidate	Evidence	# of alleles	Blosum	A.t. best HSP	name	BLAST	C.r. vs A.t.	Bayes prob	Bayes (unseq)	# add. SNPs	additional cands
Regulators	CDKA	X 6.4	Cre10.g465900	L,P	1	-2	AT3G48750.1	CDKA;1	451	6	0.97	0.02	1	0.01
	DIV48	VIII 2.6	Cre08.g372550	L,P	1	-2	AT2G38620.2	CDKB1;2	432	7	0.97	0.03	0	NA
	DIV43	IV 1.4	Cre04.g220700	L	1	0	AT2G25880	AURORA	421	6	0.96	0.04	0	NA
	DIV34	VII 4.3	Cre07.g341700	P	1	-3	AT1G77720.1	MPS1	320	4	0.96	0.04	1	<.01
	DIV38	XIII 1.3	Cre13.g562950	R,P	1	-3	AT1G78770.1	APC6	227	4	0.99*	0.01*	0	NA
	DIV23	XVII 6.0	g17912	M,L	4	0,0,-2,-2	AT2G20000.1	CDC27b	229	2,2,7,7	0.99*	0.01*	0	NA
DNA replication	DIV74	X 5.0	g11180	L	1	-3	AT4G14700.1	ORC1A	202	2	0.82	0.1	2	0.08
	DIV21	XII 3.9	Cre12.g515900	M,L	2	0,-2	AT1G77320.1	TOPBP1	157	0,4,9	0.99*	0.01*	0	NA
	DIV20	XV 0.0	g15304	M,L	2	-2,-4	AT1G27880.1	RECQ4	184	2,2	0.99*	0.01*	0	NA
	DIV65	VI 2.7	Cre06.g270250	L	1	-3	AT3G25100.1	CDC45	135	2	0.96	0.04	0	NA
	DIV37	VI 6.5	Cre06.g293000	M,L	2	2,-3	AT1G67320.1	Primase-L	336	3,4	0.99*	0.01*	0	NA
	DIV46	I 2.9	Cre01.g017450	L	1	-2	AT1G67630.1	POLA2	226	4	0.83	0.09	1	0.08
	DIV72	VII 0.05	Cre07.g312350	L	7	1	AT5G41880.1	POLA3,4	385	2	0.83	0.17	0	NA
	DIV13	IV 1.4	Cre04.g214350	M,L	3	-3,1,-3	AT5G67100.1	POLA1	848	4,5,7	0.99*	0.01*	0	NA
	DIV50	XII 4.4	Cre12.g521200	L	1	-2	AT5G22010.1	RFC1	512	4	0.87 #	0.05 #	1 #	0.08 #
	DIV28	VIII 3.3	Cre08.g374050	M,L	3	-2,-3,-3	AT2G42120.2	POLD2	353	-2,5,5	0.99*	0.01*	0	NA
	DIV45	I 2.6	Cre01.g015250	L	1	1	AT5G63960.1	POLD-cat	1285	7	0.85	0.07	1	0.08
	DIV15	XII 0.1	Cre12.g492950	M	3	-1,-5,-5	AT2G21790.1	RNR1	1278	4,5	0.99*	0.01*	0	NA
	DIV17	XII 0.1	Cre12.g491050	M	2	1,1	AT3G23580.1	RNR2	492	5,5	0.99*	0.01*	0	NA
	DIV29	III 6.0	Cre03.g190800	M,L	5	-2,-3,-3,-3,-5	AT5G59440.1	ZEU1	217	1,4,5, 11,NA	0.99*	0.01*	0	NA
	DIV64	IX 6.2	Cre09.g406050	M	2	0,0	AT1G30820.1	CTP synth	771	1,1	0.99*	0.01*	0	NA
	DIV52	XVII 2.5	Cre17.g715900	L	1	-3	AT4G34570.1	THY2	597	6	0.96	0.04	0	NA
Chromatin organization	DIV35	II 1.8	Cre02.g086650	L,R	1	-3	AT5G62410.1	SMC2	916	4	0.99*	0.01*	0	NA
	DIV19	I 1.7	Cre01.g009250	M	4	0,-3,-4,-4	AT3G23890.1	TOPII	1370	4,6,7	0.99*	0.01*	0	NA
	DIV30	I 4.3	Cre01.g029200	M,L,P	2	-2,-3	AT4G22970.1	ESP1	207	1,11	0.99*	0.01*	0	NA
Spindle/ tubulin	DIV49	XII 4.9	Cre12.g523050	L	1	-3	AT5G17410	GCP2	238	2	0.97	0.03	0	NA
	DIV51	XV 0.4	Cre12.g525500	L	1	-3	AT3G10220.1	TFC-B	229	4	0.96	0.04	0	NA
	DIV24	II 3.4	g1886	R,M	2	-1,1	AT1G71440.1	TFC-E	173	5,6	0.99*	0.01*	0	NA
Division	DIV61	VI 3.0	Cre06.g273500	M,L	2	-3,-3	AT3G04080.1	ATAPY1	310	0,9	0.99*	0.01*	0	NA
	DIV68	X 1.3	Cre10.g427250	L	1	-3	AT2G19770.1	profilin	98	3	0.92	0.06	2	0.02
	DIV31	IX 5.5	g9964	M,L	2	-1,-3	AT1G10900.1	PI4P-5K	304	-1,7	0.99*	0.01*	0	NA

Table 3.2 DIV gene candidates and map positions

1	2	3	4	5	6	7	8	9	10	11	12	13	14	15
CLASS 6 continued	GENE	Map pos.	Cre candidate	Evidence	# of alleles	Blosum	A.t. best HSP	name	BLAST	C.r. vs A.t.	Bayes prob	Bayes (unseq)	# add. SNPs	additional cands
Other/ Unknown	DIV42	XII 3.4	Cre12.g513600	L	1	-3	AT4G23570.1	SGT1A	278	7	0.95	0.02	1	0.03
	DIV44	I 7.0	Cre01.g050850	R,L	1	-3	AT4G03080.1	BSL1	933	2	0.99*	0.01*	0	NA
	DIV39	IX 4.6	g9842	R,L,P	1	-3	AT1G64570.1	DUO3	45	2	0.99*	0.01*	0	NA
	DIV47	I 7.6	Cre01.g055200	L	1	-3	AT4G00850.1	GIF3	64	4	0.89	0.1	1	0.01
	DIV55	V 0.3	Cre05.g233600	M	2	-2,-3	AT1G66750.1	CDKD1;2 @	137	7,NA	0.99*	0.01*	0	NA
	DIV60	I 5.5	Cre01.g039350	L	1	-3	AT4G24520.2	P450-reductase	528	4	0.87	0.13	0	NA
	DIV70	XIII 1.4	Cre09.g398650	L	1	-2	AT1G03910.1	CACTIN	206	0	0.79	0.1	3	0.11
	DIV57	VI 4.8	NA	NA	NA	NA	NA	NA	NA	NA	NA	0.31	1	0.69
	DIV40	XVII 1.2	(no clear cand.)	NA	1	NA	NA	NA	NA	NA	NA	0.8	1	0.2
	DIV53	XVII 5.5-6.5	(no clear cand.)	NA	1	NA	NA	NA	NA	NA	NA	0.55	3	0.45
	DIV41	VI 6.5	(no clear cand.)	NA	NA	NA	NA	NA	NA	NA	NA	0.29	4	0.71
	DIV75	IX ~2.1	None	NA	NA	NA	NA	NA	NA	NA	NA	0.99 ^	0	NA
	DIV14	IV 3.5-4.0	None	NA	3	NA	NA	NA	NA	NA	NA	0.99 ^	NA	NA
	DIV16	X 5.5-6.5	None	NA	4	NA	NA	NA	NA	NA	NA	0.99 ^	NA	NA

Table 3.2 DIV gene candidates and map positions

1	2	3	4	5	6	7	8	9	10	11	12	13	14	15
CLASS 5	GENE	Map pos.	Cre candidate	Evidence	# of alleles	Blosum	A.t. best HSP	name	BLAST	C.r. vs A.t.	Bayes prob	Bayes (unseq)	# add. SNPs	additional cands
Transcription/ translation	DIV2	XIII 2.9	Cre13.g583500	M	2	-5,-5	AT1G73960.2	TAF2	218	11,11	0.99*	0.01*	0	NA
	DIV6	XII 1.9	g12333	M	4	-5,-5,-5,-5	AT3G09180.1 #	MED27	45	11,11, 11,11	0.99*	0.01*	0	NA
	DIV33	I 6.5	g1034	M,R,L	2	-2,-2	AT1G50410.1	SNF2	471	6	0.99*	0.01*	0	NA
	DIV26	I 3.1	Cre01.g019200	M	2	-5,-5	AT5G20600.1	NOP52	161	0,11	0.99*	0.01*	0	NA
	DIV62	VI 4.9	Cre06.g279150	L	1	-3	AT4G31180.1	Asp-AARS	560	-1	0.96	0.04	0	NA
Protein folding/ proteasome	DIV27	XVI 5.9	Cre16.g677000	M	2	-1,-2	AT1G79930.1	HSP91	689	0,11	0.99*	0.01*	0	NA
	DIV69	IX 1.4	Cre09.g398550	L,P	1	1	AT3G01610.1	CDC48C	290	5	0.87	0.13	0	NA
	DIV36	X 2.8	Cre10.g439150	R,L	1	-3	AT3G05530.1	RPT5A	702	2	0.99*	0.01*	0	NA
Membranes/ lipids	DIV63	VI 6.2	Cre06.g290500	L	1	-2	AT4G29380.1	PI3K-p150 subunit	234	1	0.97	0.03	2	<0.01
	DIV5	III 8.4	g4364	M,L	4	0,-2,-3,-3	AT5G02100.1	ORP3A	390	5,6,6,6	0.99*	0.01*	0	NA
Other/ unknown	DIV54	IV 1.7	Cre04.g212300	M,L	2	-3,-3	AT5G19280.1	KAPP	102	NA,NA	0.99*	0.01*	0	NA
	DIV56	VI 4.3	g6395	L	1	0	AT3G53030.1	SRPK4	271	4	0.73	0.12	1	0.15
	DIV1	XIII 0.0	Cre13.g561800	M	4	-2,-2,-5,-5	None detected	NA	NA	NA	0.99*	0.01*	0	NA
	DIV71	XIII 1.0	(no clear cand.)	NA	NA	NA	NA	NA	NA	NA	NA	0.08	5	0.92
	DIV66	VIII 2.7	(no clear cand.)	NA	NA	NA	NA	NA	NA	NA	NA	0.4	2	0.6

Summary

This chapter described identification of about 60 causative *div* mutations, by a strategy of bulked-segregant whole-genome resequencing of genetically characterized mutants. We considered 29 of these assignments to be definitive, based on evidence from either multiple independent alleles or revertants. The remaining *div* mutants were placed on the genetic map after crossing to known markers (Appendix A2). In most cases, a single most likely causative SNP could be identified in these mutants based on linkage mapping and on statistical properties of known *div* mutations versus passenger mutations.

In chapter 2, the *div* mutants were divided into class 5 (reduced growth rate, no lysis) and class 6 (wild-type growth rate, followed by lysis), based on their growth properties and morphologies on agar. We identified mutations resulting in both class 5 and class 6 phenotypes. Mutations in genes with an established cell cycle function in other systems were exclusively found in class 6 (with the exception of *cdka-1*). These included a large number of S-phase genes and several mitotic kinases. Class 5 mutants consisted of a functionally heterogeneous set of genes, with representation of basic transcription and protein synthesis functions and membrane processes.

The mutations identified here will provide powerful tools for analyzing cell cycle control in *Chlamydomonas*. In the following three chapters we present the work beginning this analysis.

Chapter 4 Phenotypic analysis of *div* mutants

Characterization of the nuclear division cycle

Our collection of *div* mutants, representing a broad range of cell-cycle-related essential functions, allowed us to begin a systematic exploration of the genetic control of the multiple fission cell division cycle in *Chlamydomonas*, focusing on the nuclear cycle (DNA replication and chromosome segregation). We used a combination of FACS analysis and fluorescence microscopy to determine the genetic requirements for initiation and completion of DNA replication and nuclear division. We also observed progression of cytokinesis and cell division by light microscopy. In addition, we used recombinant *Chlamydomonas* Cks1 to precipitate interacting proteins with kinase activity against histone H1, as a biochemical indicator of cell-cycle progression. Cks1 is a conserved protein known to interact strongly with cyclin dependent kinases in eukaryotes. In particular, AtCKS1 was shown to pull down both A- and B-type CDKs from *Arabidopsis* lysates (De Veylder et al., 1997), and CrCKS1 was shown to pull down cell-cycle-regulated H1 kinase activity from *Chlamydomonas* (Bisova et al., 2005).

For most experiments, we employed a protocol that yielded partial cell cycle synchronization. Cells maintained on 14:10 LD cycles at permissive temperature were transferred to restrictive temperature at lights-on; since cells at the end of the dark period are almost all small newborn G1 cells, this procedure results in a long G1/cell growth period during most of the light period, followed by rapid S/M cycles starting near the time

of lights-off. This is likely similar to the pattern of growth/cell cycle control in physiological, natural conditions (Donnan and John, 1983).

In wild-type cells, initiation of the first round of replication is approximately coincident with visual signs of initiation of cell cleavage. As the S/M phase progresses, the forming daughter cells become clearly distinguishable by light microscopy. When the cell has completed all divisions, the daughter cells are released simultaneously. By FACS, dividing cells show several distinct peaks representing cells at various stages in the S/M phase (Figure 4.1B). Examination of these S/M-phase cells by fluorescence microscopy shows several clearly separated nuclei (Figure 4.3A). A general correlation exists between the proportion of cells with 1C, 2C, 4C, 8C DNA content by FACS, and the number of nuclei observed under the microscope, suggesting that, normally, DNA replication during the S/M phase is followed by nuclear division. This is in agreement with a previous study that measured the intensity of fluorescently labeled nuclei (Coleman, 1982). Immunostaining with anti-tubulin antibodies typically revealed metaphase spindles in a small fraction of S/M phase cells (Figure 4.3A). The low proportions presumably reflect a short lifetime for spindles relative to the rest of the cell cycle.

By FACS analysis, at the beginning of the time course, wild-type cells and most mutant cultures were enriched in G1 cells, as indicated by a small cell size and a 1C DNA content in 80-90% of the population (Figure 4.1B and C-E). Wild-type cells initiated DNA replication around 12-14 hours in liquid cultures (around 9 hours in the agar growth protocol, see Methods), and had completed the S/M phase and released newborn daughter

cells by 18 hours (Figure 4.1 B).

In mutant cultures, we scored three different replication phenotypes. These were (i) a near complete failure to initiate replication by 18 hours, with cells arresting uniformly with 1C DNA content and undivided nuclei (ii) initiation of DNA replication with approximately normal timing followed by a 2C arrest, also with undivided nuclei and (iii) re-replication, indicated by an arrest with multiple FACS peaks corresponding to cells with higher order DNA content (Figure 4.1 C-E); in this class, some mutants exhibited nuclear division but others retained single (presumably polyploid) nuclei.

As Table 4.1 shows, most *div* mutants either failed to complete one genome duplication, or, alternatively, arrested with substantially re-replicated DNA. Mutants that failed to initiate DNA replication included all class 5 *div* mutants tested, as well as most class 6 mutants with mutations in genes predicted to play critical roles in early S phase, such as *div20-1*/TopBP1 and *div21-1*/RecQ4 (chapter 3). No mutant without detectable replication showed divided nuclei. This observation suggests dependence of nuclear division on prior DNA replication, as was found in budding yeast (Hartwell et al., 1974), and also suggested for *Chlamydomonas* (Harper and John, 1986). Whether, in *Chlamydomonas*, this dependency is due to a 'substrate-product' relationship or checkpoint control (see Introduction) requires further investigation.

Figure 4.1: Cell-cycle analysis of class 5 (G1-arresting) and class 6 (mitotic) *div* mutants

We measured Cks1-precipitable kinase activity and DNA replication by FACS in a subset of *div* mutants grown in liquid TAP media at 33ºC. **(A)** Cks1-precipitable kinase activity was measured against histone H1. In all cases tested, class 5 mutants arrested with background levels of kinase activity, similar to newborn wild-type cells. Class 6 mutants arrested with Cks1-kinase levels comparable to or higher than wild-type mitotic cells. The very high signal from ts196 may be due to overloading (see stained histone H1 band below). **(B)** Cell growth (Coulter Counter, left) and DNA content (FACS, right) in a wild-type culture shows continuous increase in cell volume over 14 hours, at which point cell division begins, as seen by re-appearance of small daughter cells. Initiation of DNA replication is seen between 14-15 hours. Higher order FACS peaks at the 16-hour time point (4C, 8C, 16C) represent cells that are undergoing division, but have not yet released daughter cells. Daughter-cell release is seen by FACS as a return to a uniformly 1C population at 18 h. **(C-E)** Representative examples of replication phenotypes among the *div* mutants. **(C)** Arrest with unreplicated or partially replicated DNA. **(D)** Initiation of DNA replication with normal timing by 14-15 hours followed by arrest with once-replicated DNA in >50% of cells by 18 hours. **(E)** Initiation of DNA replication with normal timing, followed by re-initiation and arrest with several FACS peaks representing re-replicated DNA (4C, 8C, 16C peaks). Table 4.1 shows replication phenotypes of all *div* mutants tested.

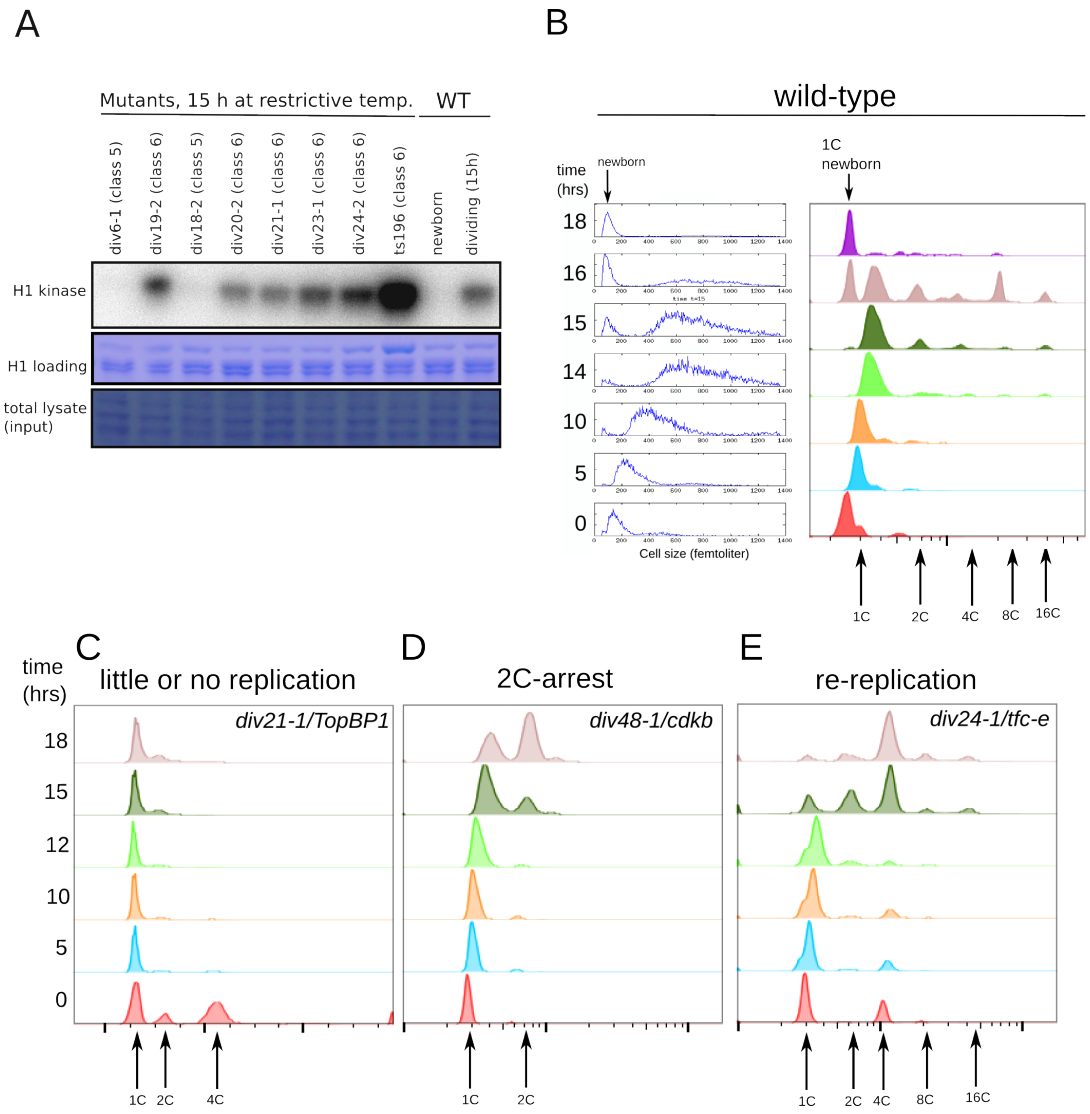

Figure 4.1: Cell-cycle analysis of class 5 (G1-arresting) and class 6 (mitotic) *div* mutants

Table 4.1: Replication phenotypes, as determined by FACS analysis, in class 5 and class 6 *div* mutants

No or partial replication		2C-arrest		re-replication	
mutant	**gene**	**mutant**	**gene**	**mutant**	**gene**
div1-1	Cre13.g561800	*div13-1*	*POL α*	*div13-2*	*POL α*
div1-2	Cre13.g561800	*div44-1*	*BSL1*	*div16-2*	unassigned
div1-3	Cre13.g561800	*div48-1*	*CDKB*	*div23-1*	*CDC27*
div2-1	*TAF2*			*div24-1*	*TFC-E*
div2-2	*TAF2*			*div24-2*	*TFC-E*
div5-1	*ORP3A*			*div34-1*	*MPS1*
div5-2	*ORP3A*			*div39-1*	*DUO3*
div6-1	g12333			*div42-1*	*SGT1*
div6-2	g12333			*div43-1*	*AURORA2*
div14-1	unassigned			*div49-1*	*GCP2*
div14-2	unassigned			*div51-1*	*TFC-B*
div15-1	*RNR2*			*div38-1*	*CDC16*
div15-2	*RNR1*				
div16-2	unassigned				
div17-1	*RNR1*				
div17-2	*RNR1*				
div18-2	dynamin-rel.				
div20-1	*RecQ4*				
div21-1	*TopBP1*				
div26-1	*NOP52*				
div27-1	*HSP70*				
div36-1	*RPT5*				
div56-1	*SRPK4?*				
TL7-51	unassigned				
cdka-1	*CDKA*				

Class 6 mutants that failed to replicate DNA nevertheless showed cytological indications of cell-cycle initiation, since they formed apparent cleavage structures around the time of wild-type S/M phase (Figure 2.4), suggesting a largely independent progression of the cytokinetic program and S phase (Harper and John, 1986). Class 6 mutants also activated Cks1-precipitable kinase activity to levels comparable to mitotic wild-type cells. In contrast, class 5 mutants (which also failed to initiate DNA replication) initiated no cytokinetic structures, and the three class 5 mutants tested (*div1-2*, *div6-1* and *div18-2*), exhibited negligible Cks1-precipitable kinase activity at restrictive temperature (Figure 4.1 A). We associated the low kinase activity, failure to initiate DNA replication and failure to form cytokinetic structures in class 5 mutants with an arrest in a G1-like state of the cell cycle, and will refer to them collectively as G1 mutants from now on.

These observations suggest that class 6 mutants all initiate the cell division program but fail in specific aspects of its execution (as an obvious example, failing in DNA replication due to presumed absence of dNTPs in ribonucleotide reductase mutants *div15* and *div17*). Class 5 mutants, in contrast, exhibited no indication of cell cycle initiation. Class 5 was originally defined operationally based on a partial cell growth defect. It is possible, therefore, that the failure of this class to initiate cell division is simply a general and non-specific consequence of slow cell growth. It is important to remember, however, that most class 5 mutants eventually exceeded the normal wild type division size. Therefore, simply a failure to reach a minimal size could not explain the failure to enter

the cell cycle in these mutants. Furthermore, the steady increase in cell size suggests that protein synthesis is ongoing in these mutants, albeit at a reduced rate. The cell-cycle arrest could potentially be explained by a requirement for some minimal growth rate, rather than cell size per se (Ko and Moore, 1990). However, we were unable to phenocopy class 6 with limiting concentrations of cycloheximide to slow but not eliminate protein synthesis; this treatment resulted only in progressively slower proliferation, but importantly, even very slow-growing cells ultimately divided at approximately the wild-type division size (not shown). Perhaps the diverse molecular defects in class 5 mutants (chapter 3) activate stress response or 'G1 checkpoint' responses that block cell-cycle initiation.

Chlamydomonas CDKA is required for cell-cycle initiation, but not for cell growth

As mentioned above (Figure 2.4), we identified one mutant, ts301, which combined features of the class 5 and class 6 mutants. The ts301 mutant carried two mutations required for ts lethality, one of which changed a conserved residue in CDKA, a CDK closely related to opisthokont Cdc2. When studied in a *MED6* background, the *cdka-1* mutant exhibited a long (up to 10 hour) delay before detectable signs of cell cycle initiation were observed. During this delay, *cdka-1* cells did not initiate DNA replication or develop apparent cytokinetic structures, and did not accumulate Cks1-precipitable H1 kinase activity. However, cell growth in the *cdka-1* mutant was unaffected for the entire duration of the delay. Therefore, CDKA is required for the transition from the G1 growth phase to cell cycle initiation. The phenotype of the *cdka-1* mutant will be discussed in

more detail in the next chapter.

Re-replication of DNA was observed in many *div* mutants

The re-replication mutants represented a diverse set of genes (Table 4.1), including genes involved in tubulin function (*div24-1*,*2*/tfc-e, *div51-1*/tfc-b and *div49-1*/gcp2) (Figure 4.2A), the kinases *div43-1*/aurora2 and *div34-1*/mps1, the Esp1/separase homologue *div30-1*, and *div39-1*, the putative homologue of the *Arabidopsis* protein DUO3. Re-replication implies at least two rounds of replication at restrictive temperature, resulting in a final DNA content of 4C or more. Clearly, scoring re-replication requires accurate determination of DNA content. Our sample preparation gave reproducible staining of DNA that was largely independent of strain background. However, small variations in the 1C value were observed by FACS, and the 1C peak generally shifted towards higher values in cells sampled later in the cell cycle, likely to a large extent reflecting an increase in organellar, particularly chloroplast, DNA content. Indeed, abundant nucleoids were generally detectable by microscopy in large cells. Consistent with the idea that overall cell size influences the absolute value of the 1C peak, small newborn cells had a distinctly lower-valued 1C peak. Frequent sampling generally facilitated assignment of peaks in the FACS profile, such that slow trends in peak shifts could be followed. The mutants in the re-replication class, arrested with at least 20% of cells (generally much higher) with a 4C or greater DNA content, as measured by FACS.

Figure 4.2: DNA re-replication in cells probably lacking normal microtubule function

(A) Analysis of microtubule mutants. The mutants *div24-1/tfc-e*, *div51-1/tfc-b* and *div49-1/gcp2* were predicted to be defective for microtubule function (see main text, chapter 3). All mutants, along with wild type, were grown in liquid TAP cultures at restrictive temperature and sampled regularly for FACS analysis. Wild type undergoes DNA replication and cell division between 14-17 hours. At 17 hours, most wild-type cells have completed division and hatched newborn 1C cells. In contrast, all mutants are completely blocked in cell division and arrest with re-replicated DNA. The fraction of cells with 4C DNA content or more (re-replicated, 2nd row) represent cells that have re-initiated DNA-replication at restrictive temperature.

B: Analysis of APM-treated wild-type cells.

Amiprophos-methyl (APM) is a microtubule poison that interferes with tubulin polymerization. Wild-type cells treated with 10 μM APM showed a complete cell cycle arrest. Asynchronous APM-treated wild-type cells (top, middle panel), untreated wild-type cells (top, left panel) as well as APM-treated S1D2-cells were grown in liquid TAP cultures at 33ºC and sampled regularly for FACS analysis. S1D2 is an independent wild-type C*hlamydomonas* isolate. Untreated cells initiated DNA replication between 12-15 hours and had largely completed cell division and released daughter cells by 18 hours. APM-treated wild-type cells initiated DNA replication by 12 hours and arrested with a majority of cells with an 8C DNA content by 18 hours. Wild-type S1D2 cells showed qualitatively similar behavior. This suggested that DNA replication could proceed independently of functional microtubules. Staining DNA in untreated cells with Sytox Green showed small newborn wild-type cells with a single nucleus (bottom row, left panel). Based on FACS data, these cells have a 1C DNA content. Staining APM-treated wild-type cells revealed only a single nucleus, implying several genome doublings without intervening nuclear division.

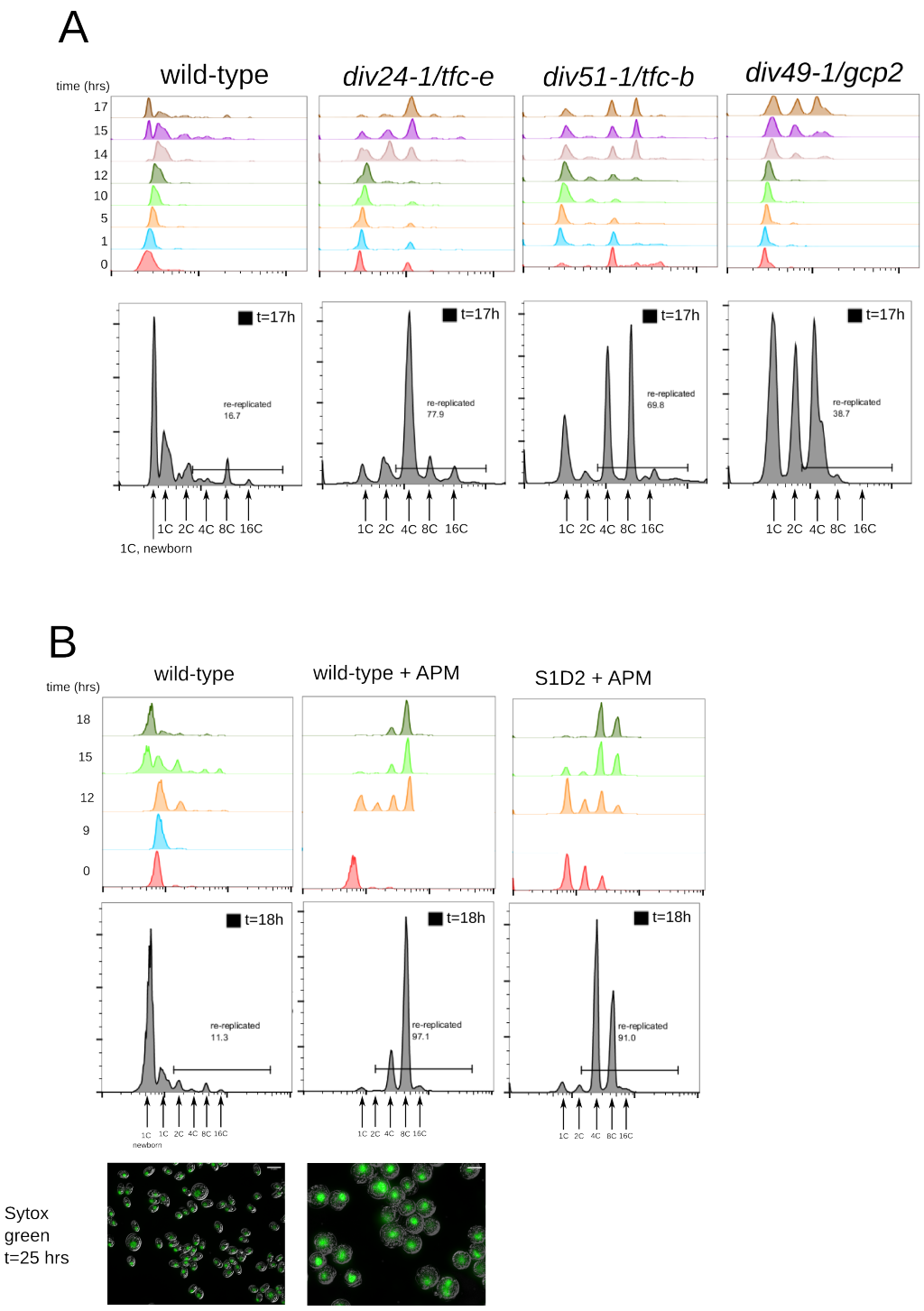

Figure 4.2: DNA re-replication in cells probably lacking normal microtubule function

Two classes of re-replication mutants: with or without nuclear division

Examination of DNA distribution by fluorescence microscopy in a subset of mutants exhibiting re-replication separated these mutants into two subgroups: apparently normal nuclear division and near-complete failure of nuclear division.

Apparently normal nuclear division was seen in the *div39-1/duo3* (Figure 4.3 A) and *div34-1*/*mps1* mutants (Figure 4.9), at times when a substantial proportion of mutant cells had re-replicated DNA. These cells had also initiated and apparently progressed through cytokinesis, as seen by formation of daughter-cell-like microclusters. However, whether this apparent cytokinesis resulted in separation of cytoplasm within the microcluster is not known. Thus, the *duo3* and *mps1* mutations appear to be compatible with both DNA replication and nuclear division, although the accuracy of chromosome segregation cannot be determined by this method. Consistent with the apparently normal nuclear division in *duo3* mutants, we observed fully formed, and apparently normal mitotic spindles in a fraction of *duo3* cells by immunostaining (Figure 4.3 A; *mps1* mutant cells were not assayed for spindle formation).

Re-replication without nuclear division was observed in *div24-1/tfc-e*, *div51-1/tfc-b*, *div49-1/gcp2* and *div30-1/esp1* (Figures 4.1 E, 4.2 A, 4.4 B): only 1-2% of mutant cells showed more than one nucleus per cell by fluorescence microscopy, at times when 20% or more of cells had re-replicated. This indicated loss of the wild-type alternation of S phase and nuclear division (see above; Coleman, 1982). Immunostaining against alpha-tubulin in *tfc-e*, *tfc-b* and *gcp2* suggested an abnormal microtubule organization,

consistent with the predicted function of these genes in tubulin folding (*tfc-e*, *tfc-b*) and nucleation of microtubule filaments (*gcp2*) (Figures 4.3A and 4.4A-B). Most importantly from the perspective of understanding the lack of nuclear division, *tfc-e*, *tfc-b* and *gcp2* showed no wild-type mitotic spindles.

Cytokinesis, or cell cleavage, in *div30-1*/*esp1* seemed farther developed compared to the tubulin folding mutants (*div24-1* and *div51-1)* and *gcp2*; microclusters containing 2-4 daughter cell-like bodies were seen by light microscopy (Figure 4.4 B). The term cytokinesis is used here only to describe the morphology of the microcluster, which suggested that some aspect of cell division was taking place. Whether the daughter-like cells within the microcluster were separated by membranes is not known. By FACS analysis, 100% of *div30-1* cells had completed one round of replication and 30% had replicated twice, arresting with 4C DNA. Strikingly, in almost all of these microclusters, the nucleus remained undivided and was found within one of the daughter-cell-like bodies, indicating a requirement for DIV30/ESP1 in nuclear division (Figure 4.4 B). This near-complete uncoupling of nuclear division from cytokinesis is an extreme version of the consequences of failed cohesion cleavage seen in yeast, where attempted division can result in one cell with a nucleus, and an ‘aploid’ cell lacking DNA (McGrew et al., 1992).

Re-replication in cells treated with the microtubule poison APM

To obtain independent confirmation that this arrest phenotype was the result of microtubule failure, we treated wild-type cells with the microtubule poison APM. APM

disrupts microtubule polymerization by binding to α-tubulin (James et al., 1993). Treating wild-type *Chlamydomonas* cultures with APM had no effect on cell growth, but resulted in a complete block to division. DNA replication started with approximately normal timing and progressed through the multiple rounds of replication typical of the S/M phase. Fluorescence microscopy detected only a single large Sytox green staining spot (DNA) in APM-treated cells, suggesting that several rounds of DNA replication occurred without intervening nuclear division. Furthermore, we obtained similar results with the independently isolated and highly polymorphic wild type strain S1D2, demonstrating that this phenotype was not associated with our particular lab strain (Figure 4.2 B).

Figure 4.3: Mutations affecting the nuclear cycle in *Chlamydomonas*

Wild type and all mutants were grown on agar plates for 11 h at restrictive temperature and prepared for microscopy. Visualization of DNA by Sytox green staining, and tubulin by alpha-tubulin immunostaining. Due to uneven staining, exposure times were adjusted between images, so variations in Sytox green intensity between images carry no meaning. DNA replication was assayed by FACS to determine proportion of re-replicated cells in A. **(A)** Arrest phenotypes of *div49-1/gcp2*, *div38-1/duo3* and *div44-1/bsl1* compared to wild-type S/M phase cells. *Wild type:* Dividing cells with separated nuclei are visible (DIC and SYTOX green). Metaphase spindles were identified by immunostaining with alpha-tubulin antibodies in ~5% of cells (white arrowheads). FACS analysis indicated that ~60% of cells had re-replicated DNA, consistent with the high proportion of multi-nucleate cells. *div49-1/gcp2:* Divided nuclei observed in 2% of cells. FACS analysis showed 4C-arrest in 40% of cells, suggesting frequent re-replication without nuclear division. A similar phenotype was observed in *div24-1/tfc-e*, *div51-1/tfc-b* and in cells treated with microtubule the poison APM (Figure 4.2). *div39-1/duo3:* Re-replication with nuclear division. DNA staining appears similar to wild type, showing separated nuclei. Immunostaining indicates ability to form normal-looking mitotic spindles (white arrowheads). FACS analysis shows progression through S/M phase with substantial fraction of 2C and 4C cells present. *div44-1/bsl1:* Arrest with once-replicated 2C DNA (FACS), and undivided nuclei (Sytox green). No morphologically normal spindles observed (tubulin).

(B) Arrest phenotype of *div48-1/cdkb-1* compared to wild-type S/M-phase cells. *Wild type*: Dividing cells with separated nuclei (DIC and Sytox green). Metaphase spindles detectable by immunostaining (white arrowhead). *div48-1/cdkb-1:* DNA-staining appeared diffuse. About 50% of cells had arrested with a single notch-structure at the time of fixation (DIC, white arrows). Development of the notch was accompanied by reorganization of anti-tubulin staining. DNA content was not measured directly, but other experiments showed a 2C arrest in *cdkb-1* cells (Figure 4.1D). Scale bar: 25 um

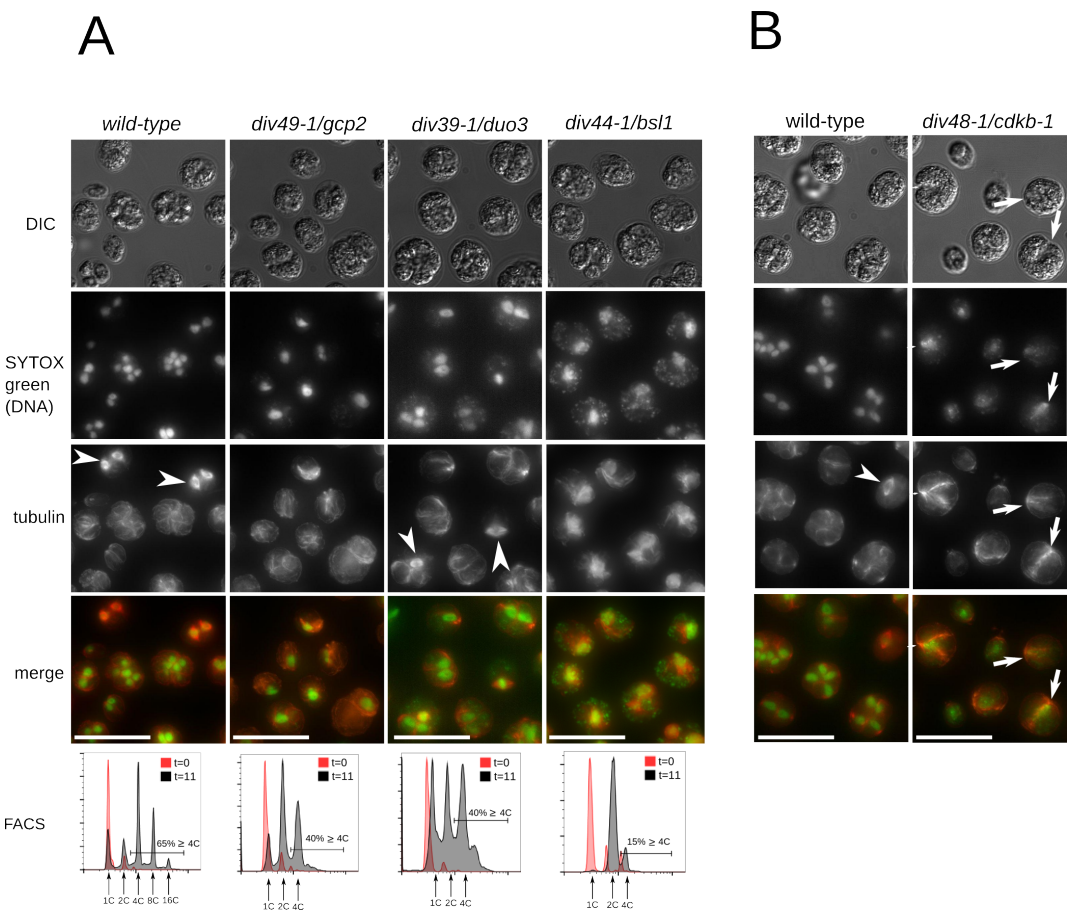

Figure 4.3: Mutations affecting the nuclear cycle in *Chlamydomonas*

Figure 4.4: DNA replication and distribution of DNA in *div24-1/tfc-e* and *div30-1/esp1*

Visualization of DNA by Sytox green staining, and tubulin by alpha-tubulin immunostaining. Due to uneven staining, exposure times were adjusted between images, so variations in Sytox green intensity between images carry no meaning.

(A) *div24-1* cells fixed after 11 hours at restrictive temperature (agar growth protocol, Methods). Parallel wild-type cells were in S/M phase. FACS analysis indicated re-replication, and 4C arrest, in about 20% of *div24-1* cells. Nuclear division was observed by Sytox green staining in 1-2% of cells. Immunostaining against alpha-tubulin revealed a disorganized tubulin distribution in several cells (white asterisks), consistent with a role of *div24-1/tfc-e* in microtubule function.

(B) *div30-1/esp1* and *div24-1/tfc-e* sampled after 15 hours at restrictive temperature (agar growth protocol, Methods). Parallel wild-type cells have completed S/M phase and released daughter cells, with a single nucleus each (DIC, Sytox green). Tubulin staining in newborn wild-type cells is characteristic of *Chlamydomonas* interphase: the region at the base of the flagella stains brightly. Cortical microtubules and flagella are also visible. *div30-1/esp1* mutant cells have formed microclusters containing daughter-cell-like bodies. Sytox green staining indicates unequal distribution of DNA within the microcluster: DNA is largely confined to one area of the microcluster. By FACS analysis, all *esp1* mutant cells have replicated DNA once, and many have undergone a second round of replication. Most *div24-1/tfc-e* mutant cells have re-replicated DNA, as determined by FACS analysis. In these cells, >95% of nuclei appeared un-divided (Sytox green), indicating extensive re-replication without nuclear division. Tubulin seemed to aggregate into several bright staining patches (white asterisks).

Scale bar: 25 um

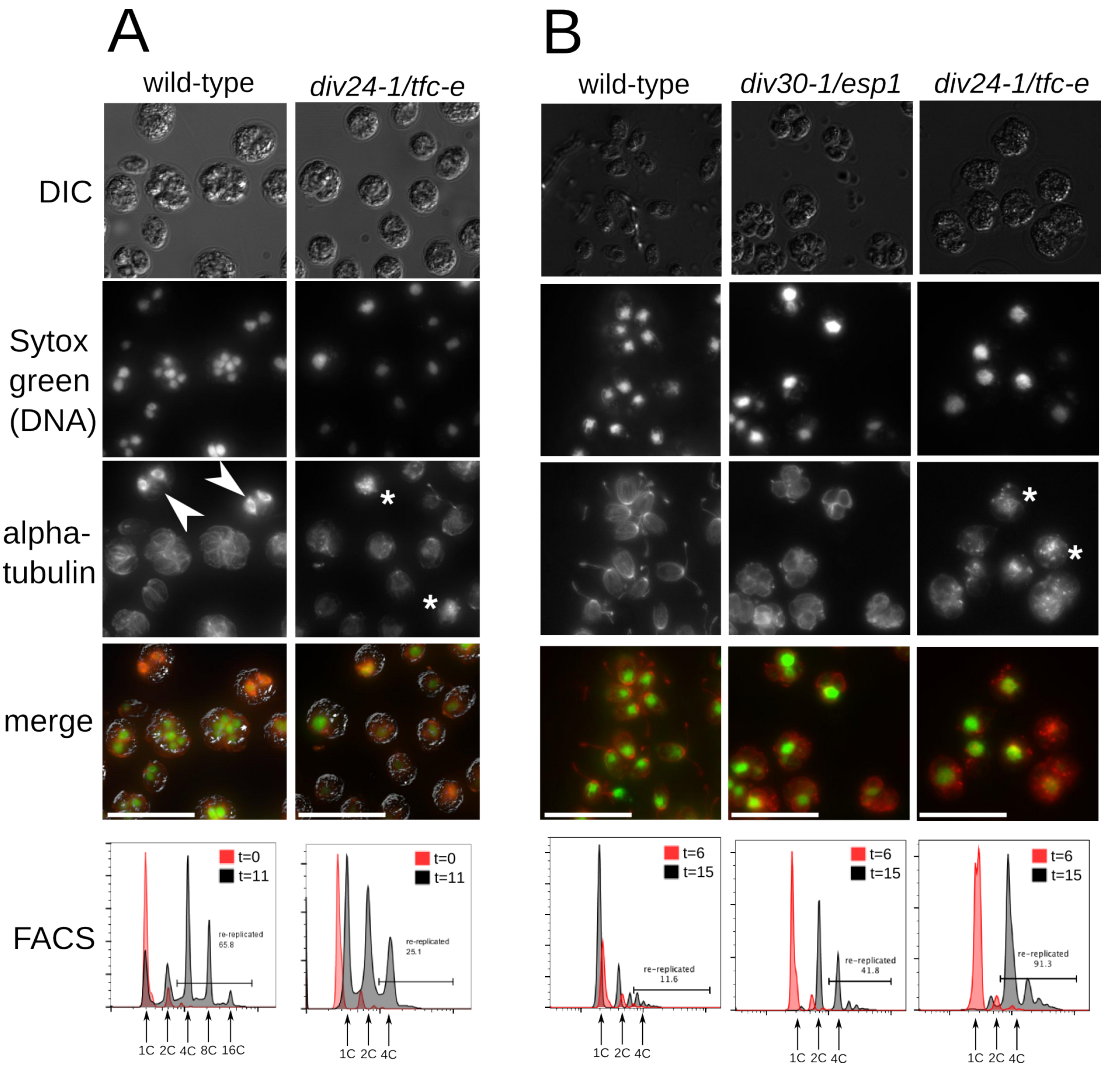

Figure 4.4: DNA replication and distribution of DNA in *div24-1/tfc-e* and *div30-1/esp1*

A 2C-arrest with undivided nuclei is a rare phenotype

Only three mutants arrested reproducibly with once-replicated DNA: *div13-1*, with a mutation in polymerase alpha, *div48-1*/*cdkb-1*, and *div44-1*/*bsl1*. The other POLA mutant, *div13-2*, displayed a weak re-replication phenotype, accompanied by nuclear division. We speculate that the two *div13* mutant proteins retain variable function at restrictive temperature, compatible with partial priming synthesis during DNA replication. Alternatively, POLA might be required only for very late-activated origins.

The *cdkb-1* mutant arrested with a single notch structure and a 2C DNA content without evidence of re-initiation of DNA replication (Figures 4.1 D, 4.7, 5.2 B). Nuclei appeared undivided, with diffuse staining of DNA in arrested *cdkb-1* cells, and development of a notch structure, characteristic of many mitotic *div* mutants, was accompanied by a striking reorganization of tubulin distribution, distinct from wild-type spindles (Figures 4.3 B and 4.7, white arrowheads). Thus, CDKB plays an essential role in mitosis, after the first round of DNA replication.

Interestingly, the *bsl1-1* mutant displayed a phenotype very similar to *cdkb-1*: a normal completion of the first S phase, followed by an arrest with 2C DNA and undivided nuclei (Figures 4.3 A and 4.5). Consistent with the failure to divide nuclei, tubulin staining suggested a disorganized microtubule organization, and a complete absence of mitotic spindles (Figure 4.3 A). BSL1 is homologous to the BSU1-family of plant phosphatases. This family plays a role in brassinosteroid signaling in *Arabidopsis*, but a direct role in cell cycle control has not been shown (see Discussion).

Figure 4.5: *DIV44/BSL1* is required for mitosis, but not for DNA replication

Wild type and *div44-1/bsl1* cells were grown in parallel on agar plates following transfer to restrictive temperature at lights-on in a 14:10 LD cycle. (Note: for unknown reasons, entry into replication was faster, and overall synchrony much better, in cells grown at low density on agar plates than in liquid medium). Cells were collected at the indicated time points, fixed and stained with Sytox green. **(A)** FACS analysis to determine DNA content. Both wild type and *div44-1*/*bsl1* cells are 1C at t=0 hours and have initiated DNA replication by t=9 hours, as seen by the appearance of higher order FACS peaks. Most wild-type cells have completed division by 11 hours and released newborn daughter cells. *div44-1/bsl1* cells complete the first round of replication with normal timing and arrest with 2C DNA content. **(B)** Fluorescence microscopy of the same preparations of cells as in **A**. Nuclear division accompanies DNA replication in wild-type cells at t=9 hours, as seen by more than one Sytox green staining area per cell body. By 11 hours, multinucleate wild-type cells in S/M phase are seen, as well as small newborn cells (DIC). By contrast, >95% of *div44-1/bsl1* cells with replicated DNA contained a single undivided nucleus at 11 hours, indicating a post-S phase, pre-mitotic block (white arrowheads).

Scale bar: 25 um

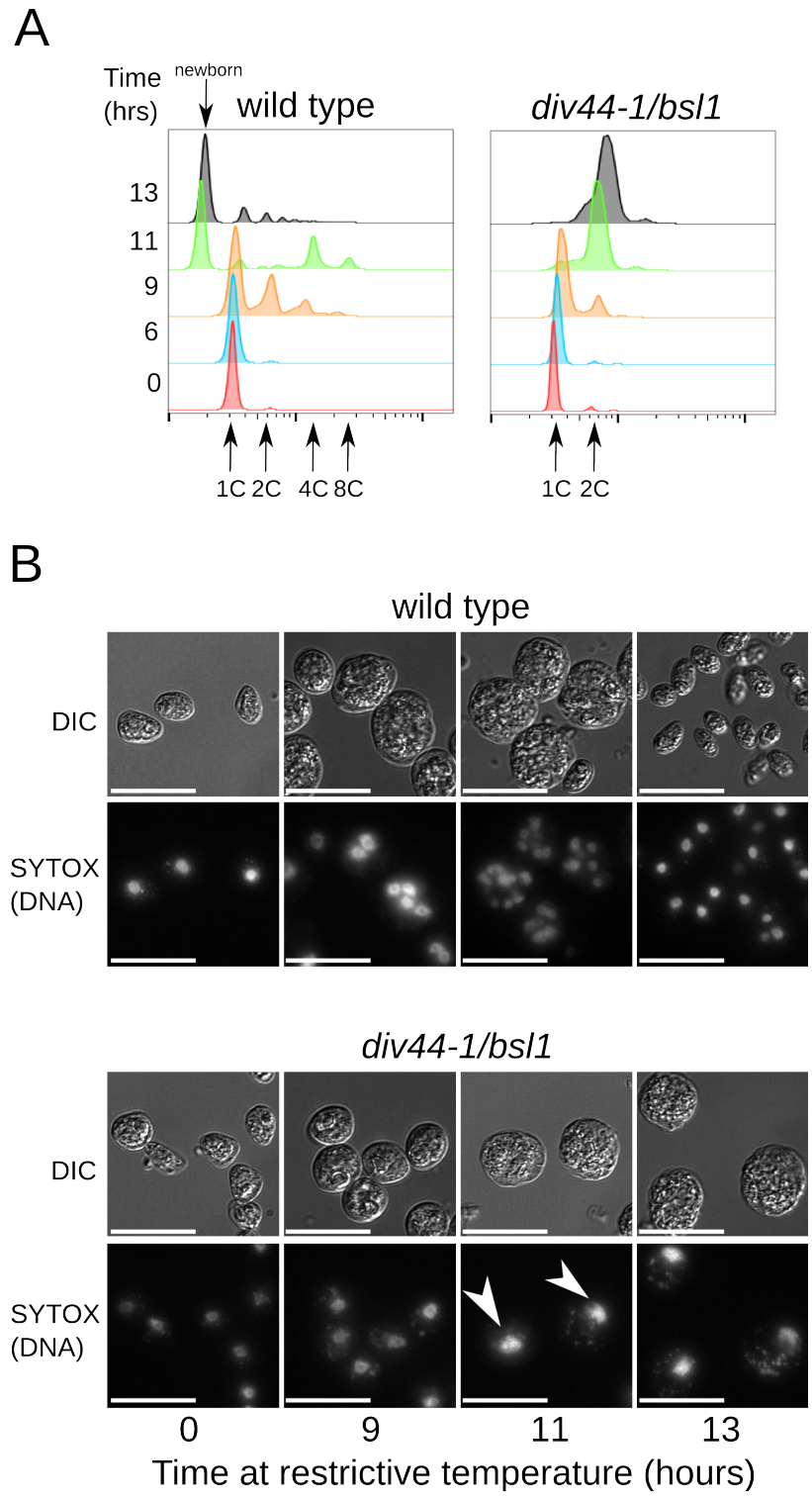

Figure 4.5: *DIV44/BSL1* is required for mitosis, but not for DNA replication

Phenotypes of mutations in two APC genes are consistent with a critical role for the APC in anaphase

We isolated two mutants, *div23-1* and *div38-1*, with mutations in genes encoding the CDC16 and CDC27 subunits of the APC (Thornton et al., 2006). These mutants accumulated a high proportion of cells with metaphase spindles, approximately 30% compared to ~5% in wild-type cells at similar cell cycle stage, indicating a requirement for the APC at the metaphase-to-anaphase transition (Figure 4.6). The metaphase block, however, appeared to be incomplete and a significant population of APC mutant cells arrested with 4C DNA content. To a first approximation, the fraction of 2C and 4C APC mutant cells in *div38-1* seemed to correlate with the fraction of mono-nucleate cells with one spindle and bi-nucleate cells with two spindles. Based on this we expect complete inactivation of the APC to result in an arrest at metaphase with once-replicated DNA; the apparent leakiness of the available mutants makes this statement somewhat provisional, however. We attempted to construct a *div23-1/div38-1* double mutant to allow definitive APC inactivation, but we were unsuccessful because the double mutant was inviable even at permissive temperature for the single mutants.

Figure 4.6: Arrest phenotypes of *div38-1/cdc16* and *div23-1/cdc27* suggests a role for the APC at the metaphase-to-anaphase transition

Wild-type cells were grown on agar plates in parallel with *div38-1/cdc16* and *div23-1/cdc27* at restrictive temperature for 11 hours. At this time, the cells were collected and stained with Sytox green to visualize DNA, and with anti-alpha tubulin antibodies to visualize tubulin. DNA content was assayed by FACS (bottom row). *wild-type:* Wild-type cells were in S/M phase, as determined by the presence of divided nuclei (white arrows) and a significant proportion of cells with 2C and 4C DNA content (FACS, bottom row). Many wild-type cells had also completed division and released daughter cells, as determined by the presence of small flagellated cells with a single nucleus (white asterisk). No mitotic spindles were seen in this preparation of wild-type cells. *div38-1/cdc16* and *div23-1/cdc27:* Most *apc* mutant cells have completed at least one round of replication, as determined by the proportion of cells with 2C and 4C DNA content, compared to cells with 1C DNA. Approximately 30% of *div38-1* and *div23-1* cells have formed apparently normal-looking mitotic spindles (white arrowheads). In cells with a mitotic spindle, DNA generally co-localizes with the spindle.

Scale bar: 50 um

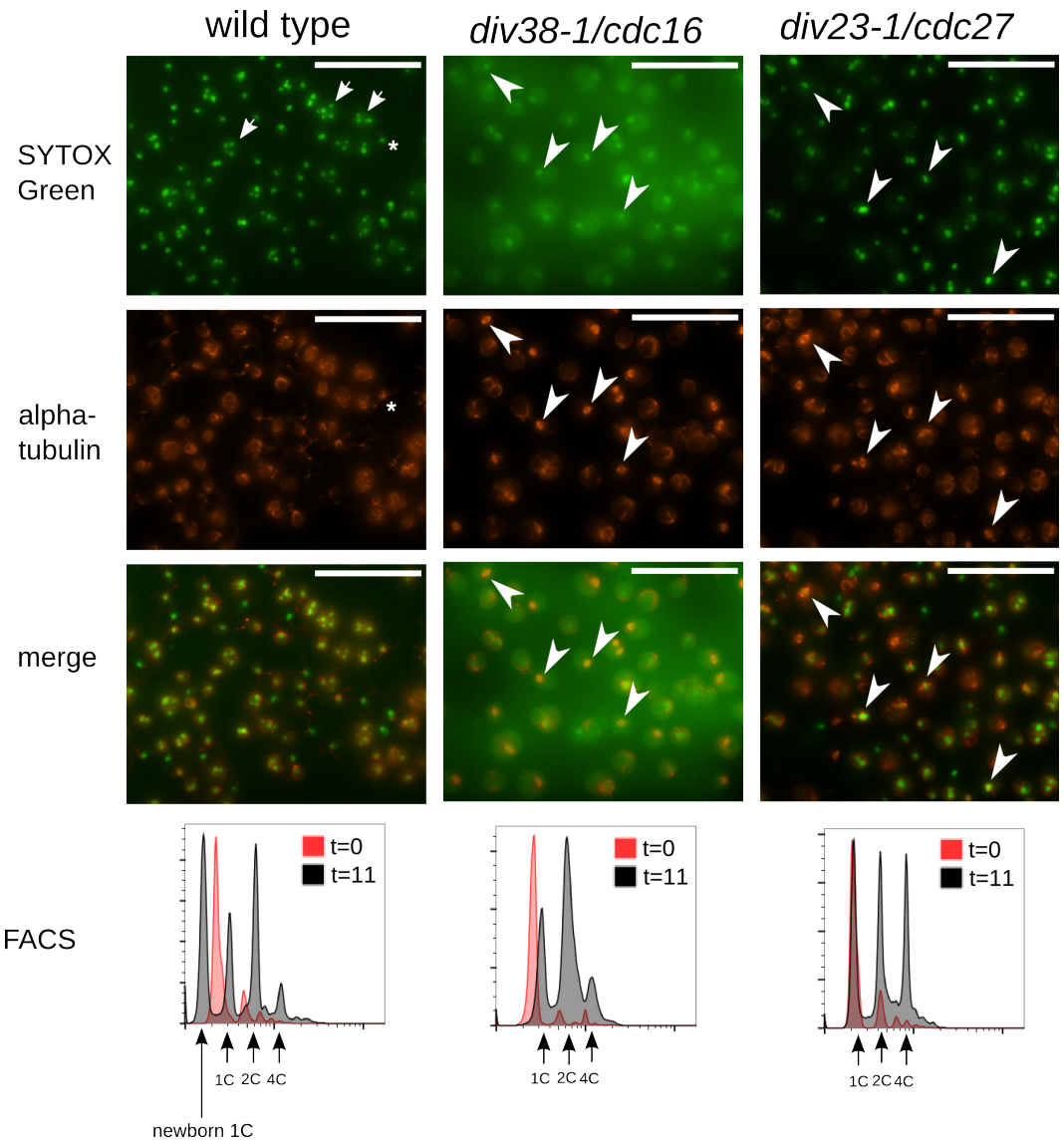

Figure 4.6: Arrest phenotypes of *div38-1/cdc16* and *div23-1/cdc27* suggests a role for the APC at the metaphase-to-anaphase transition

Discussion

Phenotypic analysis of cell division across the *div* mutant collection

We analyzed cytological and biochemical markers of the cell division program in our collection of *div* mutants: (i) replication and segregation of DNA, (ii) activation of Cks1-precipitable kinase activity and (iii) apparent initiation of cytokinesis as indicated by light microscopy. Class 5 and class 6 mutants had already been separated based on morphology and cell growth rate. This distinction between class 5 and class 6 mutants was reinforced by the more in-depth cell-cycle analysis presented in this chapter. By our assays, class 5 mutants were arrested in a G1-like state (no Cks1-precipitable kinase activity, no DNA replication, no cell lysis). Class 6 mutants entered the cell cycle, but the mutants differed from each other with respect to DNA replication, nuclear division, tubulin distribution and cell morphology.

CDKA function: at the dividing line between cell growth and cell cycle initiation

Only the *cdka-1* mutant was a clear outlier in the entire collection of *div* mutants, based on the ‘class 5 vs. class 6’ categorization discussed above. This mutant retained a normal growth rate during an extended pre-division delay. During the delay, the *cdka-1* mutant did not display any of the above-mentioned indicators of cell cycle initiation (see chapter 5). We conclude that one function of CDKA is to bridge the transition, early in the cell cycle, from growth in a G1-like state to cell-cycle entry.

Control of DNA replication and the possible absence of a spindle assembly checkpoint

The large majority of mutants exhibited either a near-complete failure to initiate DNA replication or, alternatively, exhibited repeated re-initiation of DNA replication with approximately normal timing. This re-replication phenotype resulted in a FACS profile that was similar to wild-type S/M-phase cells, with distinct peaks indicating that DNA replication was carried out in discrete rounds. The positions of the peaks was generally close to the values observed in wild-type cells with 2C, 4C and 8C DNA content, and the troughs between peaks very low, suggesting that these mutants had undergone several complete rounds of DNA replication at restrictive temperature interspersed with periods without replication (rather than random re-initiation/continuous over-replication). The FACS profiles differed from wild type in that the higher-ploidy peaks accumulated to high levels, presumably because rapid cell division and hatching in wild type, but not in the mutants, depleted the higher ploidy peaks to produce newborn single G1 cells.

Examination by fluorescence microscopy of three of the re-replicating mutants (*tfc-e*, *tfc-b*, *gcp2*) showed only a single nucleus, and a complete absence of mitotic spindles, indicating that re-initiation of DNA was not intrinsically dependent upon spindle formation or successful nuclear division (Figure 4.2; 4.3; 4.4). This observation was surprising, because opisthokonts have a well-characterized spindle assembly checkpoint (SAC) system, operating in mitosis, that actively monitors the alignment of chromosomes on the mitotic spindle (Lara-Gonzalez et al., 2012). The SAC ensures that all

chromosomes have been correctly bi-oriented before the onset of anaphase. This systems works primarily through unattached kinetochores, which generate a signal that inactivates the APC, and therefore prevents the onset of anaphase. While the checkpoint is active, mitotic cyclins are stabilized. This prevents re-licensing of replication origins (by mechanisms described in the introduction) and since re-licensing is generally required for each new round of DNA replication, cells that arrest with an active SAC do not re-replicate DNA. Disruption of microtubule function (e.g. by nocodazole treatment) is a reliable way to prevent formation of the mitotic spindle and generate a SAC-dependent cell-cycle arrest in yeast and somatic animal cells. Our observation that spindles failed to form, but re-replication occurred, with approximately normal timing, suggested that, in contrast, *Chlamydomonas* might not have a strong spindle assembly checkpoint. *Chlamydomonas* does, however, possess clear homologues of most SAC genes (Lara-Gonzalez et al., 2012), including Mad1, Mad2, Mad3, Bub1, Bub3 and Mps1. It is unclear what the function of these genes is in *Chlamydomonas*. One possibility is that the spindle checkpoint functions in meiosis, but not during the rapid S/M phases of the mitotic cycle. It is also possible that the spindle checkpoint is able to provide a short delay in anaphase, but not to prevent it for an extended period of time. In a normal cell cycle this might be sufficient to guarantee accurate chromosome segregation. Our assays would not detect very subtle defects in the timing of re-replication cycles. Another possibility is that the spindle checkpoint in *Chlamydomonas* requires some rudimentary spindle as a signaling component. Interestingly, treatment of *Arabidopsis* shoot apical meristems (a region

containing mitotically dividing cells) with the microtubule inhibitor, oryzalin, prevented cell division but led to accumulation of nuclei with increased DNA content (Grandjean et al., 2004).

It interesting to considered the similarities between the S/M phase of *Chlamydomonas*, and the rapid cell divisions of the early frog embryo. Both are essentially repeated cycles of S phase and mitosis, without much intervening growth, that reduce one large cell to many smaller cells. In *Xenopus* embryos, these cycles occur essentially without checkpoint controls; treatment with drugs that inhibit microtubule function was shown not to prevent the following S phase (Kimelman et al., 1987), similar to disruption of microtubules in *Chlamydomonas*. The successive divisions during S/M phase appear synchronous. That is, the daughters of the first division divide again almost at the same time in the second division, and so on. One speculation is that *Chlamydomonas* has evolved a system that acts globally within the dividing mother cells, such that divisions occur at the same time. Such a system might be incompatible with a strong mitotic checkpoint, and might only allow a short window of time for checkpoint action.

CDKB/DIV48 and BSL1/DIV44 act specifically at the G2/M transition

Replication of DNA only once, followed by arrest with an undivided nucleus, was a rare phenotype among the mitotic mutants. Interestingly, this behavior was observed in *div48-1*, carrying a mutation in the plant-specific B-type CDK of *Chlamydomonas*. The B-type

CDKs make up a family of cyclin-dependent kinases only found in the *Viridiplantae* (Joubès et al., 2000). *Arabidopsis* has four closely related CDKBs. These kinases have been implicated as a positive regulators of mitosis, based on overexpression studies (see Introduction), but an essential role for CDKB activity in plants has never been demonstrated. Our results strongly support a mitosis-specific function for CDKB in *Chlamydomonas.*

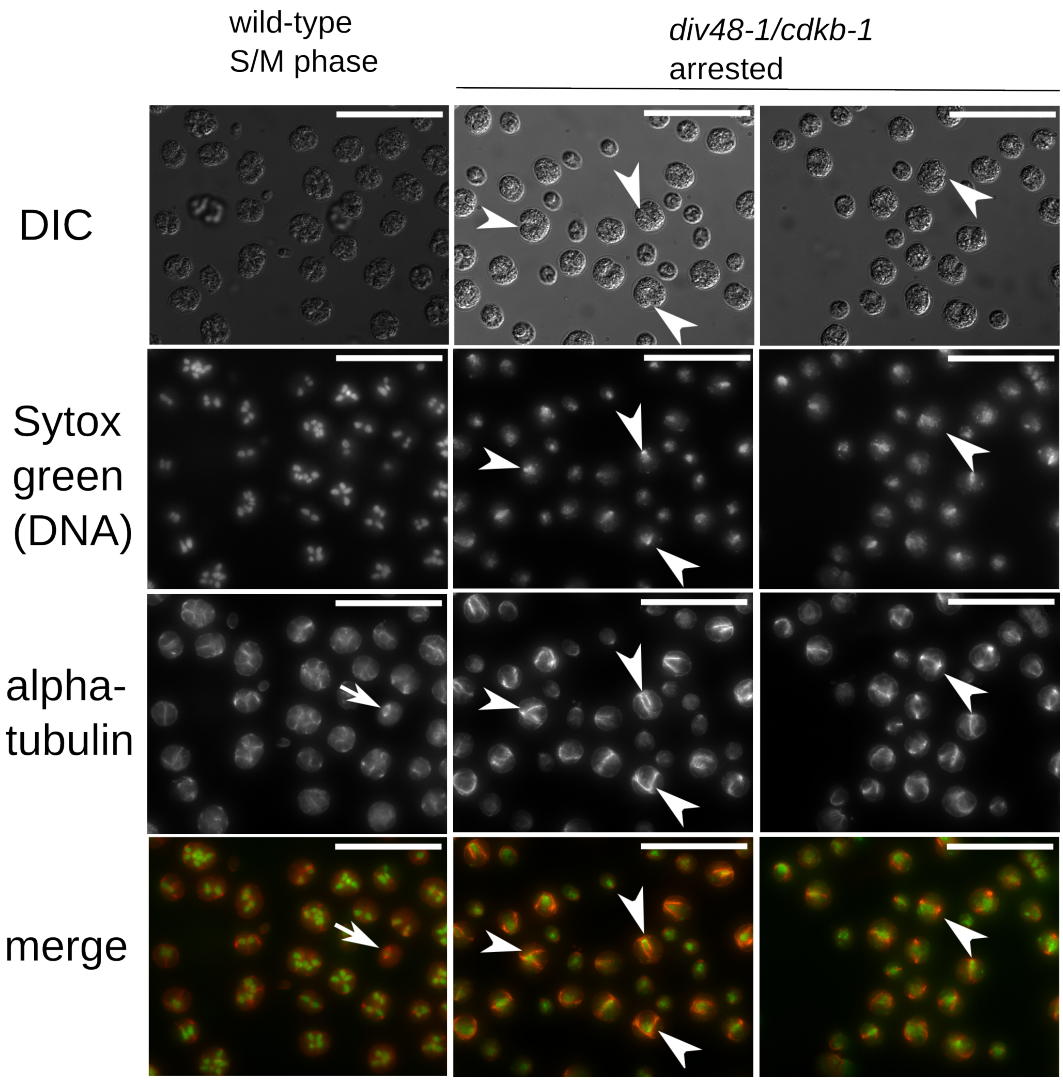

Figure 4.7: Distribution of DNA and tubulin in arrested *div48/cdkb-1* cells

Wild type: progression through the S/M phase is indicated by formation of microclusters containing daughter cells (DIC) with clearly separated nuclei (Sytox green). Metaphase spindles were rare (<5% of cells, white arrow). *cdkb-1*: Notch morphology developed in ~50% of cells (DIC, white arrowheads). Nuclei remained undivided and diffuse compared to wild type. Development of the notch morphology was accompanied by a striking reorganization of tubulin distribution into bright staining bands, which was distinct from wild-type mitotic spindles. Scale bar: 50 um

In opisthokonts, mitotic entry is controlled by Cdk1 (Nurse, 1990). The closest relative, by sequence similarity, of Cdk1 in plants is CDKA. Therefore, our results suggest that control over mitosis in *Chlamydomonas* has shifted to CDKB. To what extent this is true for *Viridiplantae* in general remains to be determined, since complete inactivation of B-type CDK activity has not yet been achieved in a plant system. The phenotype of *cdkb-1* will be discussed more in the next chapter.

The other mutant arresting with once-replicated DNA and an undivided nucleus was *div44-1*/bsl1. BSL1 belongs to a family of Kelch-domain containing phosphatases found in green plants and alveolates, but are missing from yeast and animal genomes (Guttery et al., 2012). The founding member of this family, BSU1 (bri1 suppressor), was identified in *Arabidopsis* as a positive regulator of the brassinosteroid (BR) signaling pathway, which plays an important role in regulating plant growth (Mora-Garcia et al., 2004). The BR pathway begins with reception of the brassinolide steroid signal at the cell surface by the BRI1 receptor kinase. In response, BSU1 is thought to dephosphorylate the kinase BIN2, which leads to activation of downstream gene expression (Kim and Wang, 2010). In *Arabidopsis*, the BSU1-family consists of BSU1 and three BSU1-like proteins (BSL1,2,3). Interestingly, it was recently suggested that the brassinosteroid signaling role of BSU1 might represent an evolutionary innovation in the *Brassicaceae*, and that the other members of this gene family might play BR-unrelated roles. This conclusion was based on the observed rapid evolution of the BSU1 gene in *Arabidopsis*, and a largely unaffected BR response in mutant plants lacking much of the normal BSL function, and

lethality of a BSL1,2,3 triple knockout (Maselli et al., 2014). In rice, an Asp -> Glu mutation in a conserved residue in a Kelch motif of the BSL1 homologue Os03g44500, was identified by analyzing QTLs affecting grain length (Zhang et al., 2012) (Qi et al., 2012). Notably, the amino acid associated with the grain length QTL is conserved in *Chlamydomonas.*

The BSL1 gene in *Chlamydomonas* clusters with BSL1,2,3 from *Arabidopsis*, rather than with BSU1. The causative mutation in *div44-1* changes a leucine to a proline (L46P in the *Chlamydomonas* protein) within the first Kelch motif in the N-terminal part of the protein (Adams et al., 2000). The mutated leucine is conserved in DIV44/BSL1 homologues from rice and *Arabidopsis*, and the region containing the mutation is conserved through *Viridiplantae* (Figure 4.8). Our results strongly suggest a role for DIV44/BSL1 in promoting mitosis in *Chlamydomonas*, and it will be interesting to test this idea for the BSL family in higher plants (Maselli et al., 2014).

As mentioned above, the BR signaling pathway involves several components, among them a protein kinase called BIN2 (GSK2 homolog). BIN2 is the likely direct target of inactivation by BSU in *Arabidopsis*, and *Chlamydomonas* has a clear homologue of BIN2. However, *Chlamydomonas* apparently lacks all upstream (e.g. BRI1 receptor) or downstream (e.g. BZR1 transcription factor) components of the BR signaling pathway. An interesting speculation is that the ancestral function of BSL (and BIN2) in *Viridiplantae* was in cell cycle control, and that a role in BR signaling represents subfunctionalization following gene duplications in the land plant lineage.

Yeast and animal (opisthokont) genomes lack BSL homologues, suggesting either that BSLs arose early in the *Viridiplantae* lineage, or was lost early in the opisthokont lineage. Perhaps consistent with the latter idea, BSL homologues are found in alveolates (Dorrell et al., 2013); one such homolog in the apicomplexan parasite *Plasmodium berghei* is important for sexual development (Guttery et al., 2012) (Philip et al., 2012). The divergence of alveloates relative to opisthokonts and *Viridiplantae* remains unclear, however.

Phosphatases are known to play central roles in cell cycle regulation. In fission yeast, the Cdc25 phosphatase was identified as an essential activator of mitosis, necessary for removing inhibitory phosphates on Cdc2 (Gould and Nurse, 1989) (Moreno et al., 1989). Cdc25 also plays an important role in animal cell cycle control, but a clear Cdc25 homologue has so far not been identified in plants, including *Chlamydomonas*. In fact, cell-cycle progression in *Arabidopsis* was unaffected by mutation of Thr-14 and Tyr-15 in CDKA, the residues normally at the center of regulation by Cdc25 and Wee1 (Dissmeyer et al., 2009). The consequences of inactivating phosphoregulation of B-type CDKs in *Arabidopsis in vivo*, however, remain largely unexplored. In the green alga *Ostreococcus (*Derelle et al., 2006), phosphorylated tyrosine in CKDB was detected, but the correlation with enzyme activity against histone H1 seemed poor (Corellou et al., 2005).

Cdc25 positively promotes mitosis by CDK activation; other phosphatases may antagonize mitotic entry, or promote mitotic exit, by reversing CDK phosphorylation of diverse targets (e.g. PP2A: Lorca and Castro, 2013, Cdc14: Stegmeier and Amon, 2004).

Other phosphatases regulate mitosis by dephosphorylating targets of mitotic kinases other than CDK (e.g., PP1 and AurB or Mps1 (Lesage et al., 2011)).

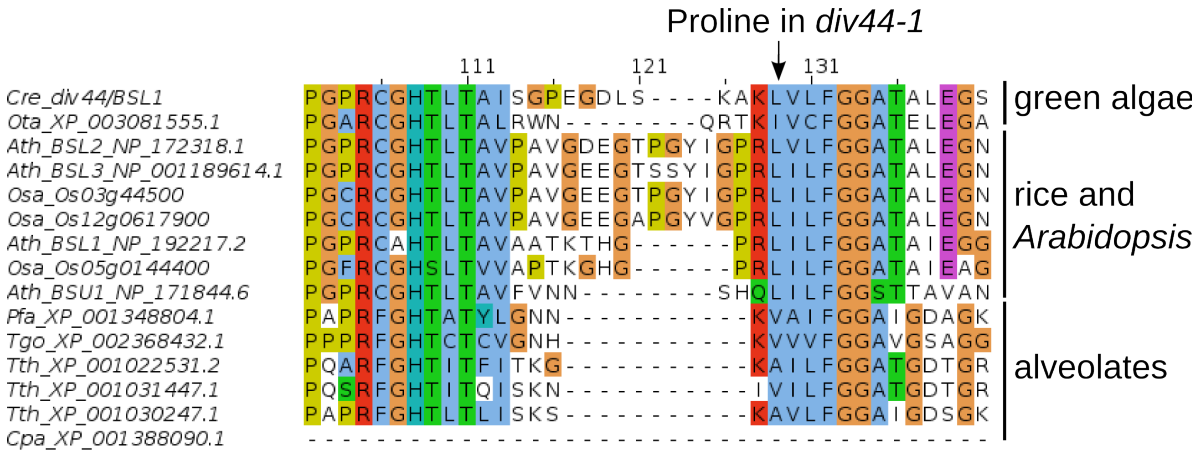

Figure 4.8: The causative mutation in div44-1/BSL1 targets a conserved residue in plant and alveolate BSL1 homologues.
The *Chlamydomonas* DIV44/BSL1 protein sequence was used in a BLAST search against the NCBI database to identify similar sequences in *Ostreococcus tauri (*Ota), *Arabidopsis thaliana* (Ath), *Oryza sativa* (Osa), *Tetrahymena thermophila* (Tth), *Plasmodium falciparum (*Pfa), *Plasmodium berghei* (Pbe), *Toxoplasma gondii* (Tgo) and *Cryptosporidium parvum* (Cpa). Proteins from all organisms aligned end-to-end, except Cpa. The location of the Leu-to-Pro mutation in *div44-1*, within the first Kelch domain, is indicated. The di-glycine is a characteristic feature of the Kelch-domain (Adams et al., 2000).

DUO3 and MPS1 act at late stages in mitotic progression

The *div39-1*/*duo3* and *div34-1/mps1* mutants exhibited re-replication of DNA to varying extents, with DNA segregated into clearly separated nuclei (Figures 4.3 A and 4.9), suggesting a block late in mitosis. MPS1 is a conserved protein with multiple functions. MPS1 is involved in spindle pole body duplication (Winey et al., 1991), in bi-orientation of chromosomes (Maure et al., 2007) and the spindle checkpoint (Winey and Huneycutt, 2002). We have not analyzed the behavior of the basal bodies in *Chlamydomonas mps1* mutants, or looked at spindle morphology. However, the fact that DNA segregated to some degree in *div34-1* at restrictive temperature suggests that spindle function is not completely eliminated (Figure 4.9).

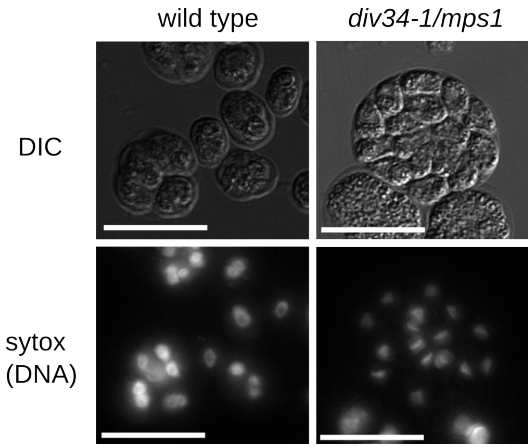

Figure 4.9: *DIV34/MPS1* is required late during S/M phase.
Sytox green staining of DNA in wild type and *div34-1/mps1*. *div34-1* re-replicated DNA at restrictive temperature as determined separately by FACS. Microscopic analysis suggested progression of the cytokinetic program, as determined by cell morphology, and formation of daughter-cell-like bodies (DIC, top). DNA distribution appeared roughly equal into each daughter-cell-like body (Sytox, DNA). Scale bar: 25 um

DUO3, a homeobox containing protein, was identified in *Arabidopsis* as required for sperm cell division during male gametophyte development. The name "duo" refers to the fact that pollen lacking DUO3 failed to undergo the second sperm cell division, leading to a mutant phenotype with only two nuclei in the pollen (one generative and one sperm nucleus). The molecular function of DUO3 in *Arabidopsis* is unclear, but it was proposed that the mitotic defects were not caused by failure to express CYCB1;1, since a CYCB1;1 reporter behaved similarly in wild-type and duo3 mutant pollen (Brownfield et al., 2009). The *Chlamydomonas* mutant *div39-1* carries a missense mutation in the most likely homologue to DUO3, although the homology is restricted to a few segments. Importantly, however, the causative mutation in *div39-1* (confirmed by isolation of a pseudo-revertant that restored viability) changes a conserved residue in one of these segments of homology. In *Chlamydomonas*, the *div39-1* mutant arrests with re-replicated DNA and divided nuclei. Microtubule staining revealed apparently morphologically normal mitotic spindles and cortical microtubules. Taken together, *div39-1* seems to be able to carry out many of the events associated with mitotic progression, although cell division was ultimately completely blocked. It will be interesting to explore the reason for the cell cycle arrest in *div39-1* further, and to determine to what extent the functions of *Chlamydomonas DIV39* and *Arabidopsis* DUO3 are conserved.

Summary

Taken together, cell-cycle analysis of many *div* mutants strengthened the initial distinction

between G1-arresting mutants (class 5) and the mitotic mutants (class 6). The defects in G1 (class 5) mutants resulted in slower cell growth and failure to exhibit any sign of cell cycle initiation (DNA replication, cytokinetic initiation, activation of Cks1-precipitable kinase), while the defects in class 6 mutants resulted in cell-cycle initiation with failure of specific aspects.

The *cdka-1* mutant is the only mutant that failed to fit in this scheme; its phenotype of absence of any signs of cell cycle initiation, combined with wild-type cell growth, suggests that CDKA functions at the border between cell growth and cell-cycle initiation.

The mitotic mutants either failed DNA replication and nuclear division, or displayed some degree of re-initiation of replication, assuming a FACS profile resembling wild type S/M-phase cells. Interestingly, in several mutants, repeated re-initiation of DNA replication continued independently of spindle formation and nuclear division. This result was surprising in the context of mitotic checkpoints that, in many cells, impose a dependency of S phase on completion of the previous mitosis. The phenotypes of *div48-1/cdkb-1* and *div44-1*/*bsl1* indicated a critical role for the CDKB and BSL1 proteins early in the G2/M transition.

Because the phenotypic analysis suggested central roles for CDKA and CDKB at different points in the cell division cycle, and because of the centrality of CDK control in opisthokont cell cycle control, we carried out a more detailed analysis of CDKA and CDKB function, described in the next chapter.

Chapter 5 CDK function in *Chlamydomonas* cell cycle control

ts mutations in *CDKA* and *CDKB*

All plants, including *Chlamydomonas*, contain both A and B-type CDKs. A-type CDK is most closely related to yeast and animal Cdc2/Cdk1, whereas B-type CDKs constitute a plant-specific family of kinases, that probably arose from *CDK* gene duplication early during evolution of the plant lineage. As for many other cell-cycle genes, *Chlamydomonas* has only a single A and B-type CKD (Bisova et al., 2005). Both A and B-type CDKs play important roles in plant cell-cycle control (De Veylder et al., 2007). A recent study contributed important insights to our understanding of CDK function in the *Arabidopsis* cell cycle, by constructing plants completely lacking CDKA (Nowack et al., 2012). Nevertheless, the current understanding of the role of CDKs in plant cell-cycle control remains far less advanced, compared to opisthokonts. The *cdka-1* and *cdkb-1* mutants isolated through this screen provide a good starting point for exploring CDK function in the green lineage in a simplified microbial setting.

As mentioned earlier, only a single *div* mutant resisted classification as either G1-arresting (class 5) or mitotic (class 6). This mutant, ts301, grew to well above division size on agar, without initiating the catastrophic division "attempts" seen in the mitotic mutants, and with substantially delayed cell lysis. The ts301 mutant was also exceptional in that two mutations were required for inheritance of the *div* phenotype: a STOP mutation early in the coding sequence of MED6 (a component of the Mediator basal

transcription machinery), and a missense mutation in *CDKA*, the *Chlamydomonas* homologue of Cdk1/Cdc2. The *CDKA* mutation (hereafter *cdka-1*) changed a Phe to a Cys in the DFG motif at the catalytic core of the enzyme (Figure 5.1). The DFG motif is universally conserved within eukaryotic protein kinases, and plays critical roles in coordinating the active state of the enzyme. The mutated phenylalanine, in particular, was proposed to be part of a hydrophobic "spine" that connects the C and N lobes of the protein (Kornev et al., 2006).

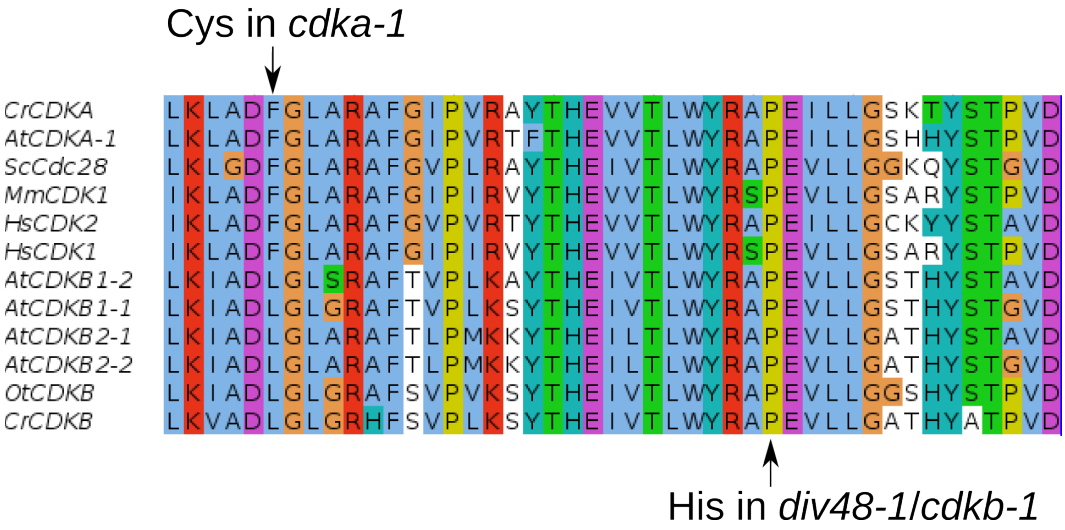

Figure 5.1: Sequence alignment of CDKA and CDKB from *Chlamydomonas* to homologous proteins from *Arabidopsis* and opisthokonts

Alignment of CDKA and CDKB protein sequences from *Chlamydomonas*, to homologous proteins from *Arabidopsis thaliana* (At), *Ostreococcus tauri* (Ot) and *Saccharomyces cerevisiae* (Sc), *Homo sapiens* (Hs) and *Mus musculus* (Mm). The causative mutations in *cdka-1* and *div48-1/cdkb-1* are indicated by black arrows.

Individually, both single mutants were viable at restrictive temperature, but exhibited distinct phenotypes, as observed by time-lapse microscopy (Figure 5.2). The mutant carrying the *med6-1* allele largely initiated division on time, but displayed a somewhat increased frequency of division failure and altered cell morphology. The *cdka-1* mutant, however, went through a normal division, but showed a prolonged pre-division delay. This delayed the onset of division by almost 10 hours relative to CDKA+/MED6+ cells. In the *cdka-1/med6-1* double mutant, this delay was converted into a tight cell cycle arrest as large undivided cells. An interesting speculation for this synthetic phenotype is that *cdka-1* cells are rescued from lethality by transcription of some Mediator-dependent genes.

The *div48-1/cdkb-1* mutant carried a Phe-to-His missense mutation in the highly conserved APE motif of the kinase (Figure 5.1) (Kornev et al., 2008). The *cdkb-1* mutant was indistinguishable from wild type at permissive temperature, but developed a characteristic "notch" phenotype after 10 hours of growth on agar at restrictive temperature, similar to many other mitotic *div* mutants, and underwent complete lysis within 20 hours (Figure 5.4). As was noted in the previous chapter, the *div48-1* mutant was nearly unique in our collection in completing only a single cycle of DNA replication, suggesting a specific role in the G2/M transition.

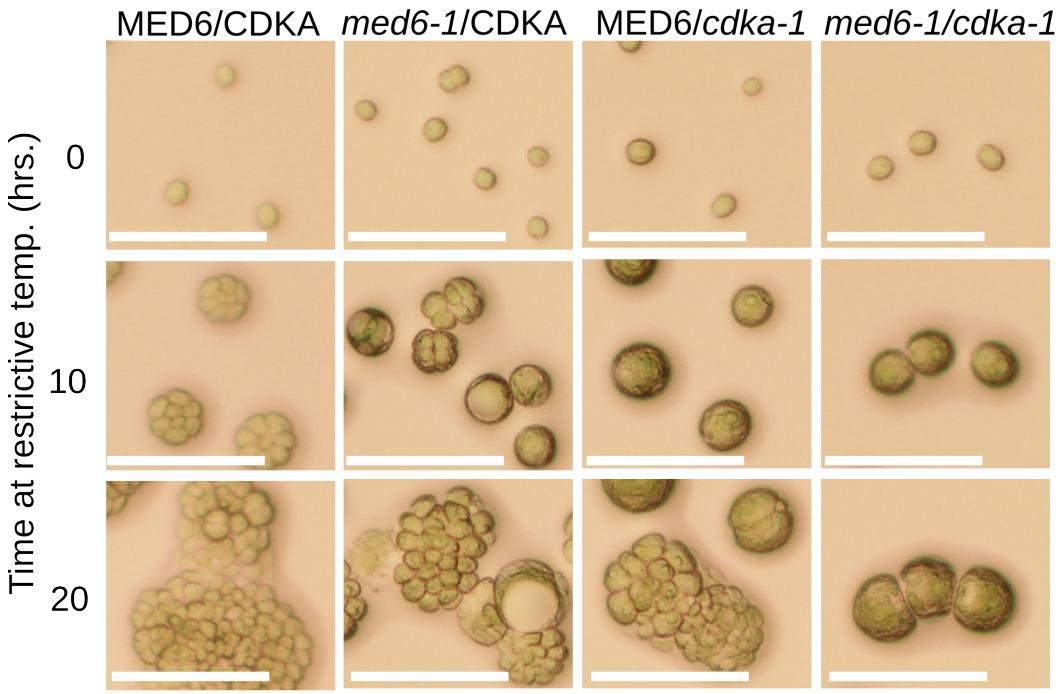

Figure 5.2: *cdka-1* is synthetically lethal with *med6-1*

The ts301 mutant (carrying the *med6-1* and *cdka-1* mutations) was crossed to wild type, and four segregants from one tetratype tetrad were analyzed by time-lapse microscopy at restrictive temperature. MED6/CDKA behaved like wild type: division initiated around 10 hours and the cells then continued to divide. The *med6-1* single mutant initiated division with approximately normal timing (around 10 hours), but displayed various morphological defects, and an increased rate of division failure. The *cdka-1* single mutant displayed a significant pre-division delay, and many cells remained undivided until the 20-hour time point. When cell division occurred in *cdka-1*, it appeared normal. The *med6-1/cdka-1* double mutant became completely arrested with a pre-division morphology. Scale bar: 50 um.

CDK function in *Chlamydomonas* cell cycle control

To further explore the functional relationship between CDKA and CDKB during the *Chlamydomonas* cell cycle, we assayed DNA replication, Cks1-precipitable kinase activity and cell morphology in parallel cultures of wild-type, *cdka-1*, *cdkb-1* and the double mutant *cdka-1*/*cdkb-1*, through a detailed time-course.

It is likely, but still unproven, that the Cks1 affinity reagent binds both CDKA and CDKB in *Chlamydomonas*, and that both CDKA and CDKB contribute to H1 phosphorylation in our assay. In *Arabidopsis* and *Ostreococcus tauri*, recombinant Cks1 protein pulled down both CDKA and CDKB (De Veylder et al., 1997)(Corellou et al., 2005). In *Ostreococcus*, differential affinity of CDKA and CDKB towards human Cks1 was used to deplete extracts of CDKA. After depletion of CDKA, CDKB could be pulled down using *Ostreococcus* Cks1, and this CDKB-containing fraction could phosphorylate histone H1 (Corellou et al., 2005).

In our time-course protocol, wild-type cells started as a uniformly small population with 1C DNA content and negligible Cks1-precipitable kinase activity (Figure 5.3: A, B, C). During the first 10 hours, wild-type cells grew in size, from about 180 to 400 femtoliters, without initiating DNA replication. This growth period was accompanied by low Cks1-precipitable kinase activity, which started to increase between 10 and 12 hours (Figure 5.3 C). Evidence of DNA replication was seen at 14 hours, accompanied by a peak in Cks1-precipitable kinase activity. By 16 hours, most wild-type cells had completed DNA replication and released daughter cells, as seen by the reappearance of

the predominantly 1C peak in the FACS profile and a sharp drop in median cell volume (Figure 5.3A). Consistent with exit from mitosis and re-entry into the G1 phase of the cell cycle, the Cks1-precipitable kinase activity at this point began to decrease. A micrograph of representative cells in the wild-type culture present at the 16 hour time point shows large pre-division cells, division clusters with 8-16 cells ready to hatch, and tiny newborn daughter cells (Figure 5.3 E).

The *cdka-1* mutant started with a larger median cell size compared to wild-type, probably reflecting an effect of the *cdka-1* mutation at permissive temperature, leading to a somewhat slowed progression through cell division in a subpopulation of *cdka-1* cells. Most *cdka-1* cells, however, had a 1C DNA content. The Cks1-precipitable kinase activity was also initially higher in *cdka-1* compared to wild type, consistent with the idea that some *cdka-1* cells had a delayed exit from the previous mitosis. After 3 hours at restrictive temperature, however, most *cdka-1* cells had released daughter cells, as indicated by a reduction in median cell size (Figure 5.3 A) and Cks1-precipitable kinase activity (Figure 5.3 C). Thus, *cdka-1* and wild-type cells had largely similar starting condition. Despite the similar starting points, initiation of DNA replication was not observed in *cdka-1* cells until the 27 hour time point, significantly delayed compared to wild-type (Figure 5.3B). Correspondingly, activation of Cks1-precipitable kinase activity was delayed by 6 hours. It is unclear how much of the defect in Cks1-precipitable kinase in the *cdka-1* mutant is due to direct defects in the mutant CDKA enzymatic activity, as compared to an indirect effect due to defective activation of CDKB in the *cdka-1* mutant.

However, the mutant form of CDKA showed reduced activity against histone H1 *in vitro* (pers. communication C. Atkins). Interestingly, the Cks1-precipitable kinase activity was only barely above background at the 27-hour time point, when *cdka-1* cells were undergoing DNA replication and cell division. Significant daughter cell release was delayed further, until the 37-hour time point (not shown), in *cdka-1* mutant cells. The newborn median cell size in *cdka-1*, however, was essentially normal, indicating that the size control mechanism normally operating during the S/M phase is not significantly affected by the *cdka-1* mutation.

The *cdkb-1* single mutant initiated DNA replication essentially on time, after 14 hours, and had almost completed one round of replication by 16 hours. This closely matched the kinetics of initiation of DNA replication observed in wild type. The *cdkb-1* mutant, however, arrested with once-replicated DNA, whereas wild type underwent several successive rounds of DNA replication during the S/M phase. This indicated that the CDKB enzyme is largely dispensable for S phase, but carries out some essential function in mitosis and is also required for additional cycles of replication seen in the wild type multiple S/M cycles. Moreover, activation of Cks1-precipitable kinase activity occurred with wild-type timing, but strikingly, activity did not decline as in wild type, instead remaining at a high level for many hours. If *cdkb-1* is catalytically inactive, the observed signal was likely due largely to CDKA. The sustained high kinase activity then, suggested that normally, CDKB is required to inactivate CDKA. Morphologically, *cdkb-1* cells developed the characteristic notch seen in many mitotic *div* mutants (Figure 5.3 E).

The absence of mitotic spindles, and nuclei that remained undivided in arrested *cdkb-1* cells was shown in chapter 4 (Figure 4.7: compare white arrows: wild-type spindles, to white arrowheads: tubulin staining in *cdkb*-1).

The *cdka-1/cdkb-1* double mutant completely failed to activate Cks1-precipitable kinase activity throughout the time course. Morphologically, the double mutant looked identical to the *cdka-1* single mutant. However, whereas the *cdka-1* single mutant eventually entered the S/M phase after 27 hours, the double mutant was terminally arrested as large undivided cells (Figure 5.3 E; 5.4 bottom row). It is possible that the small 2C peak, appearing at 27 hours (Figure 5.3 B), represents slow initiation of DNA replication in the double mutant. This behavior seems consistent with a strong effect on the onset of DNA replication mediated by the *cdka-1* mutation, and a *cdkb-1* dependent block at the 2C stage.

Taken together, these results are consistent with enzymatic activation of CDKA early in the cell cycle, leading to DNA replication and, possibly, to activation of CDKB. CDKB is required for later mitotic events, starting with the first cell division after the first round of DNA replication.

Figure 5.3: CDK function in *Chlamydomonas*

Wild type grown in parallel with *cdka-1*, *cdkb-1* and *cdka-1/cdkb-1* double mutants in liquid cultures, shifted to restrictive temperature at t=0. (**A)** Determination of cell growth (top) and cell density (bottom) by Coulter counter. Near-identical cell growth rates were observed in all strains during the first 14 hours. Wild-type cells go through S/M phase and release daughter cells between 14-16 hours as seen by a sharp drop in median cell volume and a corresponding increase in cell density. All three mutants are blocked in cell division, but largely unaffected for cell growth. **(B)** DNA by FACS. A 16C peak emerging at 14 hours indicates DNA replication in wild type. This peak represents cells undergoing multiple S/M cycles, before daughter cell release. Daughter cell release is accompanied by re-appearance of a sharp 1C peak at 16 hours. *cdka-1* cells do not replicate DNA during the 16-hour growth period, but ultimately initiate replication after 27 hours (16C peak). *cdkb-1* cells initiate DNA replication on schedule and arrest uniformly with 2C DNA content. Double mutants are completely blocked for DNA replication, but display a population of >2C cells at time=0. **(C)** Cks1-precipitable kinase activity in whole cell lysates. Activation of H1-kinase in wild type starts at 10 hours and peaks at 14 hours. A drop in kinase activity accompanies exit from the S/M phase and release of daughter cells (16-27 hours). *cdka-1* cells are significantly delayed in kinase activation, whereas *cdkb-1* cells activate kinase activity with wild-type timing to high levels that are sustained throughout the time course. The *cdka-1/cdkb-1* double mutant has negligible kinase activity throughout the time course. The activity observed at t=0 probably represents cells that are slow to exit the previous S/M phase. **(D)** Quantification of kinase activity by storage phosphor (Methods). **(E)** Representative phase images of wild-type and mutant cells at the 16-hour time point. *Wild-type*: large pre-division cells, dividing pre-hatching cells and small newborn G1-cells. *cdka-1* and *cdka-1/cdkb-1* double mutant cells are uniformly big and round at this time, whereas *cdkb-1* cells have developed a uniform notch-morphology suggesting initiation of the cytokinetic program (white arrowheads). Scale bar: 50 μm

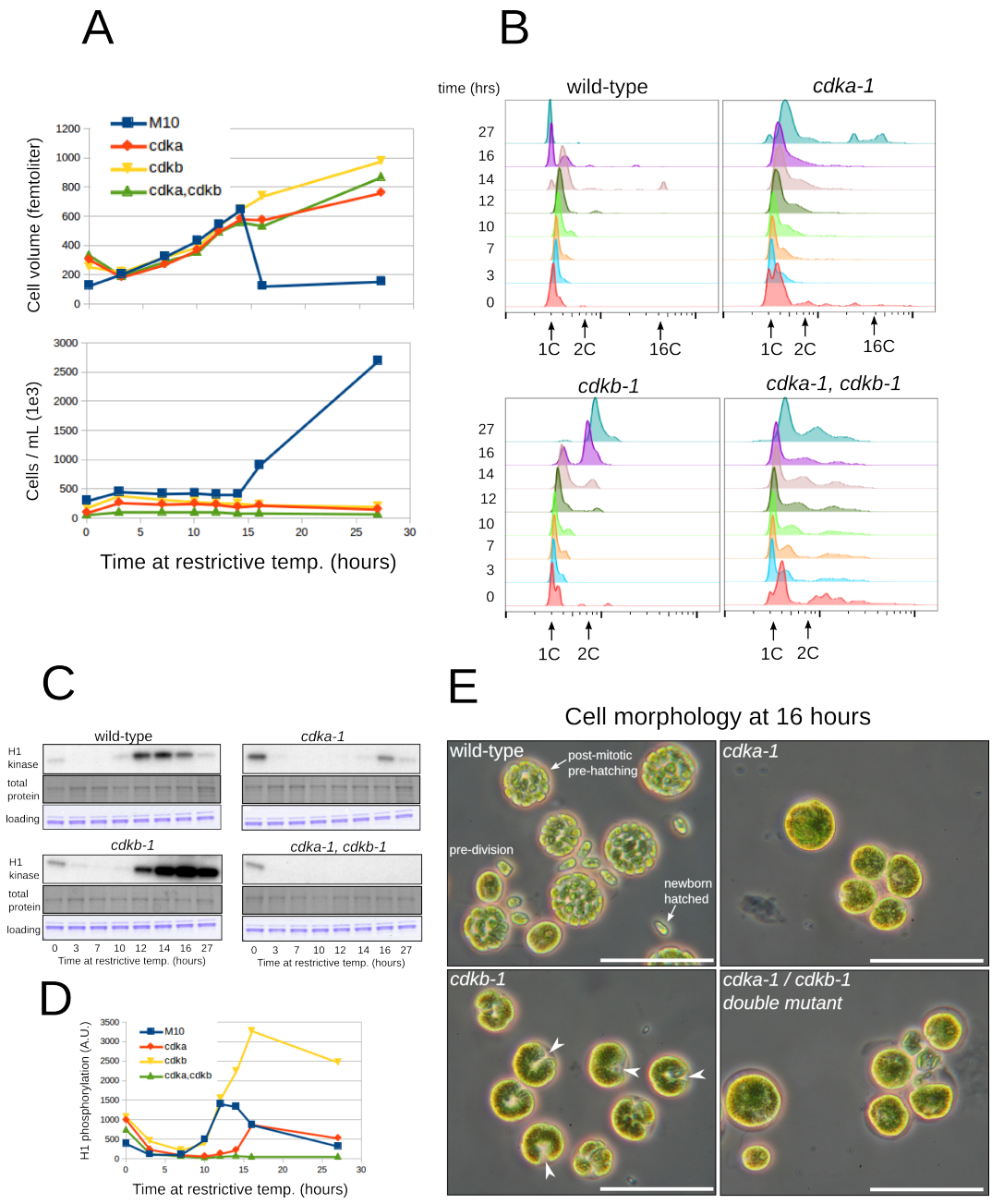

Figure 5.3: CDK function in *Chlamydomonas*

Epistasis between *cdka-1* and various *div* mutants support partial separation of function between CDKA and CDKB

The initial phenotypic characterization of the *cdka-1* mutant, as well as the time course comparing *cdka-1* and *cdkb-1* mutant behavior, suggested a role for CDKA early in the cell cycle. Epistasis experiments between *cdka-1* and a variety of *div* mutants help substantiate this finding. We know that many mitotic *div* mutants carry mutations in genes predicted based on sequence homology to be required in S phase or mitosis, e.g. *div17*/*rnr2, div13/DNApol alpha*, *div19-1*/*TopoII* and *div21-1*/*TopBP1* (Table 3.2). When grown at restrictive temperature on agar, mitotic *div* mutants generally displayed a characteristic phenotype after 10 hours, followed within 20 hours by complete cell lysis. *cdka-1*, on the other hand, does not start dividing until the 20-hour time point, after a prolonged pre-division delay. If expression of the mitotic *div* phenotype were dependent on CDKA function, then inactivating CDKA, in the *div* background, would delay expression of the *div* phenotype and preserve cell viability. Indeed, when assayed in a *cdka-1* background, the phenotype of all mitotic *div* mutants tested, including *div17-1/rnr2*, was suppressed until approximately 20 hours, the time when *cdka-1* normally initiates division (Figure 5.4). This indicated not only that normal cell cycle progression is dependent on CDKA function, but also that the aberrant cytokinesis-like events in *div17-1*/*rnr2*, as well as other mitotic *div* mutants tested, depend on an upstream CDKA-dependent step. In contrast, all class 6 G1-arresting *div* mutants tested were completely epistatic morphologically to *cdka-1*.

The observation that cells doubly mutant for *cdka-1* and any of a number of mitotic *div* mutations showed a delay of mitotic progression (as measured by incipient cytokinetic structures and subsequent cell lysis), but ultimately manifested the mitotic *div* phenotype, is likely a natural correlate of the observation that *cdka-1* single mutants are delayed, but not indefinitely blocked, for normal mitosis. There was one clear exception: the *cdka-1/ cdkb-1* double mutant showed a synthetic phenotype of complete cell cycle arrest as large undivided cells (Figure 5.4, bottom row). This finding showed that mitotic initiation (and probably a first round of replication initiation) in the *cdkb-1* mutant is dependent on CDKA, while in the *cdka-1* mutant, DNA replication, mitotic initiation and completion are dependent on CDKB. Thus despite their evident differentiation, CDKA and CDKB must have significant potential overlap in function. Interestingly, the CDKB gene is transcriptionally regulated, with two peaks of mRNA accumulation during the cell cycle: one in mitosis and one earlier, during the commitment step (Bisova et al., 2005), perhaps reflecting overlapping function of CDKA and CDKB early in the wild-type cell cycle.

Figure 5.4: Epistasis between *cdka-1* and two mitotic *div* mutants: *div17-1/rnr* and *div48-1/cdkb-1*

The mitotic *div* mutants *div17-1/rnr* and *div48-1/cdkb-1*, in wild-type background, and in *cdka-1* mutant background, were imaged at restrictive temperature by time lapse. Wild-type control cells initiated division at 10 hours (top row). The *cdka-1* single mutant displayed the pre-division delay described in the text. The *div17-1* single mutant developed a notch morphology at 10 hours (white arrowheads), which was suppressed until the 20-hour time point in the *div17-1/cdka-1* double mutant. The *cdkb-1* single mutant also developed notch morphology around 10 hours (white arrowheads). The single mutants, *div17-1* and *div48-1/cdkb-1*, as well as the *div17-1/cdka-1* double mutant eventually initiated catastrophic division events and lysed completely (20 and 30 hour time points). In contrast, the *cdka-1/cdkb-1* double mutant became blocked with a pre-division morphology (black arrow, bottom row).

Scale bar: 50 um

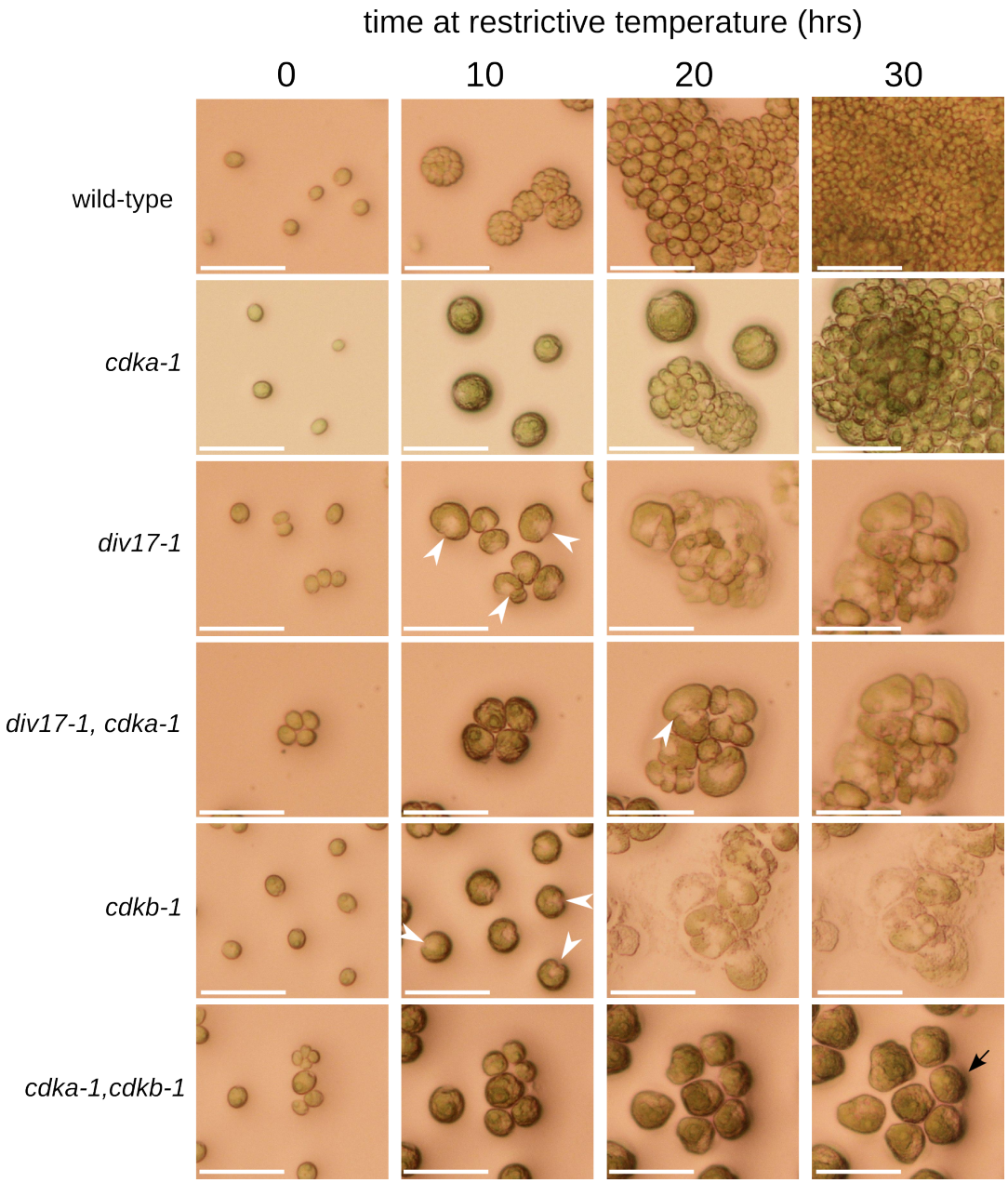

Figure 5.4: Epistasis between *cdka-1* and two mitotic *div* mutants: *div17-1/rnr* and *div48-1/cdkb-1*

Discussion

The functional separation between A- and B-type CDKs in the plant cell cycle is not clear. One reason for this is that, so far, loss-of-function alleles in all four CDKBs in *Arabidopsis* have been unavailable. The temperature sensitive alleles of CDKA and CDKB in *Chlamydomonas* provide a starting point for analyzing the functional relationship between these two kinases in plant cell cycle control.

Our results demonstrate an essential role for CDKB specifically in promoting mitosis, while being completely dispensable for execution of the early cell cycle events we assayed: activation of Cks1-precipitable kinase activity and initiation of DNA replication. An arrest before mitosis was based on the fact that *cdkb-1* mutant cells did not form mitotic spindles and did not divide nuclei, two events associated with progression through mitosis (discussed in chapter 4). *cdkb-1* mutants did, however, form apparent cytokinetic structures (the notch), suggesting an uncoupling of the mitotic and cytokinetic programs. The *cdka-1* mutant was delayed by more than 10 hours, compared to wild type, in cell cycle initiation, as determined by the timing of activation of Cks1-precipitable kinase activity and onset of DNA replication.

The Cks1-affinity reagent is thought to purify both A- and B-type CDKs, based on results in *Arabidopsis* (De Veylder et al., 1997), and both CDKA and CDKB have been shown to be able to phosphorylate histone H1. In these experiments, we interpret H1-phosphorylation as representing the bulk A- and B-type CDK activity in the cell. Although we cannot exclude contribution from other kinases, or determine the relative

contributions of CDKA and CDKB, the background level of kinase activity in the double mutant suggests that a significant part of H1 phosphorylation comes from some combination of CDKA and CDKB activities.

If the *cdkb-1* mutant kinase has severely reduced activity at restrictive temperature, then the initial rise in H1-phosphorylation in both wild type and the *cdkb-1* mutant is likely due to CDKA activity, since the rise is quantitatively comparable in the two strains (Figure 5.3 D). This activation precedes the first evidence of DNA replication by approximately two hours. Furthermore, the sustained high level of kinase activity in the *cdkb-1* mutant points to a role for CDKB in inactivating CDKA.

In the *cdka-1* mutant, Cks1-precipitable kinase activation is delayed by about 6 hours. If CDKB normally contributes significantly to the rise in H1 phosphorylation during wild type S/M phase, this would suggest a role for CDKA in activation of CDKB. In *Arabidopsis*, activation of CDKB operates to a large extent through CDKA-dependent inactivation of RBR, a transcriptional repressor of many genes, including CDKB (Nowack et al., 2012). Transcriptome analysis of *Chlamydomonas* CDK mutants (see next Chapter) indicated delayed expression of some cyclins (likely CDKB activators) and of the CDKB gene itself in *cdka-1* cells. Preliminary experiments, however, did not reveal a strong effect of deletion of MAT3, the RBR homologue in *Chlamydomonas*, on the pre-division delay in *cdka-1* cells.

The epistasis experiments suggested that the separation of function between CDKA and CDKB is incomplete. With the exception of *cdkb-1*, all other strains doubly mutant

for *cdka-1* and a mitotic *div* mutant developed the *div* phenotype after a delay. This indicated that expression of the *div* phenotype was dependent upon some upstream step controlled by CDKA. In the *cdka-1*/*cdkb-1* double mutant, however, the pre-division delay was converted into a tight cell cycle arrest as large undivided cells. This suggested that the *cdka-1* mutants might be rescued from lethality by CDKB. Functional overlap between CDKA and CDKB was demonstrated in *Arabidopsis*, where ectopic expression of CDKB1;1 could rescue many of the developmental defects in a homozygous *cdka1-/-* mutant (Nowack et al., 2012).

Currently the analysis of *Chlamydomonas* CDK mutants is limited by our inability to detect CDKA and CDKB proteins independently. This must await development of tagged versions of these kinases, or specific antibodies. Transformation of *Chlamydomonas* is generally inefficient, but the strong positive selection provided by rescue from ts lethality of the *cdkb-1* mutant or the *cdka-1/med6-1* double mutant strains should facilitate generation of rescue-strains carrying tagged alleles. Tagged alleles would also facilitate proteomic studies of the composition of the CDKA and CDKB complexes.

Chapter 6 CDKA-dependent and CDKA-independent transcription in the *Chlamydomonas* cell cycle

Introduction

The cell cycle in *Chlamydomonas* is characterized by initiation of cell growth at the beginning of the light phase. A long G1 phase then follows, where the cell actively photosynthesizes and grows in size. This period of growth ends with the entry into the S/M phase, which normally probably coincides with nightfall, when the cell starts replicating DNA and distributing it between daughter cells through the "multiple fission" cell division cycle described in the introduction. When all divisions are completed, the daughter cells re-grow flagella, break down the old mother cell wall, and emerge as tiny newborn cells. This progression through the cell cycle is likely accompanied by time-dependent changes in gene expression, reflecting changing cellular need for different proteins. Some of these changes in gene expression might be directly controlled by the cell-cycle machinery. Others might depend on the metabolic status of the cell (Fukuzawa et al., 2001), on light and temperature conditions, or on the circadian clock (Matsuo and Ishiura, 2010).

Cell-cycle-regulated transcription has not been studied in detail in *Chlamydomonas*, although there are specific examples of transcripts that vary in abundance through the wild-type cell cycle. These include a number of genes likely required for DNA replication, cell-cycle control (Bisova et al., 2005), as well as intraflagellar transport

(Wood et al., 2012), all of which showed an increase in mRNA abundance during the S/M phase.

In this chapter we present an initial analysis of transcriptomes obtained from wild-type cells, as well as the *cdka-1* and *cdkb-1* mutants, to begin to address the question of how gene expression depends on the cell cycle. The aim is to determine transcriptome changes through a single multiple fission cycle, and to determine which of these changes might be due to cell cycle progression/control.

A two-way connection between the cell cycle oscillator and transcription: examples from budding yeast

In budding yeast, distinct waves of gene expression are associated with the G1/S transition and with the entry into, and exit from, mitosis (Spellman et al., 1998). The G1/S-specific transcription includes many genes involved in early cell-cycle events, such as bud formation and DNA replication, whereas a number of genes needed in mitosis, including the mitotic cyclin Clb2 and the transcription factor Swi5, are expressed at the G2/M transition. As cells exit mitosis, a third set of genes, including the CDK inhibitor Sic1, and components of the pre-RC are transcribed. Expression of Sic1 helps maintain low CDK activity in G1, and the pre-RC components are required in G1 to load origins in preparation for the next S phase (Wittenberg and Reed, 2005).

The cell-cycle-stage specific gene transcription programs are tightly linked to CDK

activity. At the G1/S transition, Cln3-Cdc28 phosphorylates the transcriptional inhibitor Whi5, which relieves inhibition of the SBF transcription factor complex (de Bruin et al., 2004). This molecular event is critical to activation of the G1/S transcriptional program, and corresponds to the START transition, originally observed by Hartwell and colleagues as the entry point to the cell cycle (see Chapter 1, Introduction). Mitotic gene expression is also controlled by CDK activity. One important mechanism operates through phosphorylation of the protein Ndd1 (Reynolds et al., 2003b), which activates the forkhead transcription factors at specific promoters (Kumar et al., 2000).

As illustrated above, gene expression is tightly linked to and controlled by oscillations in CDK activity. In turn, the CDK oscillator depends on regulated expression of many genes, most notably the cyclins. Since the mitotic cyclins are degraded at the end of mitosis, entry into mitosis in the next cycle is critically dependent on new cyclin gene expression. Thus, rising and falling CDK activity is interdependent with regulated expression of cell-cycle genes (Haase and Wittenberg, 2014).

Wild-type transcriptome data clustered by the k-means algorithm

We sampled wild-type *Chlamydomonas* cells from three independent experiments (Figure 6.1). This generated 18 wild-type transcriptomes, which were ordered based on the time of sampling and normalized as described in the Methods section.

Multiple samples at the same time point represent true biological replicates, coming from synchronization experiments on different days. Analysis of correlations between

biological replicates indicated high reproducibility ($R^2 > 0.9$, Appendix A6). The wild-type transcriptomes were analyzed using the k-means cluster algorithm, as implemented in Matlab. The algorithm, as used here, treats each row (gene) as a vector (18-dimensional in this case) and clusters the vectors into a predefined number of clusters, k, based on Euclidean distance. The desired number of clusters is set by the user. By trying different values of k, we noticed that too few clusters ($k \sim 5$) failed to pick out small clusters of strongly regulated genes, and too many clusters ($k > 30$) resulted in many seemingly identical clusters without providing additional information. We settled for 20 clusters as a reasonable trade-off. This number of clusters is simply an arbitrary choice and does not reflect any prior knowledge about the structure of the data. Our reason for choosing k-means clustering for the data presented here was initially one of speed: the k-means algorithm is significantly faster for large data sets such as this one, compared to other commonly used clustering methods (Eisen et al., 1998). However, it is likely that re-examination of the data in the future, with additional methods, will be informative.

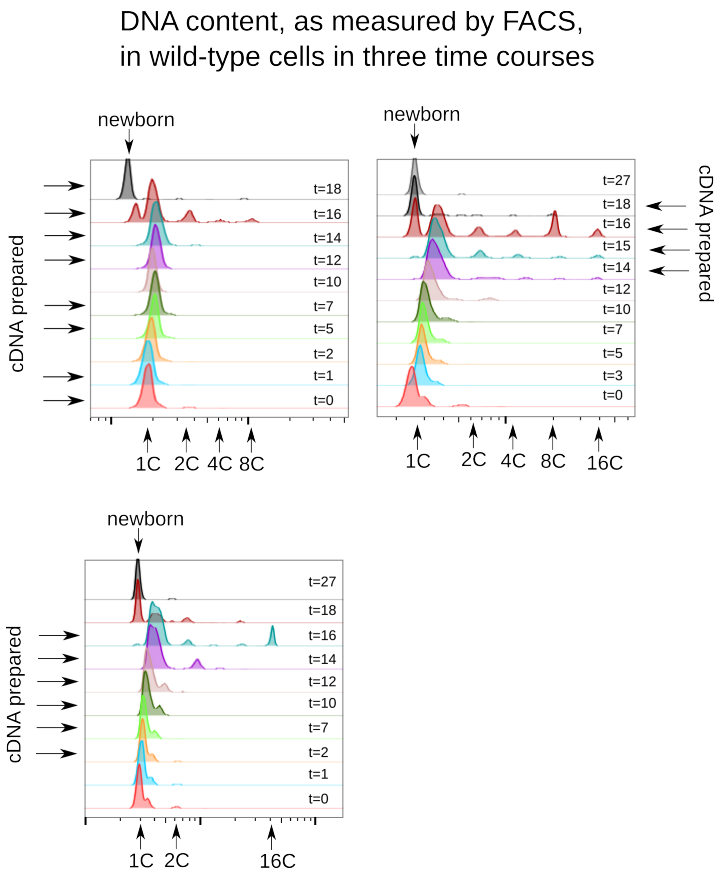

Figure 6.1: Wild-type cultures used for cDNA preparation

Wild-type cells were obtained from three independent cultures grown under similar conditions. DNA content was measured by FACS at several time points between 0 and 27 hours, following the shift to 33ºC. Samples were taken for RNA preparation at the indicated time points (black arrows). In all three cultures, cells spend the first 12 hours in G1, with a 1C DNA content. Between 14-16 hours, a significant proportion of cells go through the S/M phase, as shown by the appearance of FACS peaks corresponding to cells that have 2C of more DNA content. By 18 hours, almost all cells have completed the S/M phase and released newborn daughter cells. This is evident from the FACS plots as a return to a uniformly 1C DNA content (labeled 'newborn').

Figure 6.2: *cdk* mutant cultures sampled for cDNA preparation

cdk mutant cells were grown under the same conditions as in figure 6.1. DNA content was measured by FACS at several time points between 0 and 27 hours, following the shift to restrictive temperature. **(A-D)** Samples were taken for cDNA preparation at the indicated time points (black arrows). **(A)** The *cdkb-1* mutant replicated DNA between 16 and 18 hours. **(C-D)** In two time courses, *cdka-1* cells remained 1C for the duration of the experiment. The complicated appearance of the FACS profile at t=0h in C, is likely due to a partial cell-cycle defect in *cdka-1* cells at permissive temperature, leading to delayed completion of the previous S/M phase. **(B)** FACS profile of *cdka-1/cdkb-1* double mutant cells, showing a cell cycle defect at time = 0. The higher order peaks are likely representing cells that are still in S/M phase. Microscopic examination revealed several individual nuclei in these cells, suggesting slow cell cycle progression. At restrictive temperature, these higher order peaks gradually disappear, and the 1C peak grows, indicating delayed release of daughter cells with 1C DNA content in *cdka-1/cdkb-1* cells.

DNA content, as measured by FACS,
in *cdka-1*, *cdkb-1* and *cdka-1/cdkb-1* mutant cells
over 18 hours

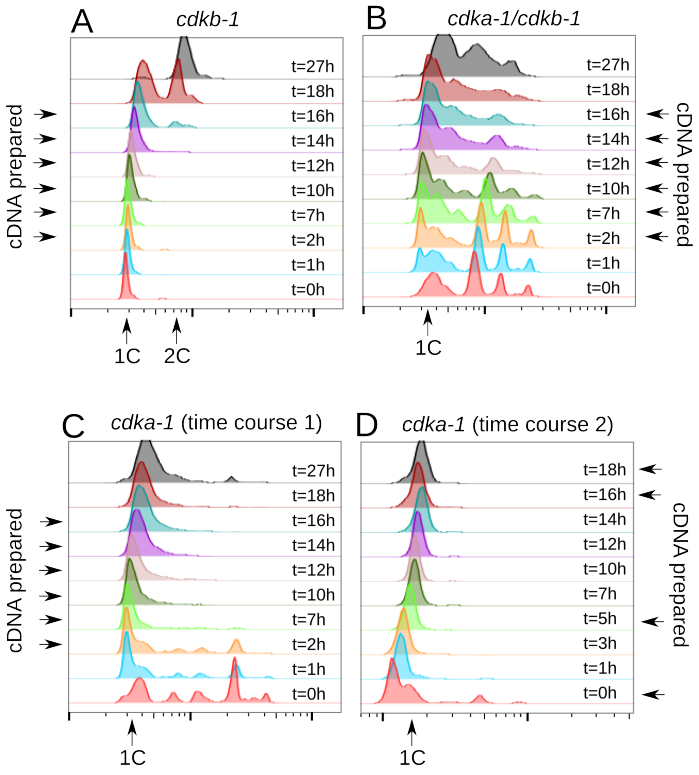

Figure 6.2: *cdk* mutant cultures sampled for cDNA preparation

Seven main patterns of transcript accumulation observed over 18 hours in wild type

The k-means clustering resulted in several clusters that appeared similar on visual inspection. That is, they contained genes that were, on average, up- or down-regulated in a similar pattern. Clusters that looked similar were grouped together manually in the following way. For each cluster, the mean relative abundance was calculated for each library (each library corresponds to one time point). Any cluster for which the maximal fold-change between any two time points was less than six-fold, was considered "unregulated"; these clusters were manually combined into a single large cluster. Clusters with a maximal average fold-change above six were grouped based on the average expression profile. This resulted in seven main patterns (Figure 6.3). In almost every case, these clusters were based on changes in expression over multiple time points, and also from changes seen at the same time points in separate experiments (biological replicates). Therefore, we have high confidence in the reproducibility of these clusters. As can be seen from figure 6.3, most genes (~14,000) showed little regulation across the 18 time-points, and fell into cluster 7. Cluster 1 (1000 genes) contained genes that increased in relative abundance between 5-7 hours, cluster 2 (1500 genes) contained genes that increased between 10-12 hours, and cluster 3 (350 genes) contained genes that increased between 12-14 hours. Cluster 4 (130 genes) showed transient down-regulation in the middle of the time-course, and cluster 6 (270 genes) showed a moderate decrease between 0-10 hours. Cluster 5 (21 genes) showed strong up-regulation specifically in the two libraries from t=7 hours. Since these samples were constructed from cells synchronized

on different days, we consider this a reliable cluster even though it only shows a strong effect at one time point.

Figure 6.3: Transcriptional trends in wild-type cells over the course of one cell cycle, and dependence on CDK

(A-B) Wild-type transcriptional patterns. **(A)** Eighteen cDNA libraries, derived from three independent wild-type cultures growing at 33ºC (Figure 6.1) were sequenced (Methods). The resulting 18 transcriptomes were ordered based on the time of sampling. This gave a matrix of 18 columns (one for each sample) and 17,737 rows (one for each gene model) containing the raw read counts for each gene model. The columns and rows were normalized based on their average read count, and the normalized read-count values were log2-transformed. The k-means clustering algorithm was used to group genes with a similar profile across the 18 samples into 20 clusters. These clusters were subsequently combined manually based on similarity into the seven clusters shown in **A**. All clusters with an arbitrarily chosen maximal fold-change of less than 6-fold were considered "unregulated", and grouped together into cluster 7. Clusters 1 (1009 genes), 2 (1496 genes) and 3 (346 genes) are characterized by an increase in relative abundance of transcripts at approximately 5, 10, and 14 hours after the shift to high temperature. Cluster 4 shows a transient decrease in abundance around 10 hours, and cluster 6 a slow continuous decrease. Cluster 5, consisting of only 21 genes, shows a sharp increase specifically in the two 7-hour libraries. **(B)** The average expression for each cluster is plotted on a linear scale. **(C)** CDK-dependence on transcript accumulation in the seven clusters. Read-count data from wild type (Figure 6.1) and *cdk* mutants (Figure 6.2) were compared. All gene models were grouped based on which wild-type cluster they belonged to (cluster 1 to 7). The average relative abundance of transcripts within each group is plotted on a linear scale.

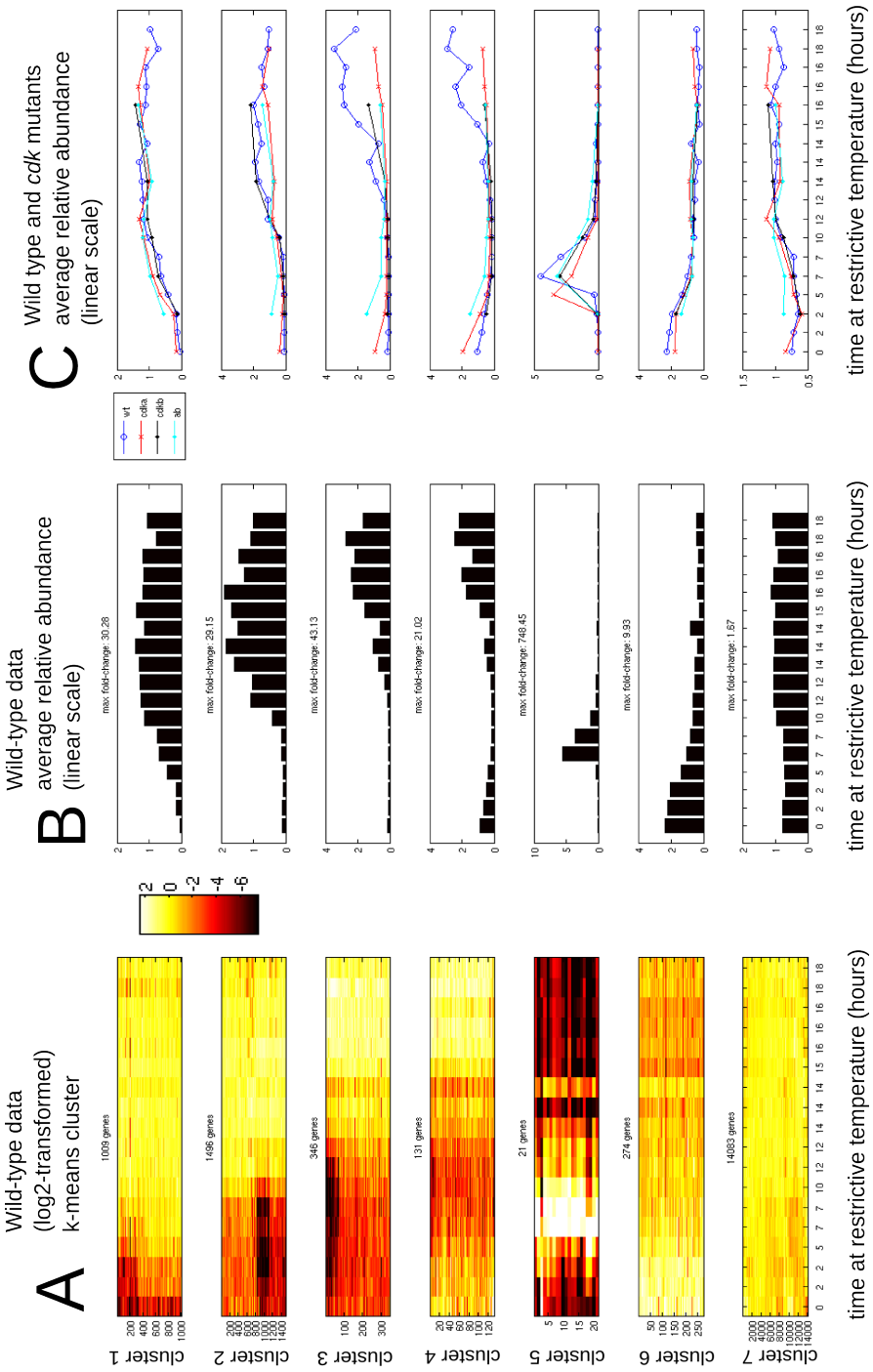

Figure 6.3: Transcriptional trends in wild-type cells over the course of one cell cycle, and dependence on CDK

CDK dependence on transcript accumulation in clusters generated from wild-type data

The seven clusters obtained from the wild-type data set (Figure 6.3 A,B) provided an overview of the major transcriptional trends over 18 hours after lights-on. Since CDK activity is known to control transcription of cell-cycle regulated genes in other organisms (Wittenberg and Reed, 2005) (Bertoli et al., 2013), we analyzed transcriptome data obtained from *cdka-1*, *cdkb-1* and *cdka-1/cdkb-1* double mutants, synchronized and grown according to the same protocol as wild type (Figure 6.2).

As shown in chapter 5, CDKA is required for timely initiation of all cell-cycle events that we monitored, accumulation of Cks1-precipitable kinase activity, DNA replication and cell division. All of these events occur after a significant delay in the *cdka-1* mutant at restrictive temperature. In contrast, CDKB is required for entry into mitosis, following the first round of DNA replication, which is usually initiated around 14-16 hours in this protocol. Notably, Cks1-precipitable kinase activity turns on with normal timing and remains at a high level for many hours in arrested *cdkb-1* cells (Figure 5.3 C).

The seven clusters obtained from the wild-type data provided a starting point for analyzing the effect of reduced CDK activity on transcript accumulation. The genes in the normalized full data set, containing transcriptomes from both wild type and *cdk* mutants, were sorted based on which wild-type cluster they belonged to: for example, the 1009 genes in cluster 1 were grouped together, the 1496 cluster 2 genes were grouped together, and so on. Next, the average relative abundance for each genotype was plotted as a

function of time (Figure 6.3 C). Cluster 1 contains genes that increase in abundance in wild type relatively early after lights-on (Figure 6.3 A). The average relative abundance of the genes in this cluster was similar in all four genetic backgrounds, with no obvious effect from the absence of normal CDK function. Cluster 2 contained about 1500 genes that increased in abundance approximately around 10 hours after lights-on. These genes behaved nearly identically in wild type and the *cdkb-1* mutant, but showed a slower increase after 10 hours in both *cdka-1* and *cdka-1/cdkb-1*. Cluster 3 and 4 contained genes that increased relatively late after lights-on, around 14 hours. These genes were down-regulated in all three *cdk* mutants: *cdka-1*, *cdkb-1* and *cdka-1/cdkb-1* at the 16 hour time point, compared to wild type.

Cluster 5, consisted of only 21 genes, up-regulated specifically at the 7 hour time points. Interestingly, this marked up-regulation was almost completely independent of CDK background; all four genotypes showed up-regulation of cluster 5 genes around the same time, and to similar extent. Note that, although this strong up-regulation was only observed at one time point, the same effect was seen in two independent wild-type libraries as well as the *cdk* mutant libraries (Figure 6.3 A), making it more likely to represent a real biological effect. Cluster 6 genes, with an initial moderate decrease in wild type, also behaved similar in our *cdk* mutants, as did the large number of essentially unregulated genes in cluster 7.

Taken together, the 1496 genes in cluster 2, which increase around 10 hours in wild type, show, on average, a moderate dependency on CDKA, which is most pronounced

around 14 hours. This effect is only partial, since the initial rise around 10 hours is approximately the same in wild type and *cdka-1*. The cluster 3 genes showed a dependency on CKDA, and probably on CDKB, and the 131 cluster 4 genes were reduced in expression in both *cdka-1* and *cdkb-1*. The double mutant *cdka-1/cdkb-1* had an elevated relative abundance of transcripts in clusters 1, 2, 3 and 4 genes. Since all these genes increase towards the end of the cell cycle, this effect can probably be attributed to the slow exit from the previous mitosis, as indicated by the presence of FACS peaks, early in the cell cycle, corresponding to dividing cells, in the *cdka-1/cdkb-1* mutant (Figure 6.2). The fact that the transient upregulation of cluster 5 genes was reproduced in all *cdk* mutants, with timing similar to wild type, suggested that *cdk* mutants retained the capacity for transcriptional control, at least at early time points.

Cluster 5 identifies genes regulated by the carbon concentrating mechanism

Cluster 5 showed a striking signature of up-regulation specifically in the two 7-hour libraries. Of the twentyone genes in this cluster, several have been shown to play a role in the carbon concentrating mechanism (Yamano and Fukuzawa, 2009). In a recent study, transcript levels of several genes involved in the carbon concentrating mechanism (CCM) were measured in 12h:12h light/dark-synchronized cultures at air-level concentration of carbon dioxide (Tirumani et al., 2014). The authors found strong up-regulation half-way through the light period for several CCM genes, followed by a reduction at the 12-hour time point. Strikingly, all of the seven genes determined to be transiently up-regulated in

the light by Rao and colleagues (Tirumani et al., 2014) were among the 20 genes with a strong up-regulation at the 7-hour time point in our transcriptome data set. In addition, we observed 13 genes with an equally strong 7-hour up-regulation.

Cluster 2 contains core S-phase genes and cell-cycle genes

As discussed in chapter 5, the *cdka-1* mutant displays a long delay before entering the cell cycle, during which Cks1-precipitable kinase activity remains low. We speculated that this delay might be connected to transcription in some way. For example, CDKA function could be directly required for transcriptional activation of genes needed to perform cell cycle functions. Alternatively, the slow cell cycle progression in *cdka-1* mutants could be unrelated to transcription. In that case, one could imagine that the cell cycle is driven by gene expression controlled by some other mechanism, and that CDKA activity is required to respond correctly to these transcriptional changes, to drive cell-cycle events.

The genes in cluster 2 displayed a pattern of accumulation suggestive of a role in the cell cycle. Their abundance was very low during the first 10 hours, during the G1-growth phase of the cell cycle, and then increased sharply between 10-12 hours in wild-type cells, roughly coinciding with the increase in Cks1-activity, and preceding detectable signs of DNA replication by a couple of hours (Figure 6.1). Furthermore, the average cluster 2 gene was weakly reduced in the *cdka-1* mutant, but appeared normal in the *cdkb-1* mutant. Expression in the double mutant was generally similar to *cdka-1*, but often higher

at early time points, probably as a consequence of the altered cell cycle behavior in this strain (Figure 6.2). Thus, the genes in cluster 2 could plausibly be connected to the observed cell cycle behavior in the *cdk* mutants. We wanted to look more closely at the genes in cluster 2, to see if the annotation could help us understand the biological significance of these transcripts, and to get a sense of the variability of CDK dependence within the cluster. It is important to note that these clusters were constructed based only on wild-type data, and show a CDKA-dependency on transcript accumulation averaged over 1500 genes. Therefore, this cluster might contain genes whose transcript accumulation deviates from the average pattern to varying extents.

We identified 40 conserved S phase genes in cluster 2 (Appendix A5). Based on sequence conservation, these were likely to be involved in diverse processes relating to pre-RC assembly (*ORC*), replication initiation (*CDC45*), elongation (*POLA*), chromosome cohesion (*SCC1*) and nucleiotide biosynthesis (*RNR1*). In fact, several of these had been identified as *DIV* genes in this screen, and have been shown to have defects in DNA replication (e.g. *div15/rnr1* and *div17/rnr2*) (chapter 4). The timing of pre-RC assembly in *Chlamydomonas* is not known. It is possible that the accumulation of pre-RC components observed around 10 hours is necessary for DNA replication in the upcoming S phase. It is also possible that G1 cells already have assembled pre-RCs and that expression of pre-RC components (for example ORC) is required only for subsequent rounds replication during the S/M phase.

All of these 40 S-phase genes behaved like the average cluster 2 gene: transcript

abundance increased in a similar pattern in wild type and *cdkb-1*, but was attenuated in *cdka-1* and *cdka-1/cdkb-1*. The average expression profiles of the 40 S-phase genes in different genetic backgrounds is shown in figure 6.5 A.

As mentioned in the introduction, the cell cycle control machinery both regulates and is regulated by cell-cycle-periodic transcription. Many cell-cycle genes, most notably the cyclins, are themselves transcriptionally controlled (Bertoli et al., 2013) (Wittenberg and Reed, 2005). In addition, the B-type family of plant CDKs are tightly regulated at the transcriptional level (De Veylder et al., 2007). We looked at nine cell-cycle genes with high sequence conservation to known cell-cycle regulators (Figure 6.4). Most of these displayed the same trend as observed for the average cluster 2 gene and for the curated set of 40 S-phase genes: attenuated transcript accumulation in *cdka-1* and *cdka-1/cdkb-1* mutant cells, compared to wild type and *cdkb-1*. The most extreme example of this trend was displayed by the cyclin gene *CYCB1*. *CYCAB1*, in contrast, was up-regulated to similar extent in all four strains. The CYCAB1 protein shows the highest sequence similarity to human cyclin A2, yeast Clb3 and CYCA1;1 from *Arabidopsis.* It was identified in a genome annotation of *Chlamydomonas* cell-cycle genes, but no function has been ascribed to it (Bisova et al., 2005).

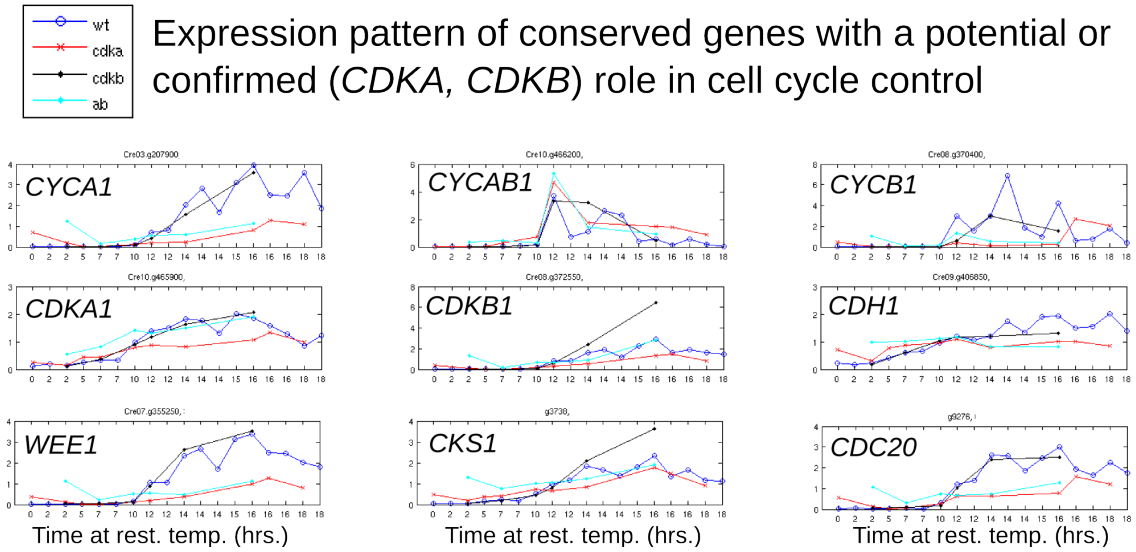

Figure 6.4: Relative transcript abundance of conserved cell-cycle genes in wild-type and *cdk* mutant backgrounds

The apparent CDKA-independent activation of the *CYCAB1* gene raised the possibility that other genes that are normally upregulated sharply around 10 hours might show a similar behavior. Using *CYCAB1* and *CYCB1* as baits, we searched for other genes with similar features: up-regulation at 10 hours that was either strongly dependent on CDKA, or not noticeably dependent on CDKA. The expression profiles of the 100 most similar genes were averaged and plotted (Figure 6.5 B and C). As expected, the 100 genes most similar to *CYCB1* displayed a reduction in transcript accumulation in the *cdka-1* and *cdkb-1* mutants, compared to wild type and *cdkb-1* (Figure 6.5 B). The 100 genes most similar to *CYCAB1*, on average, increased in abundance between 10-12 hours to a similar

extent, independent of *cdk* background. There is, of course, an issue with biological replication for the latter case, since most of this effect stems from a single time point (t=12h). Without a reliable model for estimating variability in the data, which we currently do not have, this result must be interpreted with caution. Nevertheless, the fact that many genes show strong up-regulation around 10 hours, which appears independent of CDK, makes it more likely that this represents a real biological feature.

Figure 6.5: Differential dependence on CDKA on transcript accumulation after 10 hours

Transcript abundance is shown for wild-type (blue), *cdka-1* (red), *cdkb-1* (black), and *cdka-1/cdkb-1* double mutant (cyan) cells. Cluster 2 (see Figure 6.3) contained 1500 genes that were activated around the 10 hour time point in wild-type cells. On average, this increase was attenuated in *cdka-1* mutant cells, suggesting that transcription of cluster 2 genes is CDKA dependent. **(A)** We identified 40 conserved S phase genes within cluster 2, that all increased sharply in relative abundance around 10 hours. In *cdka-1* and *cdka-1/cdkb-1* cells, this increase was attenuated compared to wild type. In contrast, expression of the 40 S phase genes appeared unaffected by the *cdkb-1* mutation. Individual examination of these 40 genes showed that there was little variability within the group. **(B-C)** Two cyclin genes, *CYCB1* and *CYCAB1* both belonged to cluster 2, that is, they turned on around 10 hours in wild type. However, they showed different behavior in the *cdka-1* mutant. For each of *CYCB1* and *CYCAB1*, 100 genes with the most similar expression profile were collected from the wild type plus *cdk* data set. To score similarity, each gene in the data set was normalized to length 1, and the inner products to all other genes were computed. The 100 genes with the highest inner products were selected. **(B)** The average expression profile of 100 genes most similar to *CYCB1* shows a significant CDKA-dependence on transcript accumulation after the 10 hour time point, although eventually abundance approaches the wild type level. **(C)** Average expression profile of 100 genes most similar to *CYCAB1*. In this case the rise in relative abundance around 10 hours is closely matched in both *cdka-1* and *cdka-1/cdkb-1* double mutants. Throughout, accumulation of transcripts in wild type and *cdkb-1* mutant cell was similar, indicating that activation of early transcription might be independent of CDKB.

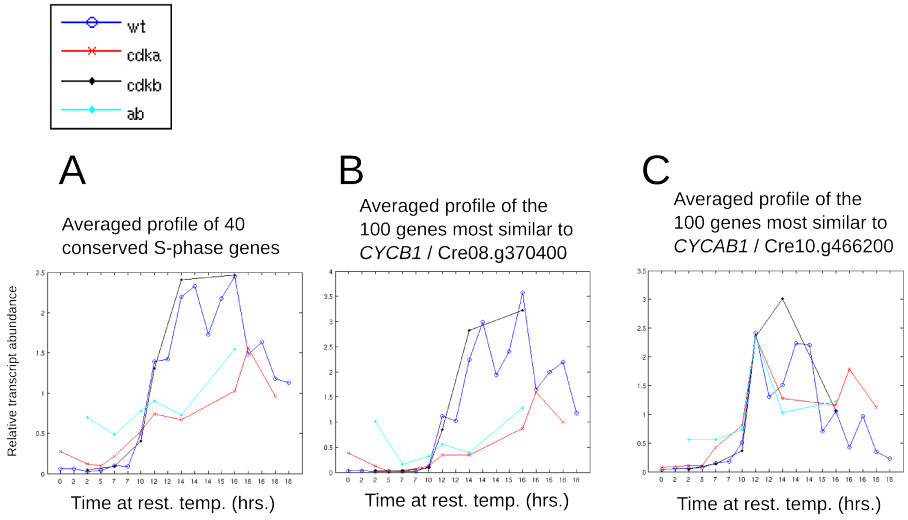

Figure 6.5: Differential dependence on CDKA on transcript accumulation after 10 hours

Patterns of transcript accumulation of *DIV* genes in wild-type and *cdk* mutant cells

For 51 *DIV* genes, we have identified high-confidence candidate causative mutations. Of these, 13 were in the 'G1' class, and the rest were 'mitotic mutants' (Chapter 3). In almost every case, 'mitotic' *DIV* genes fell into cluster 2, showing sharp up-regulation at ~10-14 hours, in parallel with the S phase gene set just discussed. In sharp contrast, G1 *DIV* genes were almost all transcriptionally unregulated, falling into cluster 7. Expression profiles of the *DIV* genes are shown in figure 6.6.

Figure 6.6: Relative abundance of transcripts from *CDKA* and *DIV* genes in wild-type and *cdk* mutant cells

Line plots showing the relative abundance (linear scale) of 49 *DIV* genes and *CDKA* in four genetic backgrounds: wild type (blue), *cdka-1* (red), *cdkb-1* (black) and *cdka-1/cdkb-1* (cyan). Many *DIV* genes display strong up-regulation, from essentially zero relative abundance, around the 10 hour time point in wild type. This behavior is also seen in the *cdkb-1* mutant. In contrast, *cdka-1* mutant cells show a reduction in activation of many *DIV* genes that are normally turned on at 10 hours (e.g. *DIV43, DIV21, DIV72, DIV15*). *cdka-1/cdkb-1* double mutants generally behave similar to *cdka-1* single mutants. Note the strong increase in abundance of *CDKB* transcripts in the *cdkb-1* mutant background.

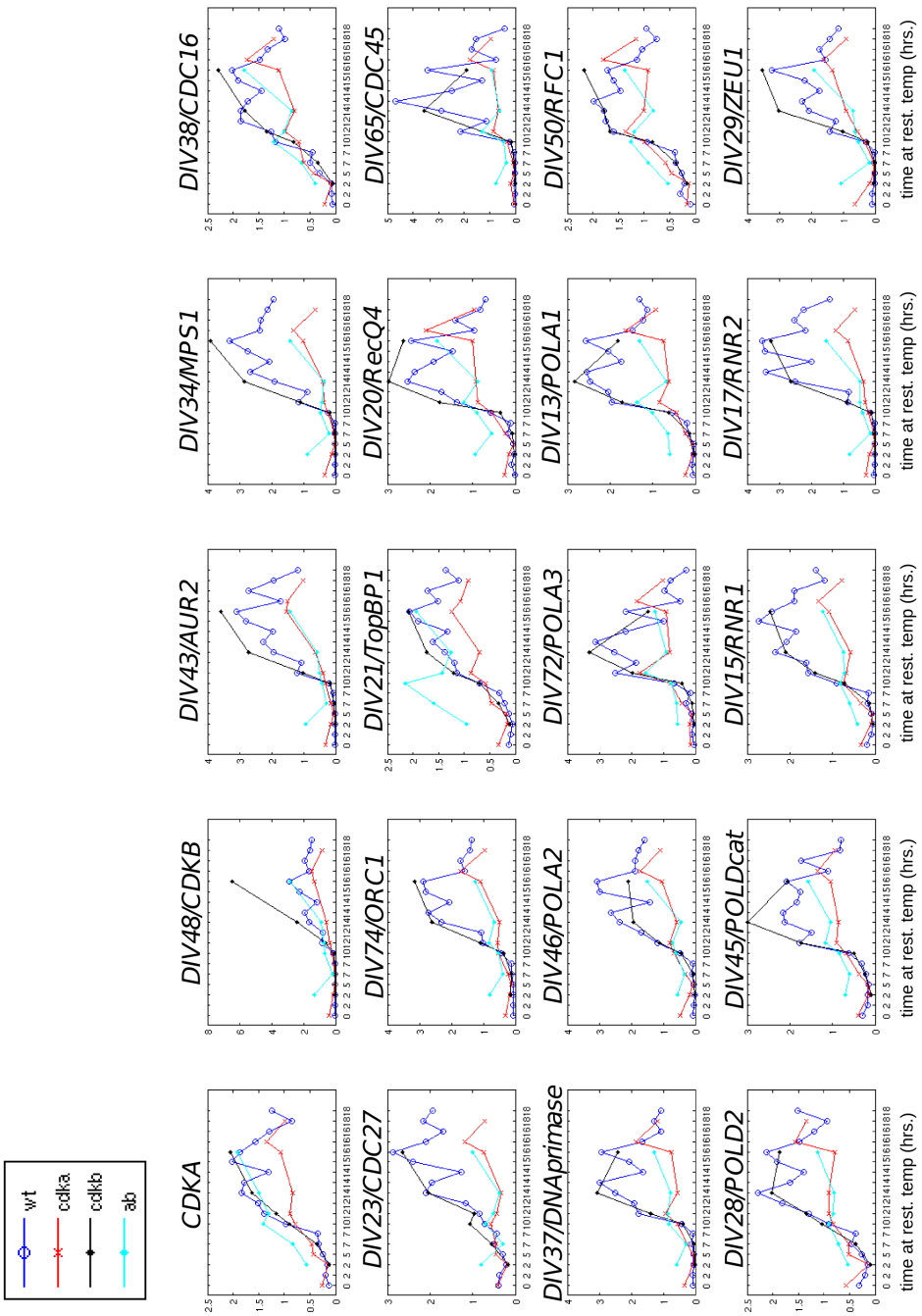

Figure 6.6: Relative abundance of transcripts from *CDKA* and *DIV* genes

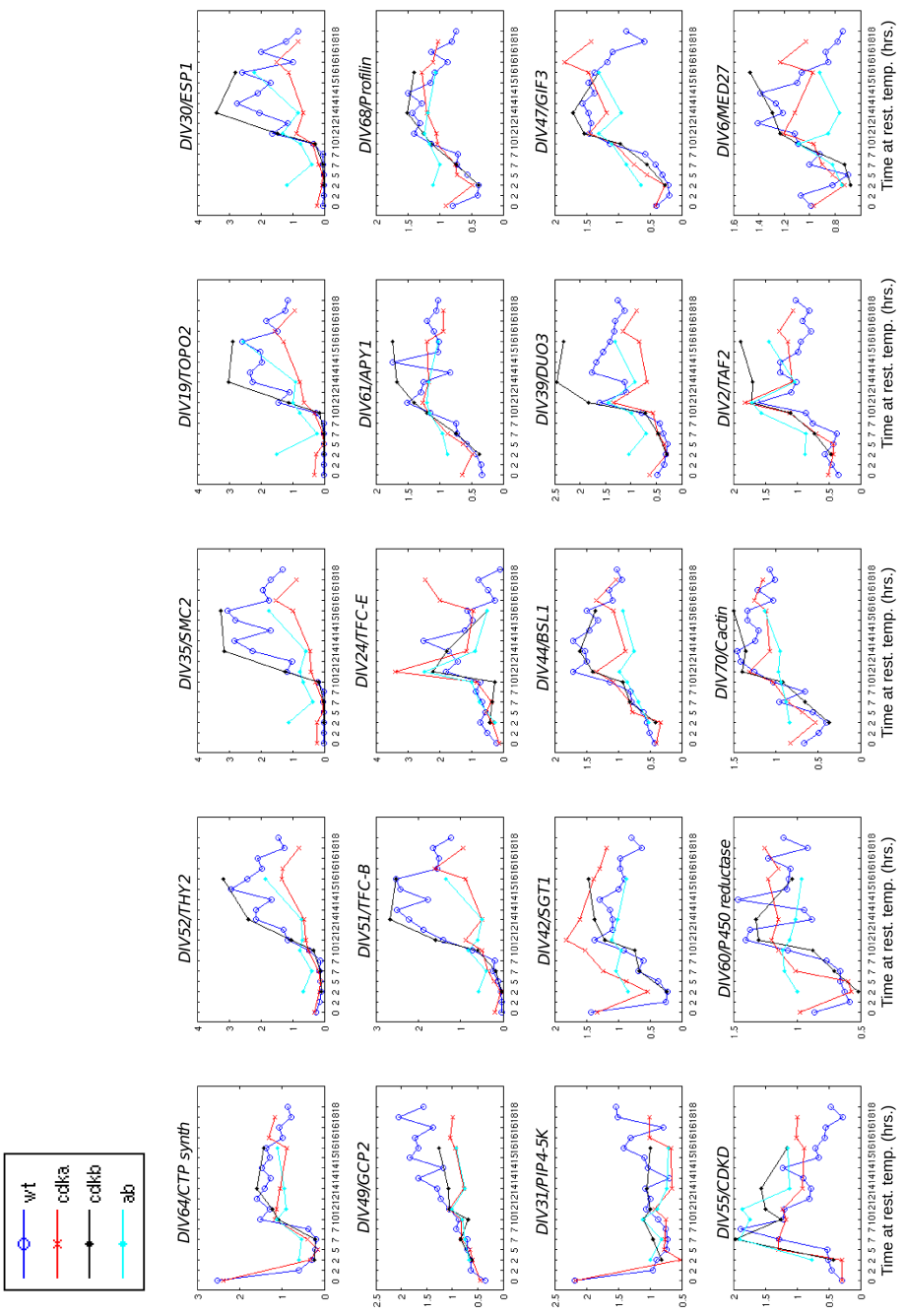

Figure 6.6: Relative abundance of transcripts from *CDKA* and *DIV* genes

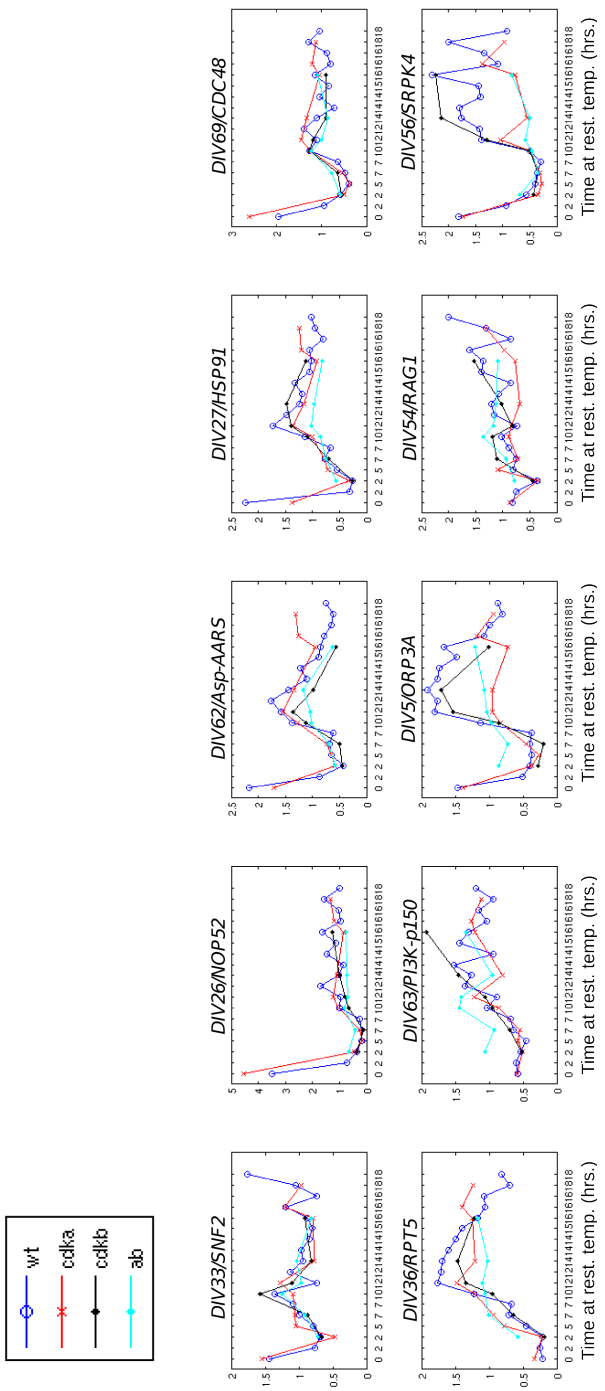

Figure 6.6: Relative abundance of transcripts from *CDKA* and *DIV* genes

Discussion

The results presented here represent an initial analysis, limited in scope, of transcriptome profiling of wild-type *Chlamydomonas* cells, along with *cdka-1* and *cdkb-1* mutants. RNA readcounts from three independent wild-type time courses over 18 hours were clustered by the k-means algorithm into groups of genes with similar expression profiles. This treatment revealed significant accumulation of a large number of transcripts (~10% of the genome) from an initially low level, starting approximately 10 hours after lights-on. Although this transcriptional program likely is the result of a combination of factors, including lights-on at t=0, lights-off at t=14h, potential circadian regulation and metabolic status of the cell (e.g. cluster 5/CCM genes), the data suggests that at least some of this regulation requires normal CDKA function. We identified specific transcripts from genes likely required for various aspects of DNA replication (Appendix A5), as well as conserved cell-cycle genes, which all increased sharply in expression in wild-type cells, but were reduced in the *cdka-1* mutant. The effect resulting from the *cdka-1* mutation was only partial, however, and would best be characterized as a slowed rate of increase in abundance, rather than a complete block; most CDKA-dependent transcripts initially increased in parallel in wild-type and *cdka-1* cultures, but leveled off in *cdka-1* cells and never reached the peak level seen in wild type. We speculate that this reduction in transcript abundance might be related to the observed cell-cycle delay in the *cdka-1* mutant (chapter 5). Among the cell-cycle genes that showed a strongly reduced accumulation in transcript levels in *cdka-1* mutants were two cyclins, *CYCA1* and

CYCB1, homologous to mitotic cyclins in opisthokonts.

In chapter 5, we suggested the possibility, based on kinase assay data, that CDKA might play a role in activating CDKB. Since CDKB almost certainly relies on a cyclin partner for enzymatic activity (Boudolf et al., 2009), and since most cyclin transcripts were present at very low levels during G1, it seems likely that new cyclin gene expression is needed to activate CDKB. This assumes, of course, that cyclin proteins are degraded at the exit from mitosis in *Chlamydomonas*, which is one of the fundamental principles of cell-cycle control in opisthokont systems (Thornton and Toczyski, 2003) (Hershko, 1999). In *Arabidopsis*, as in yeast and animals, mitotic cyclins are indeed known to be degraded upon exit from mitosis (Weingartner, 2002), so this is likely true in *Chlamydomonas* as well.

Transcripts from the *CDKB* gene itself were essentially absent during G1 and increased around 10 hours in wild-type cells. This study has shown that CDKB is essential for mitosis. Therefore, by the same argument as for cyclins, it is likely that new expression of *CDKB* is required in each cell cycle, especially since CDKB protein was reported to be degraded during mitosis and absent in G1 cells (Porceddu et al., 2001) (Sorrell et al., 2001). *CDKB* transcripts showed reduced accumulation in *cdka-1* cells, raising the possibility that timely expression of CDKB is dependent on CDKA. This delayed expression of *CDKB*, and a large number of other cluster 2 genes, might explain (or at least contribute to) the cell-cycle delay phenotype observed in the *cdka-1* mutant. This is related to the model proposed by Nowack et al. for *Arabidopsis*, in which CDKA

inactivates Rb, resulting in increased expression of many genes including CDKB; it was proposed based on genetic data that CDKB induction largely explains the CDKA requirement for efficient cell cycle initiation (Nowack et al., 2012).

Chapter 7 Discussion of the main results of the thesis

The aim of this project overall was to discover cell cycle-control components in a member of the *Viridiplantae* plant lineage, *Chlamydomonas reinhardtii*, following an unbiased methodology that was independent of prior knowledge of cell-cycle control in other organisms, especially the well-studied yeast/animal (opisthokont) systems, in order to establish fundamental similarities and differences in cell cycle control between these long-diverged lineages (Rogozin et al., 2009).

Following the strategy described in chapter 2, we identified genes acting at various stages in the *Chlamydomonas* cell cycle. A general distinction was made between G1 vs. mitotic mutants, based on cell division behavior on agar (chapter 2), as well as detailed cell-cycle timecourses (chapter 4). The G1 mutants arrested before any signs of cell-cycle initiation were observed, whereas the mitotic mutants displayed defects in specific cell-cycle processes associated with DNA replication and segregation. A small number of mitotic mutants identified genes that were required specifically at the entry to mitosis. One of these was the plant-specific kinase *CDKB.* We also identified a mutation in the *CDKA* gene, as a fortuitous double mutant (Figure 5.2). Sequence comparisons suggest that *CDKA* is the closest relative to Cdk1, the central cell-cycle regulator in opisthokonts (Bisova et al., 2005) (Vandepoele et al., 2002). The *cdka-1* mutant was unique in that it combined features of both the G1 and the mitotic mutants; it failed to show any signs of cell-cycle initiation (like the G1 mutants), but cell growth was normal (like the mitotic

mutants). This suggested to us that CDKA might play a role in bridging the transition from cell growth during G1, to cell-cycle initiation. The centrality of CDK in cell-cycle control in other systems (Nurse, 1990) suggested that a dissection of CDKA and CDKB function would be a good place to begin an analysis of cell-cycle control in *Chlamydomonas.* The initial results were presented in chapter 5, and summarized here, in the context of one *Chlamydomonas* multiple fission cell-cycle, in figure 7.1.

A proposed model for CDK function in cell-cycle control in *Chlamydomonas*

In natural conditions, it is likely that the far 'left' of the scheme in Figure 7.1 represents morning, when newborn, but quiescent, small daughters hatch from the mother cell. Previous literature on *Chlamydomonas* grown in light-dark cycles suggests that these newly hatched cells have a strong requirement for growth and/or passage of time since the last mitosis, before the classical 'commitment' event (asterisk in Figure 7.1) occurs. After the commitment step, cells will eventually divide multiple times, independent of light or further cell growth (Spudich and Sager, 1980) (Craigie and Cavalier-Smith, 1982). While some minimal growth must be required for commitment and cell division, how the commitment step is regulated is not clear, although involvement of a biological 'timer' has been proposed (Donnan and John, 1983). The time of commitment substantially precedes the time of significant activation of Cks1-precipitable kinase activity (see figure 2 in Bisova et al., 2005). The mechanistic connection between these events can now be addressed with the mutants we have isolated, and this is an interesting subject for future

work. It is interesting in this context that the *Chlamydomonas* Rb homolog MAT3 is required for restriction of commitment by growth and time (Umen and Goodenough, 2001), and CDKA has been implicated specifically in Rb inactivation in *Arabidopsis* (Nowack et al., 2012). Interestingly, while light is required for growth, blue light may also inhibit entry into the cell division cycle, by an unknown mechanism (Münzner and Voigt, 1992).

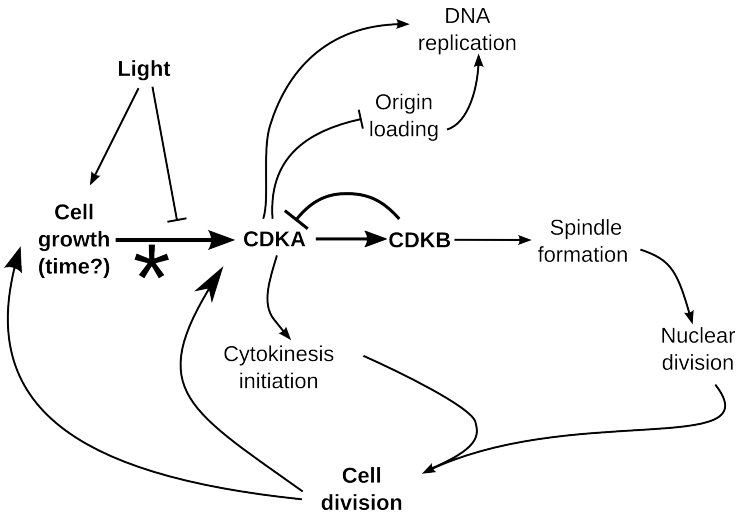

Figure 7.1: A proposed model for CDK function in cell-cycle control in *Chlamydomonas*

Newborn cells begin the cycle to the 'left' in the scheme. Following a period of light-dependent cell growth, cells pass the commitment point (asterisk), which constitutes an irreversible decision to the cell cycle. Blue light may also delay cell-cycle entry by unknown mechanisms (Münzner and Voigt, 1992). After additional post-commitment cell growth, three CDKA-dependent events are initiated: DNA replication, initiation of cytokinesis and activation of Cks1-precipitable kinase activity. CDKB is required for mitosis, specifically spindle formation and nuclear division, and may engage in a negative feedback relationship with CDKA (discussed in main text above, and chapter 5). The *cdkb-1* mutant arrests with once-replicated DNA and high Cks1-precipitable kinase activity. To explain the 2C arrest in *cdkb-1* mutant cells, we suggest the possibility, based on yeast/animal DNA replication control (Blow and Dutta, 2005), that CDKA activity prevents re-replication of DNA by inhibiting loading of origins. Depending on the size of the daughters cells after division, they may enter the scheme to the 'right' of the commitment point, with no requirement for cell growth before the next cycle, or to the 'left' of the commitment point, in which case another growth period is required. The *Chlamydomonas* homologue of the retinoblastoma protein MAT3 has been shown to be important for size control in *Chlamydomonas* (Umen and Goodenough, 2001).

The 'G1' class of mutants, with subtle defects in cell growth, all failed any detectable cell cycle initiation; we have tested three of these mutants accumulated at their blocks for Cks1-precipitable kinase activity, and found them to be at background levels, at a time when wild-type levels were very high. Therefore, we suppose these mutants are involved, at varying levels of specificity, in the transition from a newborn, pre-committed cell to a committed cell with activated CDK kinases. The identified genes in the 'G1' class have molecularly diverse roles, many of which may be subsumed under cell growth processes at some level (Table 3.2). Nevertheless, these mutants were picked up in our screen because despite a modest growth defect, they ultimately grow to a size significantly exceeding the wild-type division size, but never synthesize DNA or initiate cell division. This could be explained in several ways. Perhaps there is a requirement for a sufficiently high growth rate, as distinct from cell size per se, for cell cycle entry. Or there may be specific regulatory checkpoints restraining cell cycle initiation conditional on fully functional protein folding, ribosome biogenesis or membrane synthesis. Similar schemes have been proposed for budding yeast (Jorgensen and Tyers, 2004) (McCusker and Kellogg, 2012) (Moore, 1988).

The behavior of the *cdka-1* mutant (no growth defect, much delayed cell-cycle initiation) suggested that CDKA might play a rate-limiting role early in the cell cycle, possibly involving the commitment step. However, *cdka-1* mutant cells did eventually escape from the cell-cycle arrest and complete apparently normal cell divisions at restrictive temperature. Whether this means that CDKA function is dispensable for late

cell-cycle events, we do not know, since we do not know if the *cdka-1* mutant represents the null phenotype for CDKA. Further supporting an early role for CDKA, we have tested the effect of *cdka-1* on the phenotypes of many *div* mutants that arrest later in the cell cycle, based on initiation of cytokinesis and/or DNA replication, and in every case expression of the phenotypes of the *div* mutant was strongly delayed by the *cdka-1* mutation (Figure 5.3 C. Atkins and F. Cross, unpublished data).

CDKB is required for late cell-cycle events, specifically spindle formation, which we assayed by immunostaining (Figure 4.7). The apparent failure to form mitotic spindles also explains the failure of nuclear division in *cdkb-1* cells. In contrast, early cell-cycle events, DNA replication and activation of Cks1-precipitable kinase activity and initiation of cytokinesis-like structures, all occurred with essentially normal timing in the *cdkb-1* mutant (Figure 5.3). Since none on these things happened in the *cdka-1/cdkb-1* double mutant, we propose that these events are directly dependent on CDKA activity.

We suggest a role for CDKA in activation of CDKB (Figure 7.1). This result is consistent with comparisons of wild type to single and double *cdka-1* and *cdkb-1* mutants (Figure 5.3). In wild-type cells, Cks1-precipitable kinase activity increases sharply around 10 hours, whereas in *cdka-1* mutant cells, activation of kinase activity is delayed until the 16 hour time point. If CDKB normally contributes a non-trivial amount to the observed signal, then CDKA-dependent activation of CDKB seems plausible. The time window of this delay, between 12-16 hours, corresponds to the time when *CKDB* and mitotic cyclin transcripts increase in abundance, from a very low level, in wild type, but are delayed in

the *cdka-1* mutant (Figure 6.4).

Conversely, we propose a role for CDKB in inactivation of CDKA (Figure 7.1). This is based on the observation that Cks1-kinase activity remained at a very high level for many hours in the *cdkb-1* mutant. This assumes that the Cks1-precipitable kinase activity in the *cdkb-1* mutant primarily comes from CDKA. This seems likely, since the double mutant *cdka-1/cdkb-1* has negligible activity (Figure 5.3). To account for the absence of re-replication in the *cdkb-1* mutant, we speculate that in addition to promoting initiation of DNA replication, CDKA might also inhibit reloading of replication origins. This idea accounts elegantly for once-per-cell-cycle DNA replication in yeast and animal systems (Bell and Dutta, 2002). If this is the case also in *Chlamydomonas*, and if it is true that CDKB is needed for inhibition of CDKA, then only a single round of replication in the *cdkb-1* mutant is expected. Direct confirmation of this idea will require development of methods to detect CDKA- and CDKB-specific activities.

The *cdka-1* mutant does ultimately enter the cell division cycle after a long delay, producing viable daughters. Cell division (and even formation of incipient cytokinetic structures) in the *cdka-1* background is completely dependent on CDKB, as shown by comparison to the *cdka-1/cdkb-1* double mutant (Figure 5.4). These findings suggest some degree of functional overlap between CDKA and CDKB. In *Arabidopsis* also, significant but incomplete rescue of the phenotypes of a *cdka* null mutant can be provided by ectopic expression of CDKB (Nowack et al., 2012).

Following cell division, newborn *Chlamydomonas* cells appear to have two distinct

fates. The 2^n rule states that after commitment, *Chlamydomonas* will undergo n divisions, such that the resulting daughter cells are reduced to a constant size, which is then the size of the newborn cells released from the mother cell wall to start a new cycle (Craigie and Cavalier-Smith, 1982). Cells divided to this size appear to reenter the cell cycle at the 'left' in figure 7.1, requiring a long G1 period of growth before a new commitment and entry into new division cycles. Cells that are bigger than this size have no growth requirement and apparently enter the scheme to the 'right' of commitment in figure 7.1. The relationship of these apparently qualitatively different re-entry schemes to CDK control is an interesting subject for future studies. For example, whether CDKA is required in every division during the S/M phase could be addressed with better resolved time-lapse imaging. (Intriguingly, however, preliminary results suggest that the median size of the daughter cells produced in *cdka-1* cells is approximately normal.)

Taken together, our results indicate central, and largely distinct, roles for CDKA and CDKB in cell-cycle control in *Chlamydomonas.* Full inactivation on B-type CDK activity has never been attained in a plant system, due to genetic redundancies (Vandepoele et al., 2002). Partial inactivation has been associated with a shift from mitotic cell cycles towards endoreduplication (Boudolf et al., 2009), which is quite different from our observation of an arrest with once-replicated DNA in the *cdkb-1* mutant. It could be that full inactivation of CDKB in higher plants would result in a mitotic block without endoreduplication. Alternatively, plant cells are highly prone to endoreduplication already, most likely due to the presence of systems for cyclical activation and inactivation of

CDKA that are independent of CDKB (De Veylder et al., 2011). Such physiological endoreduplication systems should be specific to somatic cells, and are not expected to be present in *Chlamydomonas*, a single celled organism with Mendelian genetics.

Discussion of gene function during S/M phase in *Chlamydomonas*

We identified many mitotic mutants that displayed diverse cell-cycle defects during the S/M phase. These results are summarized in figure 7.2, elaborating on the putative CDK-model just discussed. A number of cell-cycle events, and some of the genes found in chapter 4 to be important for those events, are shown.

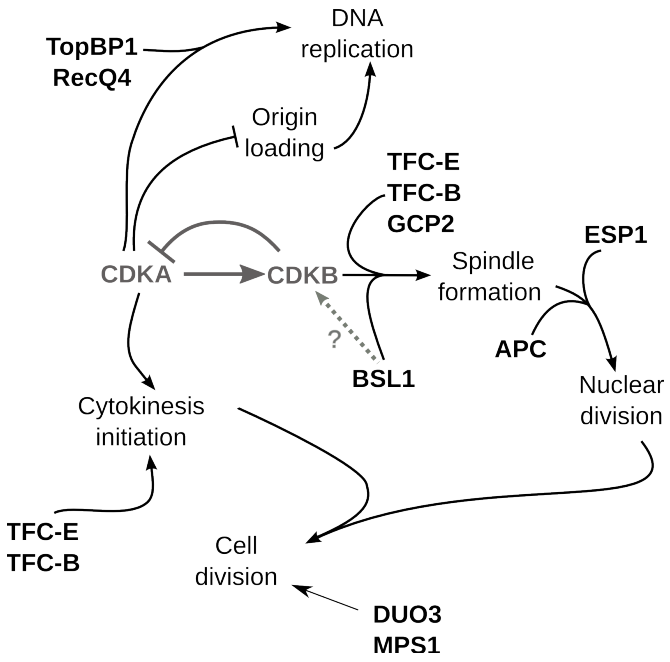

Figure 7.2: Genes required for S phase or mitosis in *Chlamydomonas*

Genes required for nuclear division

As illustrated in figure 7.2, we found five genes that are required for nuclear division: TFC-E, TFC-B, GCP2, ESP1 and BSL1. The *div24-1/tfc-e* and *div49/gcp2* mutants probably prevent nuclear division by blocking spindle formation (Figure 4.3). However, despite the absence of a spindle, the cells underwent repeated cycles of DNA replication, accumulating as much as 8-16C DNA content in some cases (Figure 4.1; 4.2). These observations were unexpected based on results in opisthokonts, where the typical response of the cell cycle machinery to spindle defects is a cell cycle arrest mediated by the spindle assembly checkpoint. The checkpoint works by inactivating the anaphase promoting complex (APC) (Lara-Gonzalez et al., 2012). During a checkpoint-mediated arrest, mitotic cyclins, which are degraded in an APC-dependent manner, are stabilized. This prevents re-loading of replication origins, and therefore re-replication of DNA (Blow and Dutta, 2005). The re-replication we observed here, under conditions where we believe microtubule function to be severely reduced, is surprising in this context. In addition, we observed a similar re-replication behavior when wild-type cells were treated with the microtubule poison APM (Figure 4.2).

Chlamydomonas does have homologues of the key components of the spindle assembly checkpoint (e.g. Mad2), but what the functions of these components are in the *Chlamydomonas* cell cycle is mysterious. Interestingly, a similar phenotype of DNA re-replication, without nuclear division, has been observed in *Arabidopsis* meristems treated

with the microtubule drug oryzalin (Grandjean et al., 2004).

Re-replication without nuclear division was also observed in the *div30-1/esp1/separase* mutant. In yeast and animals, separase is responsible for cleaving the cohesin structures that hold sister chromotids together at the metaphase-to-anaphase transition (Peters, 2002). In budding yeast, *esp1* mutant cells experienced severe chromosome segregation defects in mitosis and produced aneuploid, inviable, daughter cells (McGrew et al., 1992). The mono-nucleate, polyploid phenotype of *div30-1*, is consistent with a role for DIV30 in nuclear division.

Re-replication in these mutants, apparently occurred in complete rounds, judging from the regular spacing of the FACS peaks (Figure 4.1; 4.2), corresponding to cells with 1C, 2C, 4C and 8C DNA content. This indicated that, provided CDKA and CDKB are present, the programmed cycles of replication during S/M phase can occur despite failure in chromosome segregation.

The *bsl1-1* mutant (in addition to *cdkb-1)* was special in that not only were spindle formation and nuclear division blocked, the cells arrested with 2C DNA without re-initiating replication. Thus, the *bsl1* mutant must be different in some way compared to the other mutants blocking nuclear division. The absence of spindles cannot immediately explain the 2C arrest, given the phenotype of re-replication without spindle formation just mentioned. It is possible that the *bsl1-1* mutation produces a particular kind of defect that a potential checkpoint in *Chlamydomonas* could detect, and that inhibits the cycles of replication. Another possibility is that BSL1 inactivates CDKA, for example through

activation of CDKB. If that is the case, then according to the scheme in figure 7.2, absence of BSL1 would lead to high CDKA activity. If high CDKA activity prevents loading of origins, as is indicated in the figure (and discussed above), then only a single round of DNA replication would be expected in the *bsl1* mutant. At this point, this possibility remains a speculation.

Genes required for apparent cytokinesis initiation

We scored apparent cytokinesis initiation morphologically, based on development of notches and invaginations that frequently developed on the cell surface of mitotic *div* mutants. A few mitotic *div* mutants remained round until they lysed (compare 'notch', 'popcorn' versus 'round' in Figure 2.4). Two genes required for the apparent cytokinetic structures were the tubulin cofactors TFC-E and TFC-B (Szymanski, 2002), since both *tfc-e* and *tfc-b* mutant cells arrested with a 'round' morphology. Furthermore, the 'round' morphology of the *tfc-e* mutant was epistatic to the 'notch' and 'popcorn' morphology in all cases tested (not shown). This suggested a requirement for functional microtubules to initiate cytokinesis (and for development of the 'notch' and 'popcorn' mutant phenotypes), consistent with previous literature about microtubules involved in cell division in *Chlamydomonas* (Johnson and Porter, 1968) (Ehler and Dutcher, 1998). Also consistent with previous observations, and reflected in figure 7.2, are the independent pathways leading to initiation of cytokinesis and nuclear division (Harper & John, 1986). Note that GCP2 was different from TFC-E and TFC-B with respect to apparent cytokinesis

initiation, although all three genes were required to make spindles. GCP2 homologues in other systems are important for nucleation of microtubule filaments, as a part of the gamma tubulin ring complex (Wiese and Zheng, 2006). To what extent this difference in morphology between *tfc-e* and *tfc-b*, compared to *gcp2*, reflects different roles in microtubule dynamics, is not known.

Genes acting late during S/M phase

The DIV39 and DIV34 gene products appeared to act late in the cell cycle, since nuclear division and apparent cytokinesis occurred in the *div39-1* and *div34-1* mutants. DIV34 is the putative homologue of Mps1 in *Chlamydomonas.* In opisthokonts, the Mps1 kinase plays many roles, but is generally important for the spindle checkpoint and accurate chromosome segregation (Castillo et al., 2002) (Maure et al., 2007) (Yamagishi et al., 2012). DIV39 shares small segments of homology to DUO3 in *Arabidopsis*, a homeo-box protein shown to be important for cell cycle progression in the male gametophyte (Brownfield et al., 2009). The ultimate reason for the lethality in *div39-1* and *div34-1* is unclear, but will be an interesting topic for future studies.

APC

In figure 7.2, the APC is placed in parallel with ESP1, promoting nuclear division. This is consistent with out results showing a partial metaphase arrest in both *apc* mutants. In

opisthokonts it is well known that one of the essential functions of the APC is to promote sister chromatid separation, through activation of Esp1 (Peters, 2002). The failure to enter anaphase can be explained by a similar mechanism in *Chlamydomonas*. In addition, to account for the apparent coupling of nuclear division and replication in *apc* mutants, we speculate that the APC also plays other roles. If the scheme in figure 7.2 is correct, then one of these roles could be inactivation of CDKB, possibly by promoting degradation of specific cyclins, or perhaps CDKB itself. Due to the proposed negative interaction between CDKB and CDKA, and the suggested requirement for low CDKA levels to reload origins, this could provide coordination between nuclear division and replication control during S/M phase.

Future directions

The results presented here provide an initial outline of the cell-cycle control machinery in *Chlamydomonas.* The CDKA and CDKB enzymes play central, and largely distinct, roles. We proposed a negative feedback loop between CDKA and CDKB, based on kinase assays and transcriptome data (Figure 7.1). This model predicts that CDKB activity (and maybe protein level) will be low in the *cdka-1* mutant, and that CDKA activity will be high in the *cdkb-1* mutant. These predictions can be addressed with tagged alleles of each CDK, and work towards obtaining these is ongoing (K. Atkins, F. Cross). This undertaking is facilitated by the strong positive selection provided by rescuing *cdkb-1* from lethality by transformation with a tagged wild-type allele.

The centrality of a CDK-APC negative feedback loop in opisthokont cell-cycle control was described in the introduction. An important question to ask is: to what extent is this network architecture conserved in *Chlamydomonas*? Our results show that the APC is essential, and probably coordinates progression through the multiple fission cycles during S/M phase. Which are the essential targets of the APC ubiquitin ligase? CDKB is degraded upon exit from mitosis in tobacco (Porceddu et al., 2001). Is CDKB stabilized in an *apc* mutant background in *Chlamydomonas*?

Our results show that CDKB is essential for mitosis. Homologues of B-type CDKs are found throughout *Viridiplantae,* but their role in cell-cycle control are not understood in detail. Exploring the mechanistic basis for this mitosis-specific function in *Chlamydomonas* will be an important question for future research. With a method to detect CDKB specifically, a biochemical approach might be the best way forward. Three specific questions can be asked. First, what is the composition of the CDKB complex? With which cyclins, or other proteins does it interact? Second, is the CDKB enzyme regulated post-translationally? Tyrosine phosphorylation of CDKs is essential for timing of mitosis in many opisthokont systems, but the significance of this regulation for B-type CDKs in plants is unclear. Third, which are the important targets of CDKB-dependent phosphorylation? This question could be addressed, although not easily, by phosphopeptide proteomics, comparing wild type and *cdkb-1* cells (Bodenmiller et al., 2007). In general, the the *cdkb-1* mutant is ideal for comparative analyses because its cell-cycle behavior is essentially wild type up until the block.

The initial analysis of the transcriptional program during the cell cycle in *Chlamydomonas* indicated that a large number of genes require wild-type CDKA for robust activation. Extending this analysis, to produce a more comprehensive picture of cell-cycle regulated transcription, is a priority. This analysis will include, in addition to *cdka-1* and *cdkb-1*, transcriptomes gathered from arrested G1 and mitotic *div* mutants. As one example, we might be able to define promoter elements that are activated in a CDKA-dependent manner by comparing genes behaving like *CYCA1* (which shows a sharp CDKA-dependent upregulation before S/M phase), to genes behaving like *CYCAB1* (which show CDKA-independent activation). Validation might be done by constructing strains carrying a luciferase reporter driven by candidate promoters (Shao and Bock, 2008). If such an approach were successful, it is conceivable that screening for loss of reporter signal could identify transcription factors that drive cell-cycle regulated gene expression in *Chlamydomonas*.

The *cdka-1* allele described here has provided the opportunity for two secondary genetic screens (K. Atkins; F. Cross). One screen uses the delay-phenotype shown in figure 5.4. It was shown that survival at high temperature of certain *div* mutants is greatly enhanced, temporarily, in the *cdka-1* mutant background. Thus, by screening for 'death-delay', it might be possible to find new genes that act similarly to CDKA, that is, genes that delay cell-cycle-dependent cell death. It might also be possible to isolate non-sense mutations in CDKA this way (provided CDKA is non-essential). The other *cdka-1* based screen looks for enhancers of the *cdka-1* delay phenotype. That is, other mutations, acting

like *med6-1*, that convert the delay into a tight cell cycle block (Figure 5.2). Both of these screens have the potential to expand the CDKA pathway.

An explicit aim of this work has been to better understand cell-cycle control in plants. In this context, a number of genes, particularly *GIF3*, *DUO3* and *BSL1* are interesting because they have likely homologues (very clear homologue for *BSL1)* in *Angiosperms*, with an unclear cell-cycle function. Therefore, focusing on these genes is a natural extension of this project. As a first step, additional screening for suppressors could provide clues. This work has already begun with *bsl1*, where we have isolated, but not yet analyzed, many (>100) revertants of *bsl1* lethality. As mentioned in chapter 4, the BSU1 phosphatase (a homologue of BSL1) is involved in hormone signaling in *Arabidopsis*, where it acts on the protein BIN2 (Maselli et al., 2014), and *Chlamydomonas* has a BIN2 homologue; maybe loss of *BIN2* in *Chlamydomonas* can suppress the *bsl1* phenotype. Furthermore, testing the hypothesis of a mitotic function for BSL in *Arabidopsis*, by looking at cell division in gametophytes and early embryos of BSL1,2,3 triple knock-outs, will be an interesting objective for the future.

Another general area of interest is to integrate more of *Chlamydomonas* physiology with cell-cycle control. We mentioned the commitment point, where cell-cycle progression becomes energy independent (Donnan and John, 1983); the connection between commitment and CDK can now be addressed. For example, do *cdka-1* mutant cells require a longer time (or a larger size) to commit, or is commitment determined independently of CDKA function?

In *Chlamydomonas*, the long growth period during the light phase, followed by rapid divisions in the dark, is likely an adaptation to a photosynthetic life style, such that cell growth is coordinated with daytime. If so, it is possible that normal perception or response to light signals is required for this separation of cell growth and cell division. One question to ask is whether mutants with defective circadian rhythm (Matsuo and Okamoto, 2008) or eyespot biogenesis (Lamb et al., 1999) have altered cell-cycle behavior. An alternative hypothesis would be that cell growth rate, which is high in the light, suppresses the onset of the cell-division program independent of light.

It is also unclear how nuclear and cell division is coordinated with division of the chloroplast. These processes are likely to be regulated in *Chlamydomonas*, which has only a single large chloroplast that gets distributed among the daughters during cell division. Studying this process will probably require development of cytological techniques for monitoring chloroplast dynamics over the course of a cell cycle.

Finally, the screen for *div* mutants is only at approximately 25% saturation, so additional screening for mutants is likely to generate new genes, and the result so far has been encouraging.

Conclusion

The collection of mutants presented here (Table 3.2) represent a powerful tool for exploring cell-cycle control in the green plant superkingdom in a simplified microbial setting. We have started this investigation by by studying the functional relationship

between CDKA and CDKB in coordinating cell-cycle progression. The *Chlamydomonas* system can also be valuable for generating testable hypotheses about specific gene functions in *Angiosperms*. The potential for a mitosis-specific role for BSL1 in plants is a case in point. In this sense, we hope that *Chlamydomonas* may play a similar role for higher plants, as yeast plays for opisthokonts.

Appendix A1 Bayesian selection of candidate mutations

Meiotic mapping and sequence characteristics allow Bayesian selection of causative mutations from multiple candidates

The bulked segregant sequence analysis, using ~10 temperature-sensitive segregants from a cross of a primary temperature-sensitive mutant A to wild-type, typically resulted in detection of one or a few regions of 'uniform' SNPs (that is, all reads corresponding to an alternative version, at read depths of 20-50x). These regions were typically flanked by SNPs present at high but not uniform frequency; this is interpreted as resulting from the rightmost crossover on the left, or the converse, in the pool of 10, resulting in representation of wild-type reads in the pool. See figure A1-1, part A, for a diagrammatic representation (only one uniform region on a specific chromosome is shown).

Practically, we define the endpoints of these regions as the right-most non-uniform SNP that is left of the region, or the converse. If there is no non-uniform SNP detected from the left of the chromosome to the first uniform SNP, we take the border to be half-way to the first uniform SNP.

The problem is to determine which (if any; see below) of the linked SNPs is most likely causative.

Mapping

The observation of a small region of uniform SNPs is consistent with the causative

mutation lying within the region. This can be easily confirmed (and the correct region identified if there are multiple regions) by additional mapping. For example, if mutant A yields a uniform region on chromosome IV from 1 Megabase (Mb) to 3.5 Mb, we cross it to mutant B known to have a mutation on chromosome IV (say at 0.3 Mb). If the mutations in both A and B are on IV, the unlinked expectation of 1 parental ditype:4 tetratype:1 nonparental ditype (P:T:N) will be violated due to excess of PD over NPD. An additional qualitative signal due to linkage at longer distances is T in excess of 4 N (Harris, *Chlamydomonas* Sourcebook) due to chiasma interference. The map distance in centiMorgans (cM) between A and B is calculated as 50*(T+6N)/(P+T+N). Over the whole genome the average ratio of cM/Mb is 10 (Merchant et al. 2007). Suppose A and B are 20 cM apart; then the causative mutation in A should be located at around 0.3 +/- (20/10) Mb, therefore at -1.7 to 2.3. Only the 2.3 Mb position is sensible (and consistent with the initial uniform region); at this point we consider it reasonably proven that the causative mutation in A is between 1 and 3.5 Mb on IV, with a best-fit location at 2.3 Mb. The genetic map distance cannot be taken as giving an exact location; there are multiple sources of error. One source is experimental (fewer tetrads and greater map distance both increase error) and another source is biological: cM/Mb ratios are not uniform due to hot or cold spots for recombination. Over a large number of crosses of this kind that we have performed, in cases where we know or strongly suspect the position of the causative lesions in both mutants (Figure 3.1), we find an average relationship of about 10 cM/Mb as reported (Merchant et al. 2007), with a standard deviation of about 5 cM or 0.5 Mb.

This error is not strikingly dependent on map distance, and in all cases we are assaying enough tetrads to reduce expected statistical noise below 5 cM; therefore, we expect that most of the error is due to non-uniformity of recombination rates.

Conceptually, then, we can envision the mapping experiment as restricting the location of the mutation in a probabilistic way across the interval (Figure A1-1 C). To approximately express our degree of uncertainty about the location, we construct a probability density function for the location based on the normal distribution, using the estimated map position as means, and 0.5 Mb as standard deviation (from data; Figure 3.2).

[In some experiments, we cross a mutant to wild-type and check co-segregation of a given SNP, scored by PCR/resequencing, with temperature-sensitivity. Formally this amounts to mapping the distance between the SNP and the causative lesion in A, except that for the presumed causative lesion the predicted map distance is zero, and in such cases we have never detected recombinants.]

Finding the causative SNP: the 'unsequenceability' problem

At this point in the analysis (figure A1-1 D) we are confident that the causative mutation in A lies within a given interval, and we have a pdf for its location, with error ~0.5 Mb if the data come from a single cross, or potentially less if there are multiple crosses.

Is one of the SNPs in the uniform region causative? In the diagrammed example,

there are two uniform SNPs, at 1.2 and 2.7 Mb. If the sequence library is complete, then exactly one of these two MUST be causative. However, as discussed in Chapter 3, there are two DIV genes (DIV14 and DIV16) where despite up to 200X sequence coverage, and multiple alleles sequenced, we cannot find any causative SNP, even though we can map DIV14 and DIV16 meiotically to reasonably precise positions (on chrIV and chrX respectively; Figure 3.2; Appendix A2), and all sequenced bulked segregant pools from these mutants yield uniform SNPs in these regions (most or all non-functional, and in distinct gene models in pools from different independent alleles). We can rule out any of these as causative because there is no overlap either of gene model or of plausible physical distance for these SNPs between multiple alleles. The reasons are unknown; possibilities include the sequences of the causative genes: (i) not being present in the reference assembly (which does contain gaps); (ii) containing repetitive sequence or other features interfering with alignment of short reads; (iii) being chemically unsequenceable by Illumina technology. Therefore, in general if there are i SNPs in the uniform region, we must consider i+1 hypotheses: either one of the uniform SNPs in the region is causative, or the sequence library is incomplete (perhaps due to systematic unsequenceability, as with DIV14 and DIV16). [We neglect in principle the possibility that some phenotype is caused by multiple linked SNPs. Since we have detected almost no cases of DIV phenotypes due to two unlinked mutations, it is vastly less likely that two linked mutations cause a phenotype, since the *Chlamydomonas* genome displays the functional mosiaicism typical of eukaryotes; linked genes in general have completely

unrelated functions].

This situation is diagrammed in figure A1-1 D, with Models 1, 2 and U, where 'U' refers to 'unsequenceable'.

[More generally, 'unsequenceable' should refer to absence of the causative SNP from a given library. In our data, readcounts for mutations ultimately shown to be causative are high (~20-50); we do not see a continuous distribution of these readcounts to lower numbers, therefore it is unlikely that many causative mutations are absent from the libraries simply due to stochastic fluctuations in readcount. Therefore, we assume that in most cases, either the causative mutation is present in the library, or it is 'unsequenceable', and will not be found even with much more sequence data].

We assign a frequency of unsequenceability ('U') of 0.25. This appears conservative: for the ~60 DIV genes in Table 3.2, constituting all the genes we have mapped genetically, only three are definitively unsequenceable, and ~2-4 others lack a highly plausible candidate.

[A back-of-the-envelope calculation supporting an assignment of this magnitude: a typical result from our mutants and sequence libraries is a 1.5 Mb uniform region, and the density of coding-sequence-altering SNPs is ~1/Mb over many libraries. We observe no uniform coding sequence SNPs in ~1/20 sequence libraries. For this to happen (assuming the

causative mutation changes coding sequence), the causative mutation must be unsequenceable, AND no random passenger mutations occurred in the 1.5 Mb region. Therefore 0.05 = U*e^(-1.5) (e^-1.5 is the frequency of zero passengers if the mean is 1.5, by Poisson distribution), yielding U=0.22]

The linkage mapping function 'f' generated above gives a pdf for the location of the causative mutation, and therefore the SNPs (at positions s1 and s2) have probability density f(s1) and f(s2) for being causative. However, in the event that these SNPs are NOT causative, their likely distribution is simply uniform across the region (they must, by definition, be within the region), so non-causative SNPs have pdf 1/(length region) for their positions (FigureA1-1 E1 shows the two pdfs and the placement of the SNPs in the example on each).

The three models (1,2, and U) are mutually exclusive and exhaustive. Therefore, an explicit use of Bayes theorem applies. We take as given the mapping function f, the number of SNPs 'i' and the size of the uniform region 'W', and consider the 'data' to be just the positions of the SNPs within the region (called s_j for SNP j). We assume priors for Model k of (1-U)/i, and for Model U of U. Then the probability of Model k (SNP k is causative) given the data is:

Pr(Model k | data) = (1-U) f(s_k) / (1-U)*Sum(f(s_j)) + U i/W

and

Pr(Model U | data) = (U i/W) / (1-U)*Sum(f(s_j)) + U i/W)

These equations were confirmed to work by simulations. Figure A1-1 E2-E4, illustrates the placement of SNPs on the appropriate pdf based on the model under test.

These equations will report higher probability that a given SNP is causative if it is closer to the center of the linkage pdf, and also higher probability if it is the only SNP, or if the other SNPs are far from the center of the pdf. It will report a higher probability of unsequenceability if the SNPs are far from the center of the pdf, if there are fewer SNPs, or if the region is smaller. All of these features are qualitatively correct. In the diagrammed example, Model 2 is supported by the linkage data more than the other models since Model 1 correctly 'expects' SNP2 to occupy a probable position based on linkage; Model 1 is highly unlikely since SNP1 occupies a very improbable position on this pdf. Model U is intermediate, since the linkage mapping is not stringent enough in this example to differentiate the uniform distribution from the linkage pdf (this is typical for our data). Model U still loses to Model 1, though, because a priori it is at least 3 times as likely that the causative SNP is in the sequence data than that it is not.

As a consequence, in this hypothetical example the data presented results in an estimated probability of 0.68 vs. 0.05 that SNP2 vs, SNP1 is causative, based on the linkage data - clearly, a large refinement over the initial estimates of 0.375 ((1-U)/2) for both. The probability of the 'unsequenceable' hypothesis has hardly changed in this example (from 0.25 to 027).

An independent Bayesian criterion: BLAST/Blosum analysis

Chapter 3 describes sequence characteristics of a set of 'ground-truth' *div* mutations, and control 'passenger' mutations. The *div* mutations are more severe (based on Blosum scores) than the passenger mutations, consistent with significant interference with protein folding/function as might be expected from the temperature-sensitive phenotype. Also, the *div* mutations are much more likely to land in conserved positions of conserved genes (we used *Arabidopsis* as a standard) than the passengers, consistent with the idea that cell-cycle control is a conserved function. Thus these features are natural and plausible.

We digitized these characteristics so that any mutation fell into one of eight categories (Figure A1-2 A-B). Two features generate these categories: Blosum scores and BLAST features. Multiplication of marginals, and comparison to the data for DIV and passenger mutations, shows that these characteristics are largely independent, for both sets of mutants (Figure A1-2 C, upper bar graphs). This is useful since the marginals are much less sensitive to fluctuations in numbers (no zero categories, for example). Therefore, we used the multiplied marginals to generate likelihoods: probability of a mutation being in category j given that the mutation was or was not a *div* mutation.

Figure A1-2 C (lower left) shows the likelihood ratios for each category for DIV/passenger. The categories are clearly strong discriminators of DIV from passengers, especially since in this context, the genetics has already restricted attention to a small handful of SNPs in each case.

Returning to the case where there are some number of SNPs in an interval, we can

use these likelihoods, and apply Bayes' theorem again: we use the updated prior probabilities for each SNP being causative derived from linkage analysis, and the likelihoods derived from Blosum/BLAST categories. (We assume that linkage results and Blosum/BLAST categories are independent, again because of lack of functional clustering of the *Chlamydomonas* genome). The procedure is identical to the one for linkage, in that we discriminate between i+1 models if there are i SNPs.

Continuing with the hypothetical case in Figure A1-1, SNP2 is supposed to be a 'category 1' SNP: a strong (Leu-Pro, Blosum -3) mutation in a conserved residue in a conserved protein. (This is, in fact, the majority behavior of 'definitive' *div* mutations, and also of most of the mutations assigned as probably causative in Table 3.2). SNP1, in contrast, is supposed to be in the rather typical (for passenger mutations) category 6: the *Chlamydomonas* gene has an *Arabidopsis* BLAST hit, but the rather innocuous (Leu-Ala, Blosum -1) mutation is in a residue not aligned in the BLAST hit. Combined with the linkage data, the result in this hypothetical case is a high degree of confidence that SNP2 is causative (probability of Model 2 0.95; Figure A1-1 F). SNP1 is essentially ruled out, and unsequenceability becomes quite unlikely (probability 0.05) (Figures A1-1 E1,E3).

This procedure should obviously be considered an estimation, essentially a stopgap measure for the substantial number of cases where we have only one allele of a gene, and one or multiple SNP candidates (of which, very frequently, one is clearly by far the best candidate by the usual qualitative criteria, as in the case of CDKA). The advantage to this procedure is that it applies even statistical criteria to all candidates, and treats equally

those with high informal 'prior probabilities' such as CDKA, and other genes for which there might be no prior information suggesting a cell-cycle role.

All of these calculations are carried out in simple Matlab code, which takes as input the endpoints of the uniform interval believed to contain the causative mutation for A, the locations, Blosum scores and BLAST categories of the uniform SNPs within this interval, and for available linkage data, the physical map position(s) (in Mb) of markers and the corresponding cM distance(s) between the A mutation and these markers, and generates the probabilities for each SNP being causative, and for unsequenceability; these are the values in Table 1. (This code was used for the hypothetical example in Figure A1-1).

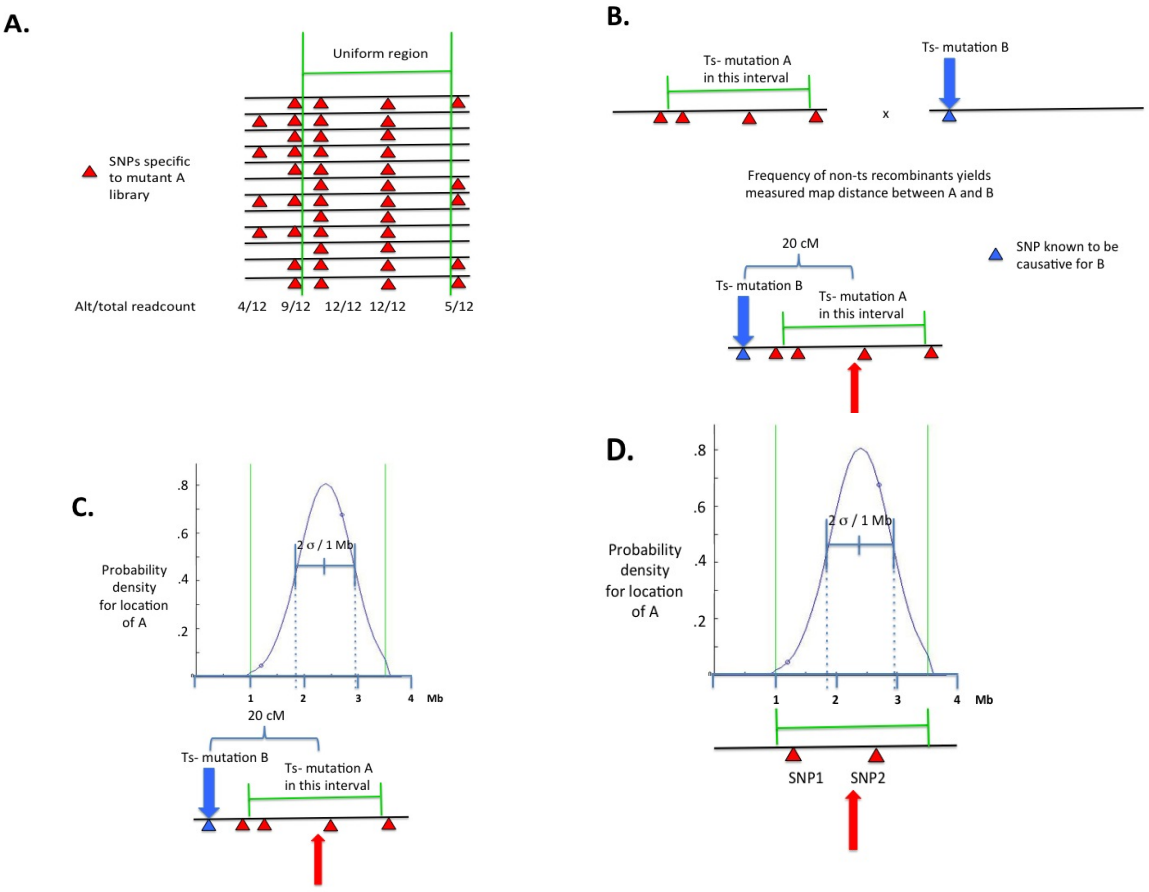

Figure A1-1, A-D: Outline of Bayes calculations for choosing among SNP candidates. (**A)** A bulked segregant pool with a central uniform region. (**B-D)** mapping the most likely location for the *div* mutation in strain A by mapping against a Ts- mutation with a known physical location.

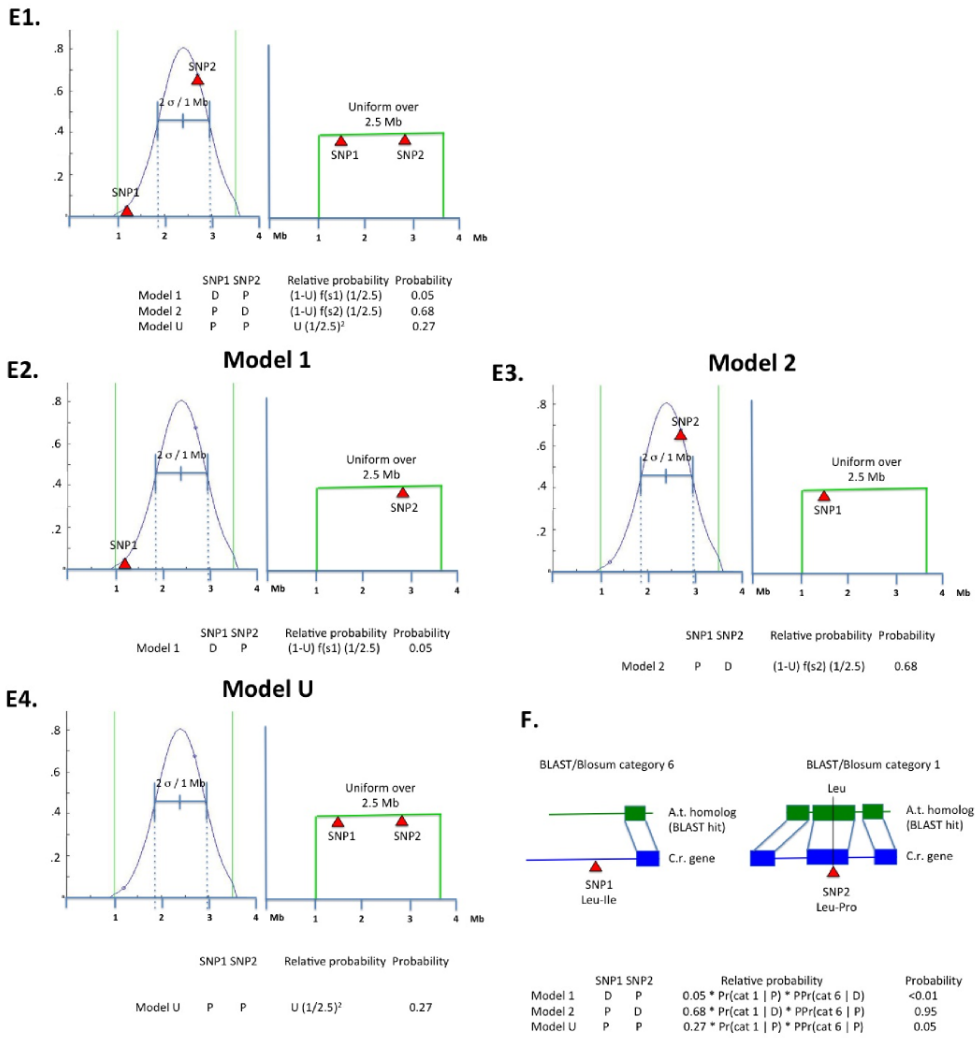

Figure A1-1, E,F: Calculation of probabilities of models based on linkage **(E1,E2,E3, E4),** and incorporating BLAST/Blosum information **(F).**

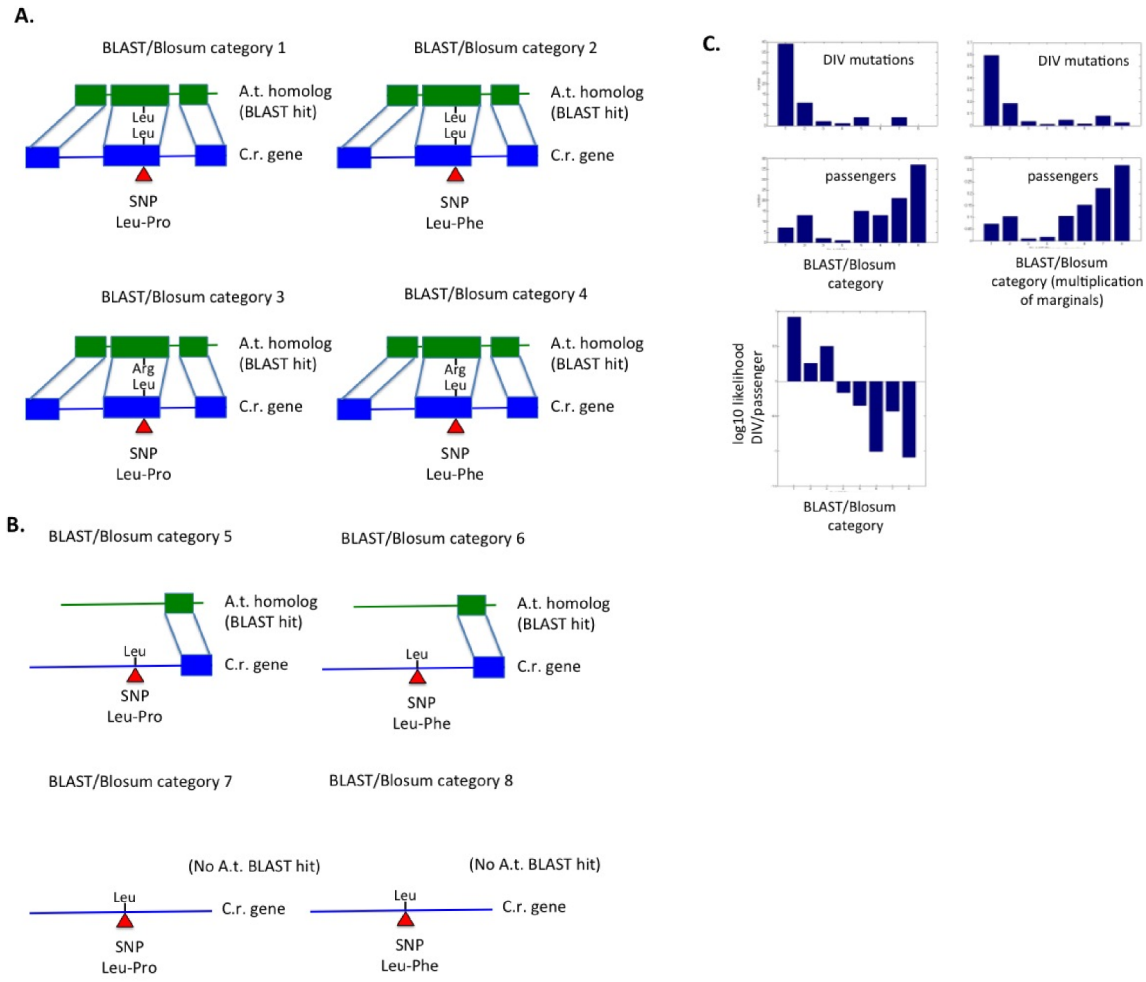

Figure A1-2: BLAST-Blosum categories. (**A, B)** Illustration of hypothetical examples of the eight categories. (**C)** Proportion of definitive *div* mutations and passengers that fall into the 8 categories, determined directly or by multiplication of marginals; **(C)** log10 likelihoods of membership in each category, *div*/passenger.

Appendix A2 Map locations of all *DIV* genes mapped

DIV genes are assigned locations on the physical map (Figure A2), based on the following requirements:

1. From bulked segregant sequence analysis, a region of uniform SNPs (functional, i.e. cds-changing, or not) that is either the only one in the library, or that is shown to be the only one consistent with other genetic linkage data;
2. At least one independent cross showing co-segregation of this uniform region with other markers on the same chromosome, with physical distances approximately consistent with location of the region and the marker (assuming an average 10 cM/Mb (Merchant et al., 2007).

DIV genes are assigned a specific gene model as described in Table 3.2: based on a SNP within the uniform region changing the gene model, where the SNP is either:

1. 'Definitively causal' based on multiple non-complementing alleles with cds-changing uniform mutations in the same gene model;
2. 'Definitively causal' based on isolation of intragenic revertants that are true or pseudo-revertants at the site of the original mutation;
3. Probably causal based on Bayesian analysis (see Chapter 3 and Appendix A1),

with a cutoff of Bayesian probability >=0.7. (This cutoff was arbitrary, and most gene models indicated have probability > 0.9; Table 3.2).

4. In some cases, no candidate is proposed (e.g. DIV14 on chr IV). This is either because the *div* mutation is apparently 'unsequenceable' (see text), or because there are multiple candidate SNPs in the interval that cannot be distinguished reliably by the Bayesian analysis (Table 3.2).

Linkage experiments were of two types. (1) Two different *div* mutants were mated, and segregation of ts lethality assessed (Ts+: Ts- ratios 2:2: PD; 1:3: T; 0:4: NPD; map distance in cM 50*(T+6 NPD)/(PD+T+NPD). In cases of distant linkage, we confirmed linkage based on excess of T over NPD indicating chiasma interference. Numbers of tetrads varied between experiments from ~20 - ~100. (2) A *div* mutant was mated to wild-type, and co-segregation of Ts- with the SNP at the indicated physical location established by PCR/resequencing, typically of 10-20 segregants from 4-viable-spore tetrads. A single map distance from such an experiment (unless the distance is ~0, as in the PCR case) is ambiguous since the linkage can be in either direction. In all cases, we could rule out one direction based on the positions of the regions of uniform SNPs, and/or on crosses with other markers and requiring approximate consistency of distances.

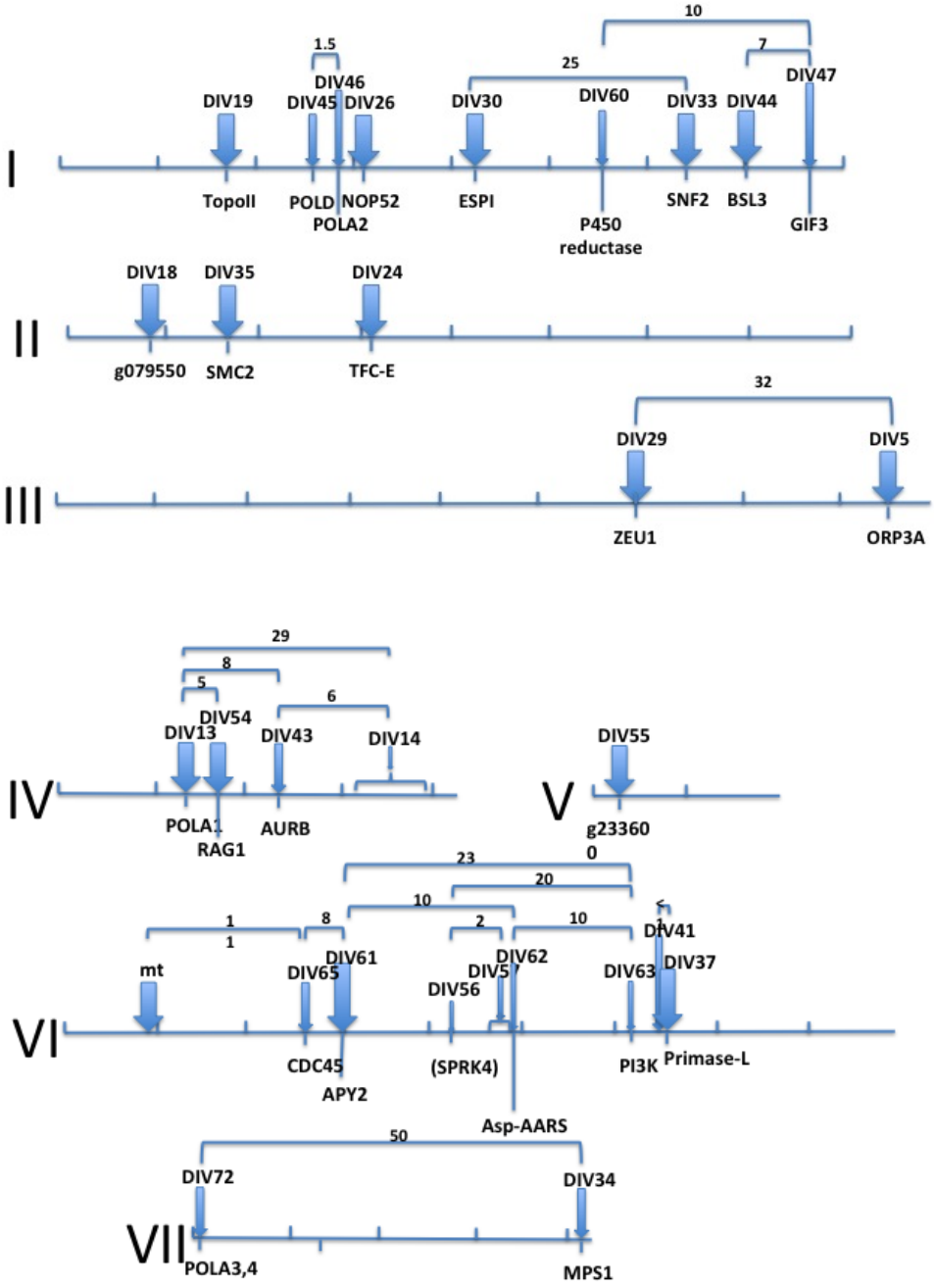

Figure A2: *DIV* genes, map positions

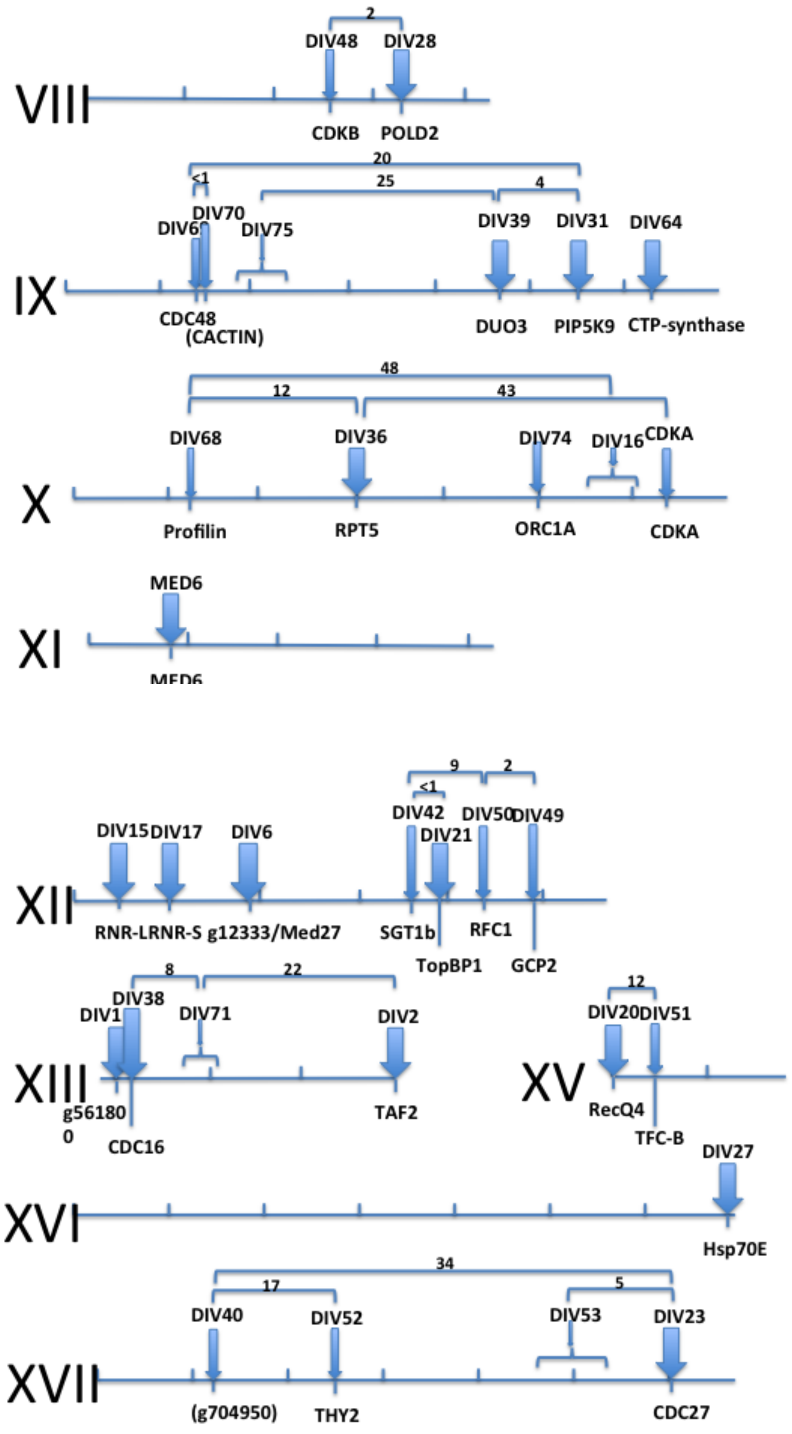

Figure A2: *DIV* genes, map positions

Appendix A3 Estimation of multiple alleles false positives rate

Suppose two mutants, A and B, each receive 100 missense mutations (typical numbers under our conditions of mutagenesis) randomly distributed between 17,000 gene models. Any given gene model is then the target of a missense mutation with 0.6% chance. So, given one particular such mutation in A, there is a 0.6% chance that the same gene model is hit in B. Conversely, there is a 99.4% chance that mutant B does not have this mutation. For 100 mutations, the chance that none of the mutations in mutant A are found in mutant B is $0.994^{100} = 0.55$, since the mutations in different strains are independent. The probability that at least one mutation is shared between the A and B mutants is thus 1 - 0.55 = 0.45. This would roughly be the chance that two independent genomes have a mutation in at least one common gene. Thus, a common hit is essentially uninformative. However, the pooled segregant strategy substantially reduces the probability. For two pools, consisting of only two segregants each, the expected overlap between the genomes is 1/16, due to random segregation. Assuming the 100 mutations are proportionally distributed, each pool would contain about six mutations uniformly present within this region. With 17,000 gene models in the *Chlamydomonas* genome, the region should contain on average 1062 genes, among which these six mutations would be distributed. Assume that mutant A has mutations in six different gene models, out of the 1062 total. That leaves 1056 gene models that can be hit in mutant B for no overlap. If the mutations are independent, the probability that all six mutations in B are different from the ones in A, is $(1056/1062)^6 = 0.97$. So with two pools made up of two segregants each, there is a

3% probability of a chance overlap. If the pools are made up of 8-10 strains, as in most of our experiments, only ~1% of the missense mutations would be in a common region, and the probability of a double hit becomes $1 - (169/170)^1 = 0.6\%$. Since we have assigned many fewer than 1/0.006=167 mutations in this way, it is very unlikely that there is an error in this list. (In many of these cases we also have sequence information for more than two alleles, as well, and a triple hit has negligible probability of occurring by chance).

Additionally, in many cases we have genetic mapping data (Figure 3.2) tightening the location of the causative mutation within the region of uniform SNPs; the mapping data are consistent with the assignments made. We conclude that even a single error in these assignments is quite unlikely.

Appendix A4 Estimating saturation of the screen

It is not possible to know with certainty how many ts lethals must be screened in order to have a good chance of covering most essential genes. Budding yeast has ~1000 essential genes (Giaever et al., 2002). In the absence of any additional information we can assume the *Chlamydomonas* number will be roughly similar. If all essential genes were equally mutable to temperature sensitivity, and assuming Poisson distribution, then any given essential gene will be in a collection of ~2,000 ts-lethals with probability 90%. Since ts lethals are about 1% of plated colonies under our conditions, this suggests a need to screen $2 * 10^5$ colonies to get high representation. Unfortunately, it is well known that not all genes mutate to temperature sensitivity at the same rate (although almost all genes are ultimately so mutable with a sufficient search). This naturally increases the number of colonies to be screened. For example, if 10% of genes are 10 times as mutable to ts as the other 90%, then of the 2000 ts lethal mutants, approximately 1000 will hit the highly mutable genes (which will get highly covered), and 1000 will be distributed among the remaining 90% of target genes. Thus, the number of ts lethals needed for the same level of saturation doubles. Also, the number of mutants needed for saturation increases in proportion to the number of target genes. *Chlamydomonas* has approximately 15,000 genes (Merchant et al., 2007), roughly three times as many as budding yeast. It seems possible that the number of essential genes will also be larger, by a factor of three. By this estimate, it is not unreasonable to assume that a couple of million colonies would to be screened to approach saturation. As mentioned in the main text, this thesis presents the

result of screening approximately 400,000 colonies, which would correspond to somewhere around 20% of the number needed for saturation. The fact that most mutants are single hits based on the complementation/recombination test (Chapter 2) is in line with the idea that many *div* mutants remain to be found.

Appendix A5 Table of annotated S-phase genes analyzed in Chapter 6

Table A1: Conserved genes with a likely function in S phase.

These genes were identified in cluster 2 (Figure 6.3), and show sharp increase in relative transcript abundance around 10 hours after lights-on in wild-type cultures (Figure 6.1). The average expression profile of these S-phase genes in wild-type and *cdk* mutant cultures in shown in Figure 6.5.

pre-RC	initiation factors	polymerases and repl. factors	chromatic cohesion/ condensation	nucleotide biosynthesis
Cre01.g023150 MCM5	Cre01.g029100 PSF2	Cre01.g017450 POLA2	Cre02.g086650 SMC2	Cre12.g491050 RNR2
Cre03.g163300 CDT1	Cre03.g161050 PSF1	Cre03.g202250 POLD3	Cre09.g412450 SCC1	Cre12.g492950 ATRNR1
Cre03.g178650 MCM6	Cre06.g251750 PSF3	Cre04.g214350 POLA1	Cre10.g440200 SMC5	Cre17.g715900 THY-2
Cre03.g199400 ORC2	Cre06.g270250 CDC45	Cre07.g337150 RFC2	Cre10.g445650 SMC3	
Cre06.g285650 ORC6	Cre07.g351400 MCM10	Cre08.g374050 POLD2	Cre12.g493400 SMC3	
Cre06.g292850 CDC6	Cre09.g393600 SLD5	Cre10.g424200 DPB2	Cre12.g525050 SMC6A	
Cre06.g295700 MCM3		Cre12.g521200 AtRFC1		
Cre07.g316850 MCM4		Cre12.g528200 DNA replication helicase		
Cre07.g355200 ORC5		Cre16.g679950 RFC3		
Cre10.g455850 MCM7		Cre17.g718850 RPA1A		
Cre17.g726500 ATORC4		g3729 2.7.7.7 POL2A		
g11180 ORC1A				
Cre07.g338000 MCM2				

Appendix A6 RNAseq basic statistics

We generated 50 bp single-end reads by sequencing cDNA libraries prepared from *Chlamydomonas* cultures (wild type, *cdka-1*, *cdkb-1* and *cdka-1/cdkb-1* double mutant cultures) sampled at different timepoints (see chapter 6). Around 10 million raw reads were generated from each sample (table A6-1). Base quality was even between samples (phred score above 30, Figure A6-1[1]). The raw reads were aligned by TopHat2.0.6 to the version 5 *Chlamydomonas* genome using the known transcripts from the version 5 gff3 file as a guide[2]. Read counts per gene model (17,737 total) were obtained using HTSeq[3]. The number of raw reads that could be mapped to the known gene models this way is shown in table A6-1 for the libraries used in this study. In most cases, around 90% of reads were aligned. Another 1-2% of reads typically aligned to the chloroplast or mitochondrial genomes, or to ribosomal RNA genes. The remaining raw reads could not be aligned for unknown reasons.

As figure 6.1 and 6.2 (chapter 6), and table A6-1 show, the data presented in chapter 6 comes from three separate experiments, with several overlapping time points. To get a sense of reproducibility, raw read counts (normalized by average read depth) for the 7 h,

---

1 The quality phred score for a base is $Q = -10\log_{10}(e)$, where e is the probability that the base is wrong. That is, a phred score of 30 implies that the probability that the base call is wrong is 1 in 1000.

2 http://genome.jgi.doe.gov/pages/dynamicOrganismDownload.jsf?organism=PhytozomeV10

3 http://www-huber.embl.de/users/anders/HTSeq/doc/overview.html

14 h and 16 h wild-type libraries were plotted and fitted to a straight line (Figure A6-2). The R^2 value indicates how well the straight line explains the variability in the data, with R^2=1 if the two libraries correlate perfectly, and R^2 close to zero for random data. Biological replicates have R^2 values above 0.9, indicating a high reproducibility. Readcount correlations between libraries prepared from wild-type cultures sampled at different timepoints have lower R^2 values: 0.71 between the t=7h/t=14h libraries and 0.56 between the t=7h/t=16h libraries (Figure A6-2). The correlation coefficients between all t7h, t14h and t16h libraries is shown in figure A6-3[4]. The distribution of the number of reads mapped was similar within biological replicates. Figure A6-4 shows, for the raw data (not normalized) the distribution of gene models with zero to ten mapped reads.

Taken toghether, these basic statistic analysis indicates that reproducibility within biological replicates is high, and that adjacent timepoints (t=14h, t=16h, during the S/M phase) are more similar to each other than to the mid-G1 samples (t=7h).

4 Correlation coefficients calculated as $R_{i,j}=C(i,j)/\sqrt{C(i,i)C(j,j)}$ where C(i,j) is the covariance between the two different libraries and C(i,i) and C(j,j) are the variances within each library.

Table A6-1: Reads generated by Illumina sequencing from three time courses.

reads reported: number of raw reads generated.

reads mapped to nuclear: number of raw reads that mapped to known gene models in the nuclear genome by TopHat.

mapped / total: fraction of mapped reads.

genotype: genotype of the strain used to prepare cDNA, and time of sampling (M10 is the wild-type strain used, see Methods).

timecourse 1	#reads reported	# reads mapped to nulcear	mapped / total	genotype
sample1	15,772,255	14,278,430	0.91	M10-0
sample2	14,797,575	13,414,482	0.91	M10-1
sample3	14,280,003	12,908,930	0.90	M10-5
sample4	14,197,998	12,763,833	0.90	M10-7
sample5	13,189,073	11,813,117	0.90	M10-12
sample6	11,790,338	10,669,558	0.90	M10-14
sample7	11,421,411	10,309,931	0.90	M10-16
sample8	15,167,908	13,552,820	0.89	M10-18
sample9	14,790,853	13,395,329	0.91	cdka t0
sample10	13,424,413	12,173,069	0.91	cdka t5
sample11	11,642,478	10,519,880	0.90	cdka t16
sample12	12,456,329	11,084,823	0.89	cdka t18

timecourse 2	#reads reported	# reads mapped to nulcear	mapped / total	genotype
sample1	12,728,287	11,314,061	0.89	M10-t14
sample2	14,592,914	13,041,490	0.89	M10-t15
sample3	12,287,157	10,973,845	0.89	M10-t16
sample4	15,126,411	13,614,793	0.90	M10-t18

timecourse 3	#reads reported	# reads mapped to nulcear	mapped / total	genotype
sample 1-1	13,942,967	12,732,926	0.91	M10-t2
sample 1-2	13,306,350	12,214,532	0.92	M10-t7
sample 1-3	14,341,531	13,042,727	0.91	M10-t10
sample 1-4	11,364,265	10,266,170	0.90	M10-t12
sample 1-5	11,350,840	10,192,010	0.90	M10-t14
sample 1-6	13,622,919	12,310,289	0.90	M10-t16
sample 1-7	12,806,277	11,565,734	0.90	cdka-t2
sample 1-8	11,229,063	10,108,316	0.90	cdka-t7
sample 1-9	12,773,722	11,560,337	0.91	cdka-t10
sample 1-10	10,556,066	9,465,793	0.90	cdka-t12
sample 1-11	13,221,351	11,874,398	0.90	cdka-t14
sample 1-12	11,337,674	10,168,650	0.90	cdkb-t16
sample 2-1	11,463,504	9,166,685	0.80	cdkb-t2
sample 2-2	10,975,375	9,931,077	0.90	cdkb-t7
sample 2-3	12,247,956	10,989,003	0.90	cdkb-t10
sample 2-4	10,584,288	8,702,170	0.82	cdkb-t12
sample 2-5	8,892,580	7,881,856	0.89	cdkb-t14
sample 2-6	12,172,520	10,988,888	0.90	cdkb-t16
sample 2-7	10,685,120	9,502,367	0.89	cdk_ab-t2
sample 2-8	9,281,884	8,305,823	0.89	cdk_ab-t7
sample 2-9	11,171,844	10,028,887	0.90	cdk_ab-t10
sample 2-10	9,840,373	9,375,224	0.95	cdk_ab-t12
sample 2-11	10,371,449	9,269,070	0.89	cdk_ab-t14
sample 2-12	10,448,379	9,392,229	0.90	cdk_ab-t16

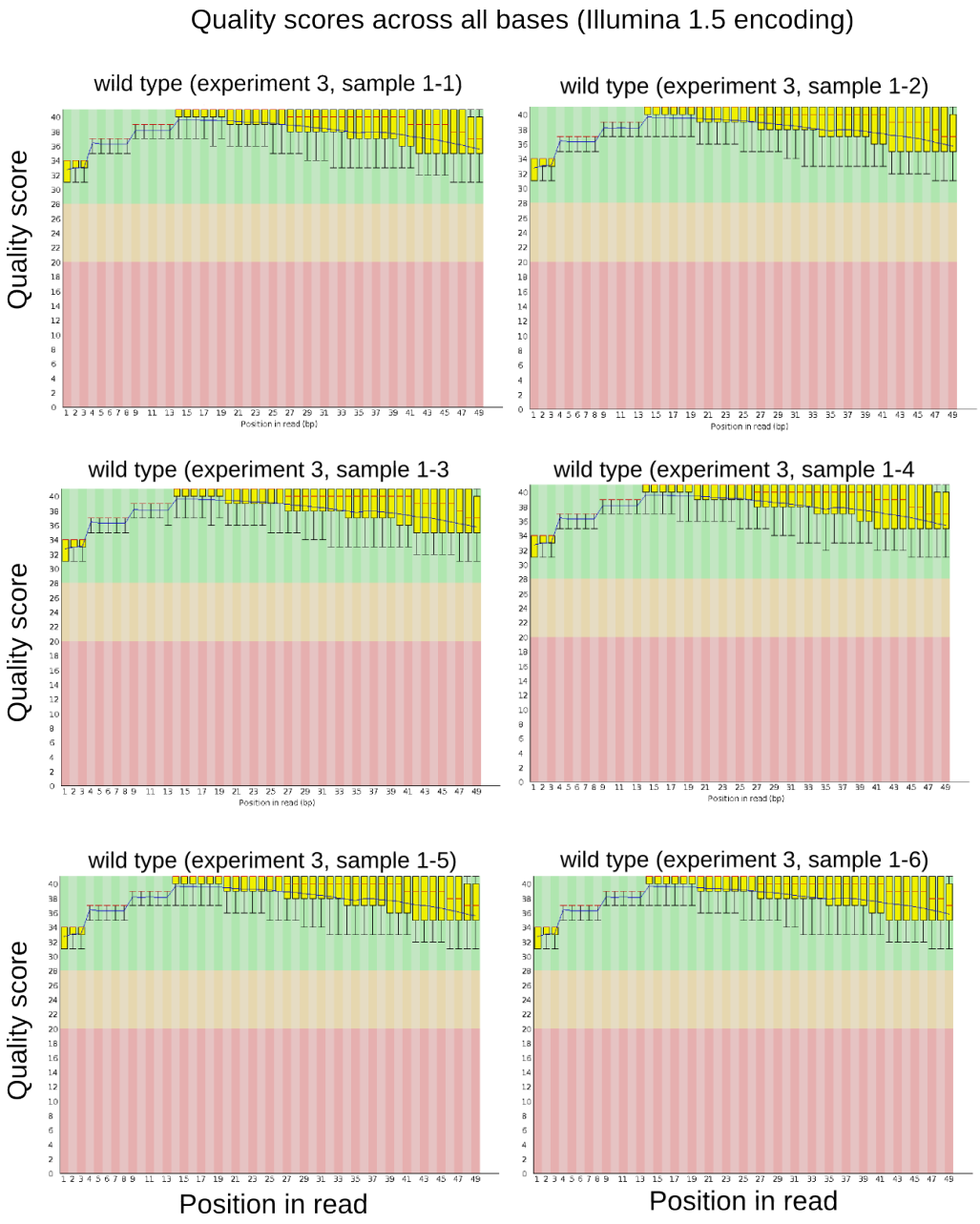

Figure A6-1: Base quality scores for six wild-type libraries (see table A6-1).

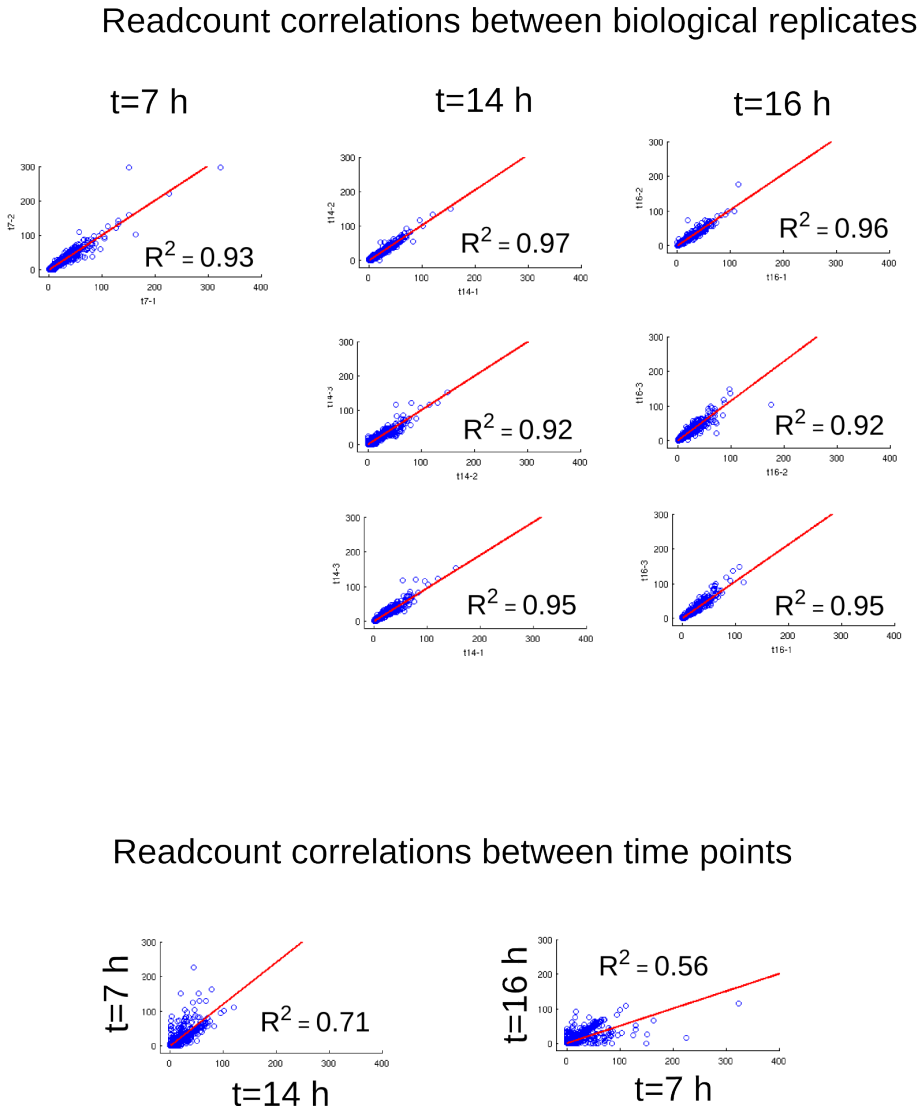

Figure A6-2: Correlation between biological replicates (top) sampled at t=7h, t=14h and t=16h. Correlation between samples from different timepoints (bottom).

	t7-1	t7-2	t14-1	t14-2	t14-3	t16-1	t16-2	t16-3
t7-1	1.00	0.96	0.85	0.82	0.87	0.75	0.78	0.72
t7-2		1.00	0.83	0.81	0.87	0.74	0.76	0.73
t14-1			1.00	0.99	0.97	0.95	0.93	0.93
t14-2				1.00	0.96	0.95	0.93	0.95
t14-3					1.00	0.91	0.90	0.91
t16-1						1.00	0.98	0.98
t16-2							1.00	0.96
t16-3								1.00

Figure A6-3: Correlation coefficients within and between biological replicates. Correlation coefficients of normalized readcounts were calculated for samples prepared at t=7h, t=14h and t=16h. Correlation coefficients within biological replicates (>0.9) are highlighted.

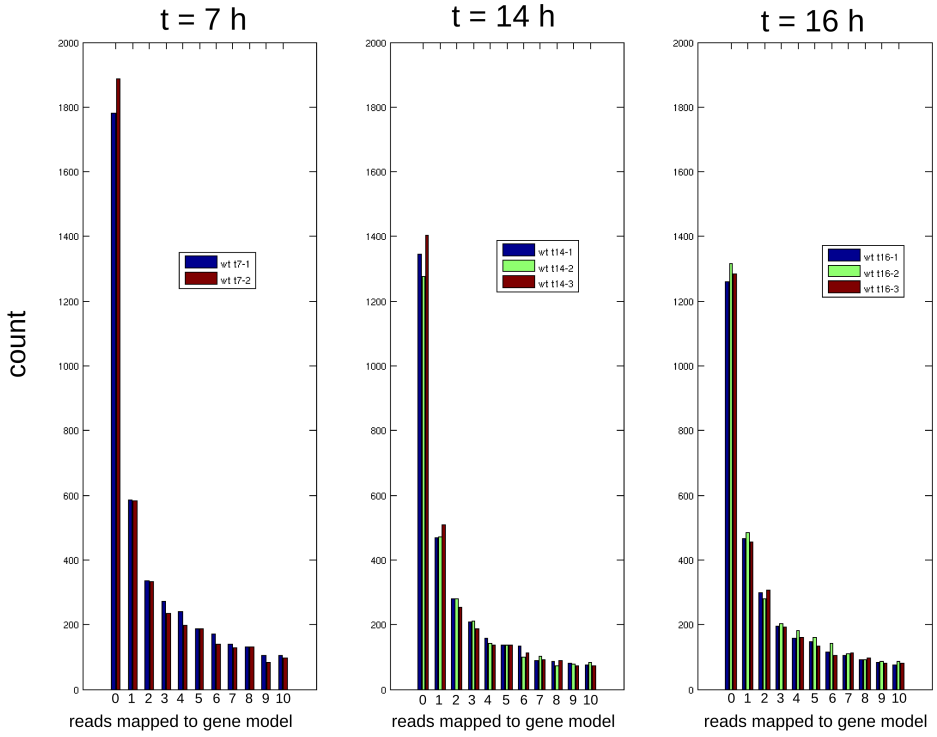

Figure A6-4: Histograms showing gene models with zero to ten mapped reads in biological replicates prepared from cells sampled at t=7h, t=14h and t=16h.

Appendix A7 Methods

Chlamydomonas reinhardtii Strains and Media

Isogenic wild-type strains M10 (mt -) and P10 (mt+) were used for mutagenesis. These were constructed by Dr. Susan Dutcher by sequential introgression of CC-125 into CC-124 ten times, and generously provided to us. S1D2 was obtained from the *Chlamydomonas* Resource Center (University of Minnesota, St Paul, MN, USA). TAP culture medium prepared as in (Harris, 2008). Mating medium for inducing gametogenesis was prepared as described in (Dutcher, 1995). Throughout the thesis, wild type refers to M10 or P10 cells.

Culturing conditions and time-course experiments

Cells were cultured in liquid TAP medium or on TAP agar plates. For time-course experiments in liquid TAP cultures, we pre-cultured the cells in TAP at permissive temperature under 14h/10h light/dark cycles (50 umol photons s-1 m-2) in glass flasks. At the start of the time-course, each culture was diluted to OD750=0.05 and shifted to a restrictive temperature (33ºC) shaking water bath, equipped with four 150 W compact fluorescent bulbs. The measured light intensity at the level of the cultures was about 15000 lux, corresponding to a photosynthetically active radiation (PAR) photon flux of about 195 umol photons s-1 m-2. This procedure resulted in partial synchronization of wild-type cells, as indicated by an enrichment of dividing cells between 14-16 hours

(light microscopy) and cells with higher order DNA content (FACS). To obtain time-course data, the cultures were sampled at regular intervals over 18-27 hours for determination of cell volume, DNA content, and Cks1-precipitable kinase activity, and microscopic imaging.

We discovered that wild-type synchrony could be greatly improved by incubation on TAP agar plates. Cells were pre-grown in liquid TAP cultures to a density of 10^6 cells/mL, and then spread evenly on agar plates, one for each time-point. After 1-2 days of pre-growth a 21ºC, the plates were incubated at restrictive temperature (33ºC) at 65 umol photons s-1 m-2. A majority of wild-type cells (~90%) were reproducibly in S/M phase after 11 hours. Cells were harvested by washing the plate with 10 mL of pre-warmed TAP medium and scrubbing gently with a glass pipette tip. We suspect that the even illumination and aeration of the cells is the reason for the fast and uniform growth of the cells on agar compared to liquid cultures, leading to faster cycling time and increased population synchrony.

Mutagenesis

An M10 or P10 culture was grown to OD750 = 0.1 in TAP medium. 25 mL was exposed to a G30T8 UV-bulb for 3-3.5 min, or 0 min for control cells, while shaking, then wrapped immediately in tin foil and incubated at 21ºC, 12 h to fix UV-induced mutations. At this point, viability test-plates were made using a 384-pin replica tool (V&P Scientific). The replica pinner made 384 spots of about 150 ul, containing about 100 cells

each. These plates were incubated at 33ºC for 20 hours, while the original UV-exposed culture was maintained in the dark. After 20 hours, the number of viable cells per pin-spot on the test plate was estimated. It was determined that untreated wild-type cells underwent one cell cycle to form a microcolony of at least 8 cells during this 20 hour incubation. Thus, the density of viable cells in the UV-exposed culture was estimated by counting 8-celled microcolonies in 40-50 spots and averaging. Next, a suitable dilution of the UV-exposed culture was prepared such that pinning to agar with the 384-pin tool gave, on average, 1 viable cell per pin-spot. Each agar plate was pinned 4 times for a total 1536 spots. Since each pin-spot was seeded with 1 viable cell, on average, this procedure yielded a maximum of 400-500 individual mutagenized colonies per plate. (An equal number of spots would be unoccupied or be seeded by more than one viable cell.) The seeded agar plates were incubated at permissive temperature (21ºC) for 7-9 days to let colonies form. Colonies were then picked robotically by the Hudson Robotics (Hudson Robotics) colony picker into 384-well plates filled with TAP medium. The picker uses automatic image analysis to only pick colonies that are round enough to likely derive from a single cell. The 384-well plates were incubated at permissive temperature for 7 days. At this point, replica plates were made with the pinning tool and incubated for 6 days at permissive (21ºC) and 3 days at restrictive (33ºC) temperature. Temperature sensitive (ts) mutants were scored either manually, or by comparing images of the 21/33ºC pair using custom MATLAB code. This yielded a set of primary ts-mutants at a frequency of about 1-5% of mutagenized survivors.

Time-lapse microscopy

To analyze the cellular phenotypes, all primary ts mutants were incubated in 96-well plates filled with TAP medium and pre-grown at 21ºC for 2 days. 10 ul of each micro-culture was transferred to a TAP agar plate using a 96-pin replica tool (V&P Scientific). The agar plate was imaged after 0, 10, 20 and 40 hours at restrictive temperature on a Leica DMIRE2 microscope with a 10x/0.25 N.A brightfield objective, in a temperature control chamber and a motorized stage for precise revisiting of positions. Images were collected with a Canon EOS Rebel T2i. The vast majority of ts mutants fell into one of six phenotypic categories (see main text). Only classes 5 and 6, making up about 5% of total ts mutants, were considered *div* mutants.

Genetic analysis and complementation/recombination testing

Genetic crosses were carried out as described in (Dutcher, 1995) with the following modifications. After zygospores had matured on a 1.5% agar TAP plates, unmated cells were scraped away with a sharp razor blade. Then 200 ul M-N/5 medium was applied to the plate and zygospores were detached from the agar surface using a roughened razor blade. The resuspended zygospores were transferred to a new agar plate and incubated at permissive temperature for 20 hours in constant illumination. When the spores had undergone meiosis, they were dissected on a Zeiss Axioscope 40 microscope, equipped with a dissection microneedle.

Each *div* mutant was backcrossed to M10 or P10. This served three purposes. First, it allowed us to assess segregation of the *div* phenotype. In most cases we observed 2:2 segregation. Second, we could isolate the original *div* mutation in both mating types (mt- and mt+) for complementation/recombination testing. Third, we could isolate between 10-12 *div* segregants from each cross for bulked segregant DNA preparation and sequencing (see below).

To asses allelism between different div-mutants, we devised a recombination/complementation test that would allow us to prepare a large number of crosses in parallel and score recombination between *div* alleles in the meiotic progeny. When crossing *Chlamydomonas*, only a minority of mated cells produce vegetative diploid cells (Dutcher, 1995), and the remainder enter the meiotic program. Thus, our assay represents to a large degree linkage between different *div* genes. We did not determine the relative contributions of wild-type recombinants versus complementing diploids.

The complementation test was performed by inoculating 5 mL M-N/5 mating medium with mt- and mt+ versions of each *div* mutant separately for 12 hour incubation at 21^{o}C in continuous illumination to let the cells undergo gametogenesis. Each mt- strain was crossed to each mt+ strain in several 96-well plates, using a Multi-drop plate filler (Thermo Scientific). This way, between 500-1000 crosses could be prepared in parallel. After 1.5 hours mating, 10 ul of each cross was spotted on agar using a 96-channel pipette (Rainin, Cat. no. LIQ-96-200) in duplicates. One copy was incubated for 5 days at

restrictive temperature under continuous illumination, and the other for 5 days at permissive temperature in the dark. In parallel, each *div* parent was spotted at restrictive temperature as a control. Generally, *div* parents were completely lethal at restrictive temperature, as were self-crosses between the same *div* mutation in opposite mating types (Figure 4.5). Two different *div* mutants were considered allelic if (i) both reciprocal crosses failed to produce colonies at restrictive temperature, and (ii) zygospores were produced on the dark-plate, indicating successful mating.

The spots contained around 10^4 cells each. Mating efficiency varied greatly, as determined by counting quadriflagellated cells. Thus, the number of cells that made up the signal in the assay varied between crosses. With 10% mating (a fairly typical number), about 1000 cells have mated and have a chance to recombine to form wild-type recombinants, or produce complementing diploid cells. Thus, complete failure to reconstitute wild-type growth at restrictive temperature through recombination indicates linkage at ~0.1 cM for the most part.

Isolation of revertants

Revertants were isolated by growing 50 mL of a given original mutant to OD_{750} ~ 0.1 (in total around $5*10^7$ cells). The cells were spun down and resuspended in fresh TAP medium and plated on agar, ~1 mL per plate. The plates were exposed to UV light from the G30T8 bulb as above. Immediately after UV exposure, the plates were wrapped in tin foil and placed at 21°C for ~12 hours. At this point, the foil was removed and revertants

were selected at 33ºC. DNA was prepared directly from the colonies by placing a small amount of cells in 17 uL d-H_2O, 2 uL 10x Vent buffer (200 mM Tris-HCl pH 8.8, 100 mM KCl, 100 mM $(NH_4)_2SO_4$, 20 mM $MgSO_4$, 1% Triton-X-100), 1 uL proteinase K, and heating in a thermal cycler 1 h at 58ºC, 30 min at 95ºC. 1 uL of the DNA preparation was used for PCR reactions using PuReTaq beads (GE Healthcare, Cat. No. 27-9557-02) with gene-specific primers designed using the online NCBI primer-BLAST tool (http://www.ncbi.nlm.nih.gov/tools/primer-blast/). The PCR product, containing the mutated residue was sequenced by Sanger sequencing.

target gene	PRIMER NAME	sequence (5' -> 3')	product size
Cre10.g465900	CDKA-for	CCAGAACCTTGCGCGCTCGT	438
	CDKA-rev	CCGTCACGCCGCCCTGTATT	
g11589	MED6-for	CCGCGCCTCTGTGTTGTTCA	401
	MED6-rev	ACGGCACGGTGTCTGTGACT	
Cre07.g341700	MPS1-for	TCATCCGGCTGTACTGGCAGC	411
	MPS1-rev	GCGCAAGACACCACGACAGG	
g1886	TFCE2-FOR	GTGGCAGGCGGGAATAAG	198
	TFCE2-REV	TCTGTCCAGCTCGTTGACAC	
Cre13.g562950	APC6-for	GCAACCCTACGGCGAGCTGA	406
	APC6-rev	GGTCAGTGCCTGTACCCGCT	
g9842	DUO3-for	TGCTGTTAACGCCTGACCGC	185
	DUO3-rev	TGCATGGCGACAGCCAGGAG	
Cre01.g050850	BSL1-for	CCAGCCCTGTCCCCAGGC	200
	BSL1-rev	CACCGACTGAGACTCGGCCC	
Cre08.g372550	CDKB-for	GCCCAGCTTCCAGCCGTAGT	196
	CDKB-rev	GGACCACATGTCCACGGGGG	

DNA preparation for genome sequencing

To prepare DNA for bulk segregant pooled sequencing, each *div* mutant was backcrossed to M10 or P10 and 10-12 ts segregants were isolated. These were incubated on TAP agar plates until a dense patch had grown up. At this point all segregants were combined in one 200 mL TAP culture, incubated for 1-2 days or until OD750 was ~ 0.5. The cells were collected by centrifugation and resuspended in 8 mL TEN buffer (10 mM Tris, 10 mM EDTA, 150 mM NaCl, pH 8) with 0.5% SDS and 0.1 mg/mL proteinase K. The lysis mixture was heated to 50^{o}C for 2 hour, with sonication to break open the cells after 1 hours. Extraction twice with 16 mL phenol:chloroform. Aqueous phase was transferred to 50 mL tube and precipitated with 16 mL 100% ethanol. The precipitate was rinsed with 70% ethanol and resuspended in TE buffer (10 mM Tris, 1mM EDTA, pH 8). Next, NaCl was added to 1M final concentration, and the solution extracted again with phenol-chloroform. The aqueous phase was transferred to an eppendorf tube and precipitated with 1 mL 100% ethanol, washed in 70% ethanol and resuspended in 200 ul TE. RNAse was added and the mixture was incubated at 37oC for 1h. Concentration estimate by nanodrop was about 600 ng/ul at this point. To further purify the DNA, we used the Qiaex Gel Extraction Kit (Qiagen Cat. no. 20021) according to manufacturers instructions. Total amount of high molecular weight DNA recovered was roughly 1mg by gel estimate. The DNA was fragmented by sonication (Covaris S2 Focused Ultrasonicator) to get get an average fragment length of 300 bp. After fragmentation, 5 ug of sonicated DNA was end-repaired (New England Biolabs, End Repair Module, E6050) and dA-tailed (New

England Biolabs, dA-tailing Module, E6053) according to manufacturers instructions. Illumina sequencing adapters (TruSeq DNA LT Sample Prep Kit, Ilumina) were ligated to dA-tailed DNA by Quick ligase (New England Biolabs, Quick Ligation Kit, M2200). Finally, adaptor-ligated DNA was run on a 1.3% agarose TAE gel and fragments between 300-600 bp excised and extracted (Qiagen Gel extraction, Cat. no. 28704). DNA concentration estimated by NanoDrop (Thermo Scientific) and by gel was usually between 2-10 ng/ul. For multiplex DNA sequencing, samples with different indices were pooled with equal representation based on the concentration estimates. Typically 7 samples were pooled and sequenced in one lane. Sequencing, 100 bp paired-end, was carried out on an Illumina HiSeq2000 instrument by Beijing Genomics Institute (BGI, Hong Kong).

FACS and Coulter Counter analysis

The equivalent of 10 mL culture, OD750~0.05 was spun down and resuspended in EtOH:HAc 3:1 and incubated at room temp. for 2 hours. Cells were then spun down, washed once in 5 mL PBS and resuspended in 2 mL PBS with RNAse, 2 h at 37^{o}C, spun down again and resuspended in PBS + 500 nM Sytox Green (Invitrogen Cat. no. C34858). FACS analysis was carried out on either a BD FACSCalibur or a BD Accuri C6 instrument (BD Biosciences), equipped with a 488 nm laser. For analysis, a FSC/SSC gate was applied and FL-1 fluorescence plotted as a histogram. The scatter profile was useful for following cell growth and division, with a clear separation between small

newborn (low FSC and SSC) and large dividing (high FCS and SSC) cells. Assignment of cell populations representing 1C, 2C, 4C, 8C and 16C DNA content was determined based on wild-type cells. Frequently, the population of 1C-cells was split into two closely spaced peaks at the beginning of the time-course. The two peaks corresponded to two cell populations with different side scatter (SSC) and likely reflected different-sized daughter cells that could result from the multiple fission cell division mechanisms of *Chlamydomonas*. The SSC and fluorescence of the 1C-populations drifted towards higher values through-out the time-course. DNA replication was seen as an increase in a distinct population of 2C-cells that appeared between 12-16 hours. Shortly after the appearance of FACS peaks corresponding to dividing cells, the low SSC 1C-cells population started to increase, indicating release of newborn daughter cells. After 16 hours, >80% of cells were found in this population, indicating that most cells had completed cell division.

Cell volume data was obtained by fixing cells in 1% glutaraldehyde and using the Z2 Coulter Counter (Beckman Coulter).

Fluorescence microscopy and immunostaining

For indirect immunofluorescence, cell were spun down and resuspended in microtubule stabilizing buffer (MT buffer: 30 mM Tris-acetate, 5 mM MgSO4, 5 mM EDTA, 25 mM KCl, 1 mM dithiothreitol, pH 7.4) and then adhered to poly-L-Lysine (Sigma Cat. no. P4707) coated coverslips for 5 min. Excess liquid was removed and cells were fixed in ice cold methanol, 20 min. Coverslips were rehydrated in PBS, 5 min and blocked in PBS

+ 5% newborn goat serum, 1 h at room temp. The coverslips were incubated 12 h at 4ºC with a monoclonal anti-α-tubulin antibody produced in mouse (Sigma-Aldrich, clone B512) at a 1:500 dilution in PBS. Next, the coverslips were washed three times in PBS and incubated with a secondary anti-mouse antibody coupled to the Alexa 568 fluorophore (Invitrogen, Cat. no. P36930), 1 h at room temp in the dark. Coverslips were then washed three times in PBS, incubated 30 min in PBS + 500 nM Sytox Green, then washed once in PBS. Imaging was performed on a Zeiss Axioplan 2 microscope with a Zeiss PLAN APOCHROMAT 63x/1.40 N.A. Oil DIC objective, equipped with an AttoArc HBO 100W mercury arc bulb. Images were collected with a Hamamatsu CCD camera (Hamamatsu, C 4742-95). A filter cube for FITC was used to acquire Sytox Green fluorescence and a filter cube for CY3 was used for Alexa 568 fluorescence. Stacks of 5-7 images were collected and merged using the Openlab acquisition software.

Cks1-precipitable kinase assay

For determination of Cks1-precipitable kinase activity, 20 mL of OD750=0.05 culture was used. The cell suspension was added to crushed ice to cool rapidly, spun down and resuspended in 1 mL ice-cold water, then spun down again and the liquid aspirated off. The pellet was stored at -80ºC until all samples were collected. Cells were mixed with 400 υλ acid washed glass beads (Sigma, Cat. no. G8772) and 400 υλ LSHNN buffer (50 mM NaCl, 10 mM HEPES, 10% glycerol, 0.1% NP-40, pH 7.5) with protease and phosphatase inhibitors Aprotinin 100 υλ/mL (Sigma Cat no. A6279), PMSF 0.5 mM

leupeptin/pepstatin 0.01 mg/mL, NaPPi 10 mM. Cells were lysed using a FastPrep (Thermo Scientific) vortexer, and extracts cleared by centrifugation. Total protein sample collected by adding 20 ul of the cleared lysate to 40 ul sample buffer and heating at 95ºC, 5 min. The remaining lysate was bound to Cks1-GST beads, 1h rotating at 4ºC. The beads had been prepared by expressing and in-frame fusion of *Chlamydomonas* Cks1-GST construct in E. coli, and covalently linking the purified protein to dynabeads functionalized with epoxy groups (Invitrogen, Cat. no. 14302). The beads were washed 4 times with LSHNN buffer, twice with HSN buffer (250 mM NaCl, 10 mM HEPES, 10% glycerol, 0.1% NP-40, pH 7.5) and once with kinase buffer (10 mM HEPES, 10 mM MgCl2, 1 mM DTT, pH 7.5). Finally, beads were resuspended in 60 ul kinase buffer. Kinase reactions were performed by adding 15 ul of the beads to a mixture of 1 υλ [g-32P]ATP (NEN Radiochemicals, Cat. no. BLU502A001MC), 1ul d-H2O, 1 υλ histone H1 (2mg/ml; Roche Applied Science, Cat. no. 10223549001) and 2 ul of 50 μM ATP (Jena Bioscience, Cat. no. NU-1173). The kinase reactions were incubated at 30oC, 10 min with shaking every 2-3 minutes. The reactions were stopped by adding 20 υλ 2x sodium dodecyl sulfate (SDS) sample buffer and heating to 95ºC, 5 min. Kinase reaction samples and total protein samples were run on Tris-HCl 4-15% gradient gels. The kinase gel was exposed to film and developed. The total protein gel was stained with commassie brilliant blue. For quantification, histone H1 was transferred to a polyvinyl diffluoride membrane and exposed to a storage phosphor screen (Molecular Dynamics), and imaged on an Amersham Biosciences Typhoon 9400 Variable Imager. To quantify signal intensity,

a box was drawn around the histone H1 band, and an equal sized box was placed just above the band to quantify the background. The reported intensity is the difference in total intensity between signal and background.

Sequence analysis and alignment

Sequenced reads were aligned to the published *Chlamydomonas* genome (Phytozome v5.3) using bowtie2.0.6 (Langmead and Salzberg, 2012). Identification of SNPs was carried out by custom written awk and MATLAB scripts.

Preparation of cDNA and sequencing

A volume of *Chlamydomonas* liquid culture, normalized by OD to correspond to 30 ml of an OD_{750} = 0.05 culture, was collected for each time point and added to crushed ice. Cells were spun down and washed once with water. The pellet was lyzed in TriZol (Life Technologies, Cat. No 10296) according to manufacturer's instructions. RNA integrity was assessed on a Agilent 2100 Bioanalyzer, and RNA concentration was measured by NanoDrop (Thermo Scientific). By this estimate, 2 ug total RNA was used to prepare cDNA libraries using the TruSeq RNA kit (# 15026495) from Illumina according to manufacturer's instructions. Size distribution of adapter-ligated cDNA was centered around 260 bp, as determined on a 2200 TapeStation (Agilent Technologies). 12 cDNA libraries, with different bar codes were pooled in equal proportions by NanoDrop estimate and sequenced in one lane on a HiSeq2000 instrument (Illumina) by Beijing Genomics

Institute (BGI, Hong Kong), using 50 bp single-end reads. Alignments to the reference genome was done by TopHat (Kim et al., 2013), with the published genome (Phytozome v5.3) annotation as a guide, generating between 10-14 million mapped fragments per library, distributed over the 17737 gene models. Read counts per gene model were obtained using the HTSeq software (http://www-huber.embl.de/users/anders/HTSeq/doc/overview.html). For basic statistics about cDNA libraries used in this study see Appendix A6.

Data pre-treatment and normalization for transcriptome analysis

The raw read-count data per gene model was normalized in two ways. First, the read counts in each library were normalized by the average read count for that library. Second, the read counts for each gene was normalized by the average read count across all libraries. The first normalization accounts for differences in read depth between libraries. The second normalization standardizes the average expression for each gene to one. Finally, the normalized values were log2-transformed to make fold-changes symmetric around zero. In the main text, 'relative transcript abundance' is used to refer to increases or decreases in a particular gene, relative to its average value across all libraries. Thus, genes that change in expression in a similar pattern, but with different absolute number of reads mapped, will appear similar in the analysis. It should be pointed out that, since the total number of RNA molecules sampled is similar for all libraries, this simple normalization is sensitive to the differences in composition between libraries. For

example, consider two samples A and B, where all transcripts present in sample A are also present in sample B. If, however, sample B contains additional transcript molecules, not present in sample A, then the fixed read depth (through RNA input equalization and library size normalization) will result in under-sampling of the shared transcripts. In the analysis, this would appear as a reduction in relative transcript abundance for the under-sampled transcripts. This effect is expected to be minor, provided that the bulk of transcripts vary little between strains or conditions. This situation seems to apply here (Figure 6.3).

References

Adams, J., Kelso, R., and Cooley, L. (2000). The kelch repeat superfamily of proteins: propellers of cell function. Trends Cell Biol. **10**: 17–24.

Adams, K.L. and Wendel, J.F. (2005). Polyploidy and genome evolution in plants. Curr. Opin. Plant Biol. **8**: 135–41.

Aparicio-Fabre, R., Guillén, G., Estrada, G., Olivares-Grajales, J., Gurrola, G., and Sánchez, F. (2006). Profilin tyrosine phosphorylation in poly-L-proline-binding regions inhibits binding to phosphoinositide 3-kinase in Phaseolus vulgaris. Plant J. **47**: 491–500.

Backues, S.K., Korasick, D. a, Heese, A., and Bednarek, S.Y. (2010). The Arabidopsis dynamin-related protein2 family is essential for gametophyte development. Plant Cell **22**: 3218–31.

Baldwin, K.L., Dinh, E.M., Hart, B.M., and Masson, P.H. (2013). CACTIN is an essential nuclear protein in Arabidopsis and may be associated with the eukaryotic spliceosome. FEBS Lett. **587**: 873–9.

Bäurle, I. and Laux, T. (2003). Apical meristems: the plant's fountain of youth. Bioessays **25**: 961–70.

Beach, D., Durkacz, B., and Nurse, P. (1982). Functionally homologous cell cycle control genes in budding and fission yeast. Nature **300**: 706–709.

Bell, S.P. and Dutta, A. (2002). DNA replication in eukaryotic cells. Annu. Rev. Biochem. **71**: 333–74.

Bertoli, C., Skotheim, J.M., and de Bruin, R. a M. (2013). Control of cell cycle transcription during G1 and S phases. Nat. Rev. Mol. Cell Biol. **14**: 518–28.

Bishop, a C. et al. (2000). A chemical switch for inhibitor-sensitive alleles of any protein kinase. Nature **407**: 395–401.

Bisova, K., Krylov, D., and Umen, J. (2005). Genome-wide annotation and expression profiling of cell cycle regulatory genes in Chlamydomonas reinhardtii. Plant Physiol. **137**: 475–491.

Blow, J.J. and Dutta, A. (2005). Preventing re-replication of chromosomal DNA. Nat. Rev. Mol. Cell Biol. **6**: 476–86.

Bodenmiller, B., Mueller, L.N., Mueller, M., Domon, B., and Aebersold, R. (2007). Reproducible isolation of distinct, overlapping segments of the phosphoproteome. Nat. Methods **4**: 231–7.

Boos, D., Frigola, J., and Diffley, J.F.X. (2012). Activation of the replicative DNA helicase: breaking up is hard to do. Curr. Opin. Cell Biol. **24**: 423–30.

Boudolf, V. et al. (2009). CDKB1;1 forms a functional complex with CYCA2;3 to suppress endocycle onset. Plant Physiol. **150**: 1482–1493.

Bracken, A.P., Ciro, M., Cocito, A., and Helin, K. (2004). E2F target genes: unraveling the biology. Trends Biochem. Sci. **29**: 409–17.

Brownfield, L., Hafidh, S., Durbarry, A., Khatab, H., Sidorova, A., Doerner, P., and Twell, D. (2009). Arabidopsis DUO POLLEN3 is a key regulator of male germline development and embryogenesis. Plant Cell **21**: 1940–56.

Brueggeman, A.J., Gangadharaiah, D.S., Cserhati, M.F., Casero, D., Weeks, D.P., and Ladunga, I. (2012). Activation of the carbon concentrating mechanism by CO2 deprivation coincides with massive transcriptional restructuring in Chlamydomonas reinhardtii. Plant Cell **24**: 1860–75.

De Bruin, R. a M., McDonald, W.H., Kalashnikova, T.I., Yates, J., and Wittenberg, C. (2004). Cln3 activates G1-specific transcription via phosphorylation of the SBF bound repressor Whi5. Cell **117**: 887–98.

Carmena, M. and Earnshaw, W.C. (2003). The cellular geography of aurora kinases. Nat. Rev. Mol. Cell Biol. **4**: 842–854.

Castillo, A.R., Meehl, J.B., Morgan, G., Schutz-Geschwender, A., and Winey, M. (2002). The yeast protein kinase Mps1p is required for assembly of the integral spindle pole body component Spc42p. J. Cell Biol. **156**: 453–65.

Champoux, J.J. (2001). DNA topoisomerases: structure, function, and mechanism. Annu. Rev. Biochem. **70**: 369–413.

Cheeseman, I.M. and Desai, A. (2008). Molecular architecture of the kinetochore-microtubule interface. Nat. Rev. Mol. Cell Biol. **9**: 33–46.

Churchman, M.L. et al. (2006). SIAMESE, a plant-specific cell cycle regulator, controls endoreplication onset in Arabidopsis thaliana. Plant Cell **18**: 3145–57.

Classon, M. and Harlow, E. (2002). The retinoblastoma tumour suppressor in development and cancer. Nat. Rev. Cancer **2**: 910–7.

Coleman, A. (1982). THE NUCLEAR CELL CYCLE IN CHLAMYDOMONAS (CHLOROPHYCEAE). J. Phycol. **18**: 192–195.

Corellou, F., Camasses, A., and Ligat, L. (2005). Atypical regulation of a green lineage-specific B-type cyclin-dependent kinase. Plant Physiol. **138**: 1627–1636.

Craigie, R. and Cavalier-Smith, T. (1982). Cell volume and the control of the Chlamydomonas cell cycle. J. Cell Sci. **191**: 173–191.

Cross, F.R. (2003). Two redundant oscillatory mechanisms in the yeast cell cycle. Dev. Cell **4**: 741–52.

Cross, F.R., Buchler, N.E., and Skotheim, J.M. (2011). Evolution of networks and sequences in eukaryotic cell cycle control. Philos. Trans. R. Soc. Lond. B. Biol. Sci. **366**: 3532–44.

Cui, X., Fan, B., Scholz, J., and Chen, Z. (2007). Roles of Arabidopsis cyclin-dependent kinase C complexes in cauliflower mosaic virus infection, plant growth, and development. Plant Cell **19**: 1388–402.

Derelle, E. et al. (2006). Genome analysis of the smallest free-living eukaryote Ostreococcus tauri unveils many unique features. Proc. Natl. Acad. Sci. U. S. A. **103**: 11647–52.

Diaz-Trivino, S., del Mar Castellano, M., de la Paz Sanchez, M., Ramirez-Parra, E., Desvoyes, B., and Gutierrez, C. (2005). The genes encoding Arabidopsis ORC subunits are E2F targets and the two ORC1 genes are differently expressed in proliferating and endoreplicating cells. Nucleic Acids Res. **33**: 5404–14.

Dieckmann, C.L. (2003). Eyespot placement and assembly in the green alga Chlamydomonas. Bioessays **25**: 410–6.

Dissmeyer, N., Weimer, A.K., Pusch, S., De Schutter, K., Alvim Kamei, C.L., Nowack, M.K., Novak, B., Duan, G.-L., Zhu, Y.-G., De Veylder, L., and Schnittger, A. (2009). Control of cell proliferation, organ growth, and DNA damage response operate independently of dephosphorylation of the Arabidopsis Cdk1 homolog CDKA;1. Plant Cell **21**: 3641–54.

Doherty, C.J. and Kay, S. a (2010). Circadian control of global gene expression patterns. Annu. Rev. Genet. **44**: 419–44.

Donnan, L. and John, P. (1983). Cell cycle control by timer and sizer in Chlamydomonas. Nature **304**: 630–633.

Dorrell, R.G., Butterfield, E.R., Nisbet, R.E.R., and Howe, C.J. (2013). Evolution: unveiling early alveolates. Curr. Biol. **23**: R1093–6.

Dutcher, S.K. (1995). Mating and tetrad analysis in Chlamydomonas reinhardtii. Methods Cell Biol. **47**: 531–40.

Dyson, N. (1998). The regulation of E2F by pRB-family proteins. Genes Dev. **12**: 2245–

2262.

Ebel, C., Mariconti, L., and Gruissem, W. (2004). Plant retinoblastoma homologues control nuclear proliferation in the female gametophyte. Nature **429**: 776–80.

Edgar, B. a and Orr-Weaver, T.L. (2001). Endoreplication cell cycles: more for less. Cell **105**: 297–306.

Edgar, B. a., Zielke, N., and Gutierrez, C. (2014). Endocycles: a recurrent evolutionary innovation for post-mitotic cell growth. Nat. Rev. Mol. Cell Biol. **15**: 197–210.

Ehler, L.L. and Dutcher, S.K. (1998). Pharmacological and genetic evidence for a role of rootlet and phycoplast microtubules in the positioning and assembly of cleavage furrows in Chlamydomonas reinhardtii. Cell Motil. Cytoskeleton **40**: 193–207.

Eisen, M.B., Spellman, P.T., Brown, P.O., and Botstein, D. (1998). Cluster analysis and display of genome-wide expression patterns. Proc. Natl. Acad. Sci. U. S. A. **95**: 14863–8.

Evans, T., Rosenthal, E.T., Youngblom, J., Distel, D., and Hunt, T. (1983). Cyclin: a protein specified by maternal mRNA in sea urchin eggs that is destroyed at each cleavage division. Cell **33**: 389–96.

Fang, G., Yu, H., and Kirschner, M.W. (1999). Control of mitotic transitions by the anaphase-promoting complex. Philos. Trans. R. Soc. Lond. B. Biol. Sci. **354**: 1583–90.

Fang, S.-C., de los Reyes, C., and Umen, J.G. (2006). Cell size checkpoint control by the retinoblastoma tumor suppressor pathway. PLoS Genet. **2**: e167.

Fang, W., Si, Y., Douglass, S., Casero, D., Merchant, S.S., Pellegrini, M., Ladunga, I., Liu, P., and Spalding, M.H. (2012). Transcriptome-wide changes in Chlamydomonas reinhardtii gene expression regulated by carbon dioxide and the CO2-concentrating mechanism regulator CIA5/CCM1. Plant Cell **24**: 1876–93.

Fukuzawa, H., Miura, K., Ishizaki, K., Kucho, K.I., Saito, T., Kohinata, T., and Ohyama, K. (2001). Ccm1, a regulatory gene controlling the induction of a carbon-concentrating mechanism in Chlamydomonas reinhardtii by sensing CO2 availability. Proc. Natl. Acad. Sci. U. S. A. **98**: 5347–52.

Gadal, O., Strauss, D., Braspenning, J., Hoepfner, D., Petfalski, E., Philippsen, P., Tollervey, D., and Hurt, E. (2001). A nuclear AAA-type ATPase (Rix7p) is required for biogenesis and nuclear export of 60S ribosomal subunits. EMBO J. **20**: 3695–704.

Giaever, G. et al. (2002). Functional profiling of the Saccharomyces cerevisiae genome. Nature **418**: 387–91.

Goodrich, J. a and Tjian, R. (2010). Unexpected roles for core promoter recognition factors in cell-type-specific transcription and gene regulation. Nat. Rev. Genet. **11**: 549–58.

Goto, K. and Johnson, C.H. (1995). Is the cell division cycle gated by a circadian clock? The case of Chlamydomonas reinhardtii. J. Cell Biol. **129**: 1061–9.

Gould, K. and Nurse, P. (1989). Tyrosine phosphorylation of the fission yeast cdc2+ protein kinase regulates entry into mitosis. Nature **342**: 39–45.

Grandjean, O., Vernoux, T., and Laufs, P. (2004). In vivo analysis of cell division, cell growth, and differentiation at the shoot apical meristem in Arabidopsis. Plant Cell **16**: 74–87.

Gray, W. and Muskett, P. (2003). Arabidopsis SGT1b is required for SCFTIR1-mediated auxin response. Plant Cell **15**: 1310–1319.

Grossniklaus, U. and Schneitz, K. (1998). The molecular and genetic basis of ovule and megagametophyte development. Semin. Cell Dev. Biol. **9**: 227–38.

Guertin, D. (2002). Cytokinesis in eukaryotes. Microbiol. Mol. Biol. Rev. **66**.

Gusti, A., Baumberger, N., Nowack, M., Pusch, S., Eisler, H., Potuschak, T., De Veylder, L., Schnittger, A., and Genschik, P. (2009). The Arabidopsis thaliana F-box protein FBL17 is essential for progression through the second mitosis during pollen development. PLoS One **4**: e4780.

Guttery, D.S. et al. (2012). A unique protein phosphatase with kelch-like domains (PPKL) in Plasmodium modulates ookinete differentiation, motility and invasion. PLoS Pathog. **8**: e1002948.

Gutzat, R., Borghi, L., and Gruissem, W. (2012). Emerging roles of RETINOBLASTOMA-RELATED proteins in evolution and plant development. Trends Plant Sci. **17**: 139–48.

Haase, S.B. and Wittenberg, C. (2014). Topology and control of the cell-cycle-regulated transcriptional circuitry. Genetics **196**: 65–90.

Hardwick, K.G., Li, R., Mistrot, C., Chen, R.H., Dann, P., Rudner, A., and Murray, a W. (1999). Lesions in many different spindle components activate the spindle checkpoint in the budding yeast Saccharomyces cerevisiae. Genetics **152**: 509–18.

Harper, J. (1999). Chlamydomonas Cell Cycle Mutants. Int. Rev. Cytol. **189**: 131–176.

Harper, J. and John, P. (1986). Coordination of division events in the Chlamydomonas cell cycle. Protoplasma **131**: 118–130.

Harper, J., Wu, L., Sakuanrungsirikul, S., and John, P. (1995). Isolation and partial characterization of conditional cell division cycle mutants inChlamydomonas. Protoplasma **186**: 149–162.

Harper, J.D., McCurdy, D.W., Sanders, M. a, Salisbury, J.L., and John, P.C. (1992). Actin dynamics during the cell cycle in Chlamydomonas reinhardtii. Cell Motil. Cytoskeleton **22**: 117–26.

Harper, J.D.I., Salisbury, J.L., John, P.C.L., and Koutoulis, A. (2004). Changes in the centrin and microtubule cytoskeletons after metaphase arrest of the Chlamydomonas reinhardtii met1 mutant. Protoplasma **224**: 159–165.

Harper, J.W. and Elledge, S.J. (1998). The role of Cdk7 in CAK function, a retro-retrospective. Genes Dev. **12**: 285–9.

Harris, E. (2001). Chlamydomonas as a model organism. Annu. Rev. Plant Biol. **52**: 363–406.

Harris, E. (2008). The Chlamydomonas Sourcebook: Introduction into Chlamydomonas and its laboratory use.

Hartwell, L., Culotti, J., Pringle, J., and Reid, B. (1974). Genetic control of the cell division cycle in yeast. Science (80-.). **183**: 46–51.

Hartwell, L. and Weinert, T. (1989). Checkpoints: controls that ensure the order of cell cycle events. Science (80-.). **246**: 629–34.

Hartwell, L.H., Mortimer, R.K., Culotti, J., and Culotti, M. (1973). Genetic Control of the Cell Division Cycle in Yeast: V. Genetic Analysis of cdc Mutants. Genetics **74**: 267–86.

Henikoff, S. and Henikoff, J.G. (1993). Performance evaluation of amino acid substitution matrices. Proteins **17**: 49–61.

Hershko, A. (1999). Mechanisms and regulation of the degradation of cyclin B. Philos. Trans. R. Soc. Lond. B. Biol. Sci. **354**: 1571–5; discussion 1575–6.

Hirano, T. (2005). Condensins: organizing and segregating the genome. Curr. Biol. **15**: R265–75.

Holmes, J.A. and Dutcher, S.K. (1989). Cellular asymmetry in Chlamydomonas reinhardtii. J. Cell Sci. **94 (Pt 2)**: 273–85.

Howell, S.H. and Naliboff, J.A.Y.A. (1973). Conditional mutants in chlamydomonas reinhardtii blocked in the vegetative cell cycle. J. Cell Biol. **57**: 760–772.

Inzé, D. and De Veylder, L. (2006). Cell cycle regulation in plant development. Annu. Rev. Genet. **40**: 77–105.

Ito, H., Mutsuda, M., Murayama, Y., Tomita, J., Hosokawa, N., Terauchi, K., Sugita, C., Sugita, M., Kondo, T., and Iwasaki, H. (2009). Cyanobacterial daily life with Kai-based circadian and diurnal genome-wide transcriptional control in Synechococcus elongatus. Proc. Natl. Acad. Sci. U. S. A. **106**: 14168–73.

Iwakawa, H., Shinmyo, A., and Sekine, M. (2006). Arabidopsis CDKA; 1, a cdc2 homologue, controls proliferation of generative cells in male gametogenesis. Plant J. **45**: 819–31.

Jager, S. de and Scofield, S. (2009). Dissecting regulatory pathways of G1/S control in Arabidopsis: common and distinct targets of CYCD3; 1, E2Fa and E2Fc. Plant Mol. Biol. **71**: 345–365.

James, S.W., Silflow, C.D., Stroom, P., and Lefebvre, P.A. (1993). A mutation in the alpha 1-tubulin gene of Chlamydomonas reinhardtii confers resistance to anti-microtubule herbicides. J. Cell Sci. **106**: 209–218.

Jenik, P.D., Gillmor, C.S., and Lukowitz, W. (2007). Embryonic patterning in Arabidopsis thaliana. Annu. Rev. Cell Dev. Biol. **23**: 207–36.

Jiao, Y., Lau, O.S., and Deng, X.W. (2007). Light-regulated transcriptional networks in higher plants. Nat. Rev. Genet. **8**: 217–30.

Johnson, U.G. and Porter, K.R. (1968). Fine structure of cell division in Chlamydomonas reinhardi. Basal bodies and microtubules. J. Cell Biol. **38**: 403–25.

Johnston, G.C., Pringle, J.R., and Hartwell, L.H. (1977). Coordination of growth with cell division in the yeast Saccharomyces cerevisiae. Exp. Cell Res. **105**: 79–98.

Jorgensen, P. and Tyers, M. (2004). How cells coordinate growth and division. Curr. Biol. **14**: R1014–27.

Joubès, J., Chevalier, C., Dudits, D., Heberle-Bors, E., Inzé, D., Umeda, M., and Renaudin, J.P. (2000). CDK-related protein kinases in plants. Plant Mol. Biol. **43**: 607–20.

Kampinga, H.H. and Craig, E. a (2010). The HSP70 chaperone machinery: J proteins as drivers of functional specificity. Nat. Rev. Mol. Cell Biol. **11**: 579–92.

Kim, D., Pertea, G., Trapnell, C., Pimentel, H., Kelley, R., and Salzberg, S.L. (2013). TopHat2: accurate alignment of transcriptomes in the presence of insertions, deletions and gene fusions. Genome Biol. **14**: R36.

Kim, T.-W. and Wang, Z.-Y. (2010). Brassinosteroid signal transduction from receptor kinases to transcription factors. Annu. Rev. Plant Biol. **61**: 681–704.

Kimelman, D., Kirschner, M., and Scherson, T. (1987). The events of the midblastula transition in Xenopus are regulated by changes in the cell cycle. Cell **48**: 399–407.

Kitagawa, K., Skowyra, D., Elledge, S.J., Harper, J.W., and Hieter, P. (1999). SGT1 encodes an essential component of the yeast kinetochore assembly pathway and a novel subunit of the SCF ubiquitin ligase complex. Mol. Cell **4**: 21–33.

Knizewski, L., Ginalski, K., and Jerzmanowski, A. (2008). Snf2 proteins in plants: gene silencing and beyond. Trends Plant Sci. **13**: 557–65.

Ko, H. and Moore, S. (1990). Kinetic Characterization of a Prestart Cell Division Control Step in Yeast. J. Biol. Chem. **265**: 21652–21663.

Kornev, A.P., Haste, N.M., Taylor, S.S., and Eyck, L.F. Ten (2006). Surface comparison of active and inactive protein kinases identifies a conserved activation mechanism. Proc. Natl. Acad. Sci. U. S. A. **103**: 17783–8.

Kornev, A.P., Taylor, S.S., and Ten Eyck, L.F. (2008). A helix scaffold for the assembly of active protein kinases. Proc. Natl. Acad. Sci. U. S. A. **105**: 14377–82.

Kozminski, K.G., Johnson, K.A., Forscher, P., and Rosenbaum, J.L. (1993). A motility in the eukaryotic flagellum unrelated to flagellar beating. Proc. Natl. Acad. Sci. U. S. A. **90**: 5519–23.

Kumar, R., Reynolds, D., and Shevchenko, A. (2000). Forkhead transcription factors, Fkh1p and Fkh2p, collaborate with Mcm1p to control transcription required for M-phase. Curr. Biol. **10**: 896–906.

Kusano, H., Testerink, C., Vermeer, J.E.M., Tsuge, T., Shimada, H., Oka, A., Munnik, T., and Aoyama, T. (2008). The Arabidopsis Phosphatidylinositol Phosphate 5-Kinase PIP5K3 is a key regulator of root hair tip growth. Plant Cell **20**: 367–80.

Labib, K. (2010). How do Cdc7 and cyclin-dependent kinases trigger the initiation of chromosome replication in eukaryotic cells? Genes Dev. **24**: 1208–19.

Lamb, M.R., Dutcher, S.K., Worley, C.K., and Dieckmann, C.L. (1999). Eyespot-assembly mutants in Chlamydomonas reinhardtii. Genetics **153**: 721–9.

Langmead, B. and Salzberg, S.L. (2012). Fast gapped-read alignment with Bowtie 2. Nat. Methods **9**: 357–9.

Lara-Gonzalez, P., Westhorpe, F.G., and Taylor, S.S. (2012). The spindle assembly checkpoint. Curr. Biol. **22**: R966–80.

Lassing, I. and Lindberg, U. (1985). Specific interaction between phosphatidylinositol 4, 5-bisphosphate and profilactin. Nature **314**: 472–474.

LeDizet, M. and Piperno, G. (1986). Cytoplasmic microtubules containing acetylated alpha-tubulin in Chlamydomonas reinhardtii: spatial arrangement and properties. J. Cell Biol. **103**: 13–22.

Lee, B.H., Ko, J.-H., Lee, S., Lee, Y., Pak, J.-H., and Kim, J.H. (2009). The Arabidopsis GRF-INTERACTING FACTOR gene family performs an overlapping function in determining organ size as well as multiple developmental properties. Plant Physiol. **151**: 655–68.

Lee, L. a and Orr-Weaver, T.L. (2003). Regulation of cell cycles in Drosophila development: intrinsic and extrinsic cues. Annu. Rev. Genet. **37**: 545–78.

Lee, M.G.. and Nurse, P. (1987). Complementation used to clone a human homologue of the fission yeast cell cycle control gene cdc2. Nature **327**: 31–35.

Lee, Y., Kim, E.-S., Choi, Y., Hwang, I., Staiger, C.J., Chung, Y.-Y., and Lee, Y. (2008). The Arabidopsis phosphatidylinositol 3-kinase is important for pollen development. Plant Physiol. **147**: 1886–97.

Lemmon, M. (2004). Pleckstrin homology domains: not just for phosphoinositides. Biochem. Soc. Trans. **32**: 18–22.

Lesage, B., Qian, J., and Bollen, M. (2011). Spindle checkpoint silencing: PP1 tips the balance. Curr. Biol. **21**: R898–903.

Li, H., Handsaker, B., Wysoker, A., Fennell, T., Ruan, J., Homer, N., Marth, G., Abecasis, G., and Durbin, R. (2009). The Sequence Alignment/Map format and SAMtools. Bioinformatics **25**: 2078–9.

Lindmo, K. and Stenmark, H. (2006). Regulation of membrane traffic by phosphoinositide 3-kinases. J. Cell Sci. **119**: 605–14.

Liu, X. and Winey, M. (2012). The MPS1 family of protein kinases. Annu. Rev. Biochem. **81**: 561–85.

Liu, Y., Tsinoremas, N.F., Johnson, C.H., Lebedeva, N. V, Golden, S.S., Ishiura, M., and Kondo, T. (1995). Circadian orchestration of gene expression in cyanobacteria. Genes Dev. **9**: 1469–1478.

Logan, M. and Mandato, C. (2006). Regulation of the actin cytoskeleton by PIP2 in cytokinesis. Biol. Cell **98**: 377–88.

Lorca, T. and Castro, A. (2013). The Greatwall kinase: a new pathway in the control of the cell cycle. Oncogene **32**: 537–43.

Ma, H. and Sundaresan, V. (2010). Development of flowering plant gametophytes. Curr. Top. Dev. Biol. **91**: 379–412.

Magyar, Z., Horváth, B., and Khan, S. (2012). Arabidopsis E2FA stimulates proliferation and endocycle separately through RBR-bound and RBR-free complexes. EMBO J. **31**: 1480–1493.

Majka, J. and Burgers, P.M.J. (2004). The PCNA-RFC families of DNA clamps and clamp loaders. Prog. Nucleic Acid Res. Mol. Biol. **78**: 227–60.

Malik, S. and Roeder, R.G. (2010). The metazoan Mediator co-activator complex as an integrative hub for transcriptional regulation. Nat. Rev. Genet. **11**: 761–72.

Manabe, Y., Bressan, R. a, Wang, T., Li, F., Koiwa, H., Sokolchik, I., Li, X., and Maggio, A. (2008). The Arabidopsis kinase-associated protein phosphatase regulates adaptation to Na+ stress. Plant Physiol. **146**: 612–22.

Maselli, G.A., Slamovits, C.H., Bianchi, J.I., Vilarrasa-Blasi, J., Caño-Delgado, A.I., and Mora-García, S. (2014). Revisiting the evolutionary history and roles of protein phosphatases with kelch-like domains in plants. Plant Physiol. **164**: 1527–41.

Masumoto, H., Muramatsu, S., Kamimura, Y., and Araki, H. (2002). S-Cdk-dependent phosphorylation of Sld2 essential for chromosomal DNA replication in budding yeast. Nature **415**: 651–5.

Matsuno, K., Kumano, M., Kubota, Y., Hashimoto, Y., and Takisawa, H. (2006). The N-terminal noncatalytic region of Xenopus RecQ4 is required for chromatin binding of DNA polymerase alpha in the initiation of DNA replication. Mol. Cell. Biol. **26**: 4843–52.

Matsuo, T. and Ishiura, M. (2010). New insights into the circadian clock in Chlamydomonas. In International review of cell and molecular biology (Elsevier Inc.), pp. 281–314.

Matsuo, T. and Okamoto, K. (2008). A systematic forward genetic analysis identified components of the Chlamydomonas circadian system. Genes Dev. **22**: 918–930.

Maure, J., Kitamura, E., and Tanaka, T. (2007). Mps1 kinase promotes sister-kinetochore bi-orientation by a tension-dependent mechanism. Curr. Biol. **17**: 2175–82.

McCusker, D. and Kellogg, D.R. (2012). Plasma membrane growth during the cell cycle: unsolved mysteries and recent progress. Curr. Opin. Cell Biol. **24**: 845–51.

McDonald, M.J. and Rosbash, M. (2001). Microarray analysis and organization of circadian gene expression in Drosophila. Cell **107**: 567–78.

McGarry, T.J. and Kirschner, M.W. (1998). Geminin, an inhibitor of DNA replication, is degraded during mitosis. Cell **93**: 1043–53.

McGrew, J.T., Goetsch, L., Byers, B., and Baum, P. (1992). Requirement for ESP1 in the nuclear division of Saccharomyces cerevisiae. Mol. Biol. Cell **3**: 1443–54.

McKinney, J.D., Chang, F., Heintz, N., and Cross, F.R. (1993). Negative regulation of FAR1 at the Start of the yeast cell cycle. Genes Dev. **7**: 833–843.

Meldau, S., Baldwin, I.T., and Wu, J. (2011). For security and stability: SGT1 in plant defense and development. Plant Signal. Behav. **6**: 1479–82.

Menges, M. and Murray, J. (2002). Synchronous Arabidopsis suspension cultures for analysis of cell-cycle gene activity. Plant J. **30**: 203–12.

Merchant, S.S. et al. (2007). The Chlamydomonas genome reveals the evolution of key animal and plant functions. Science **318**: 245–250.

Molendijk, a J. and Irvine, R.F. (1998). Inositide signalling in Chlamydomonas: characterization of a phosphatidylinositol 3-kinase gene. Plant Mol. Biol. **37**: 53–66.

Moore, S. (1988). Kinetic evidence for a critical rate of protein synthesis in the Saccharomyces cerevisiae yeast cell cycle. J. Biol. Chem. **263**: 9674–9681.

Mora-García, S., Vert, G., Yin, Y., Caño-Delgado, A., Cheong, H., and Chory, J. (2004). Nuclear protein phosphatases with Kelch-repeat domains modulate the response to brassinosteroids in Arabidopsis. Genes Dev. **18**: 448–60.

Moreno, S., Hayles, J., and Nurse, P. (1989). Regulation of p34 cdc2 protein kinase during mitosis. Cell **58**: 361–372.

Mueller, A., Keaton, M., and Dutta, A. (2011). DNA Replication: Mammalian Treslin–TopBP1 Interaction Mirrors Yeast Sld3–Dpb11. Curr. Biol. **21**: R638–40.

Müller, S., Wright, A.J., and Smith, L.G. (2009). Division plane control in plants: new players in the band. Trends Cell Biol. **19**: 180–8.

Münzner, P. and Voigt, J. (1992). Blue light regulation of cell division in Chlamydomonas reinhardtii. Plant Physiol. **99**: 1370–5.

Murphy, S.M., Urbani, L., and Stearns, T. (1998). The mammalian gamma-tubulin complex contains homologues of the yeast spindle pole body components spc97p and spc98p. J. Cell Biol. **141**: 663–74.

Murray, A. and Kirschner, M. (1989). Dominoes and clocks: the union of two views of the cell cycle. Science (80-.). **246**: 614–621.

Musacchio, A. and Hardwick, K.G. (2002). The spindle checkpoint: structural insights into dynamic signalling. Nat. Rev. Mol. Cell Biol. **3**: 731–41.

Nguyen, V.Q., Co, C., and Li, J.J. (2001). Cyclin-dependent kinases prevent DNA re-replication through multiple mechanisms. Nature **411**: 1068–73.

Nowack, M.K., Harashima, H., Dissmeyer, N., Zhao, X., Bouyer, D., Weimer, A.K., De Winter, F., Yang, F., and Schnittger, A. (2012). Genetic framework of cyclin-dependent kinase function in Arabidopsis. Dev. Cell **22**: 1030–40.

Nurse, P. (1990). Universal control mechanism regulating onset of M-phase. Nature **344**: 503–508.

Nurse, P., Thuriaux, P., and Nasmyth, K. (1976a). Genetic control of the cell division cycle in the fission yeast Schizosaccharomyces pombe. Mol. Gen. Genet. MGG **146**: 167–178.

Nurse, P., Thuriaux, P., and Nasmyth, K. (1976b). Genetic control of the cell division cycle in the fission yeast Schizosaccharomyces pombe. Mol. Gen. Genet. **146**: 167–78.

Page, D.R. and Grossniklaus, U. (2002). The art and design of genetic screens: Arabidopsis thaliana. Nat. Rev. Genet. **3**: 124–36.

Di Paolo, G. and De Camilli, P. (2006). Phosphoinositides in cell regulation and membrane dynamics. Nature **443**: 651–7.

Park, S., Tian, G., Roelofs, J., and Finley, D. (2010). Assembly manual for the proteasome regulatory particle: the first draft. Biochem. Soc. Trans. **38**: 6–13.

Peters, J. (2002). The anaphase-promoting complex: proteolysis in mitosis and beyond. Mol. Cell **9**: 931–43.

Philip, N., Vaikkinen, H.J., Tetley, L., and Waters, A.P. (2012). A unique Kelch domain phosphatase in Plasmodium regulates ookinete morphology, motility and invasion. PLoS One **7**: e44617.

Pines, J. (2011). Cubism and the cell cycle: the many faces of the APC/C. Nat. Rev. Mol. Cell Biol. **12**: 427–38.

Pomerening, J.R., Sontag, E.D., and Ferrell, J.E. (2003). Building a cell cycle oscillator: hysteresis and bistability in the activation of Cdc2. Nat. Cell Biol. **5**: 346–51.

Porceddu, a, Stals, H., Reichheld, J.P., Segers, G., De Veylder, L., Barroco, R.P., Casteels, P., Van Montagu, M., Inzé, D., and Mironov, V. (2001). A plant-specific cyclin-dependent kinase is involved in the control of G2/M progression in plants. J. Biol. Chem. **276**: 36354–60.

Qi, P., Lin, Y.-S., Song, X.-J., Shen, J.-B., Huang, W., Shan, J.-X., Zhu, M.-Z., Jiang, L., Gao, J.-P., and Lin, H.-X. (2012). The novel quantitative trait locus GL3.1 controls rice grain size and yield by regulating Cyclin-T1;3. Cell Res. **22**: 1666–80.

Qin, H., Wang, Z., Diener, D., and Rosenbaum, J. (2007). Intraflagellar transport protein 27 is a small G protein involved in cell-cycle control. Curr. Biol. **17**: 193–202.

Raychaudhuri, S. and Prinz, W. a (2010). The diverse functions of oxysterol-binding proteins. Annu. Rev. Cell Dev. Biol. **26**: 157–77.

Reynolds, D., Shi, B.J., McLean, C., Katsis, F., Kemp, B., and Dalton, S. (2003). Recruitment of Thr 319-phosphorylated Ndd1p to the FHA domain of Fkh2p requires Clb kinase activity: a mechanism for CLB cluster gene activation. Genes Dev. **17**: 1789–802.

Ringo, D. (1967). Flagellar motion and fine structure of the flagellar apparatus in Chlamydomonas. J. Cell Biol. **33**: 543–571.

Rochaix, J. (1995). Chlamydomonas reinhardtii as the photosynthetic yeast. Annu. Rev. Genet. **29**: 209–30.

Rogozin, I.B., Basu, M.K., Csürös, M., and Koonin, E. V (2009). Analysis of rare genomic changes does not support the unikont-bikont phylogeny and suggests cyanobacterial symbiosis as the point of primary radiation of eukaryotes. Genome Biol. Evol. **1**: 99–113.

Rudner, a D. and Murray, a W. (2000). Phosphorylation by Cdc28 activates the Cdc20-dependent activity of the anaphase-promoting complex. J. Cell Biol. **149**: 1377–90.

Saavedra, L., Mikami, K., Malhó, R., and Sommarin, M. (2012). PIP kinases and their role in plant tip growing cells. Plant Signal. Behav. **7**: 1302–5.

Sabelli, P.A. and Larkins, B.A. (2009). The contribution of cell cycle regulation to endosperm development. Sex. Plant Reprod. **22**: 207–19.

Salisbury, J., Baron, A., and Sanders, M. (1988). The centrin-based cytoskeleton of Chlamydomonas reinhardtii: distribution in interphase and mitotic cells. J. Cell Biol. **107**: 635–641.

Sanchez-Pulido, L., Diffley, J., and Ponting, C. (2010). Homology explains the functional similarities of Treslin/Ticrr and Sld3. Curr. Biol. **20**: R509–10.

Saravanan, R. and Slabaugh, E. (2009). The targeting of the oxysterol-binding protein ORP3a to the endoplasmic reticulum relies on the plant VAP33 homolog PVA12. Plant J. **58**: 817–30.

Savino, T.M., Bastos, R., Jansen, E., and Hernandez-Verdun, D. (1999). The nucleolar antigen Nop52, the human homologue of the yeast ribosomal RNA processing RRP1, is recruited at late stages of nucleologenesis. J. Cell Sci. **112 (Pt 1**: 1889–900.

Schaffer, R., Landgraf, J., Accerbi, M., Simon, V., Larson, M., and Wisman, E. (2001). Microarray analysis of diurnal and circadian-regulated genes in Arabidopsis. Plant Cell **13**: 113–23.

Shao, N. and Bock, R. (2008). A codon-optimized luciferase from Gaussia princeps facilitates the in vivo monitoring of gene expression in the model alga Chlamydomonas reinhardtii. Curr. Genet. **53**: 381–8.

Sherr, C.J. and Roberts, J.M. (1999). CDK inhibitors: positive and negative regulators of G1-phase progression. Genes Dev. **13**: 1501–12.

Shultz, R.W., Tatineni, V.M., Hanley-Bowdoin, L., and Thompson, W.F. (2007). Genome-wide analysis of the core DNA replication machinery in the higher plants Arabidopsis and rice. Plant Physiol. **144**: 1697–714.

Sorrell, D. a, Menges, M., Healy, J.M., Deveaux, Y., Amano, C., Su, Y., Nakagami, H., Shinmyo, A., Doonan, J.H., Sekine, M., and Murray, J. a (2001). Cell cycle regulation of cyclin-dependent kinases in tobacco cultivar Bright Yellow-2 cells. Plant Physiol. **126**: 1214–23.

Sousa, E., Kost, B., and Malhó, R. (2008). Arabidopsis phosphatidylinositol-4-monophosphate 5-kinase 4 regulates pollen tube growth and polarity by modulating membrane recycling. Plant Cell **20**: 3050–64.

Spellman, P.T., Sherlock, G., Zhang, M.Q., Iyer, V.R., Anders, K., Eisen, M.B., Brown, P.O., Botstein, D., and Futcher, B. (1998). Comprehensive identification of cell cycle-regulated genes of the yeast Saccharomyces cerevisiae by microarray hybridization. Mol. Biol. Cell **9**: 3273–97.

Spudich, J.L. and Sager, R. (1980). Regulation of the Chlamydomonas cell cycle by light and dark. J. Cell Biol. **85**: 136–45.

Stack, J.H., DeWald, D.B., Takegawa, K., and Emr, S.D. (1995). Vesicle-mediated protein transport: regulatory interactions between the Vps15 protein kinase and the Vps34 PtdIns 3-kinase essential for protein sorting to the vacuole in yeast. J. Cell Biol. **129**: 321–34.

Stegmeier, F. and Amon, A. (2004). Closing mitosis: the functions of the Cdc14 phosphatase and its regulation. Annu. Rev. Genet. **38**: 203–32.

Szymanski, D. (2002). Tubulin folding cofactors: half a dozen for a dimer. Curr. Biol. **12**: 767–769.

Takatsuka, H., Ohno, R., and Umeda, M. (2009). The Arabidopsis cyclin-dependent kinase-activating kinase CDKF;1 is a major regulator of cell proliferation and cell expansion but is dispensable for CDKA activation. Plant J. **59**: 475–87.

Taylor, N.G. (2011). A role for Arabidopsis dynamin related proteins DRP2A/B in endocytosis; DRP2 function is essential for plant growth. Plant Mol. Biol. **76**: 117–29.

Thornton, B.R., Ng, T.M., Matyskiela, M.E., Carroll, C.W., Morgan, D.O., and Toczyski, D.P. (2006). An architectural map of the anaphase-promoting complex. Genes Dev. **20**: 449–60.

Thornton, B.R. and Toczyski, D.P. (2003). Securin and B-cyclin/CDK are the only essential targets of the APC. Nat. Cell Biol. **5**: 1090–4.

Tichtinsky, G., Vanoosthuyse, V., Cock, J.M., and Gaude, T. (2003). Making inroads into plant receptor kinase signalling pathways. Trends Plant Sci. **8**: 231–7.

Tirumani, S., Kokkanti, M., Chaudhari, V., Shukla, M., and Rao, B.J. (2014). Regulation of CCM genes in Chlamydomonas reinhardtii during conditions of light-dark cycles in synchronous cultures. Plant Mol. Biol.

Toker, A. (1998). The synthesis and cellular roles of phosphatidylinositol 4,5-bisphosphate. Curr. Opin. Cell Biol. **10**: 254–261.

Trunnell, N.B., Poon, A.C., Kim, S.Y., and Ferrell, J.E. (2011). Ultrasensitivity in the Regulation of Cdc25C by Cdk1. Mol. Cell **41**: 263–74.

Tyson, J.J., Chen, K.C., and Novak, B. (2003). Sniffers, buzzers, toggles and blinkers: dynamics of regulatory and signaling pathways in the cell. Curr. Opin. Cell Biol. **15**: 221–231.

Umeda, M., Shimotohno, A., and Yamaguchi, M. (2005). Control of cell division and transcription by cyclin-dependent kinase-activating kinases in plants. Plant Cell Physiol. **46**: 1437–42.

Umen, J.G. and Goodenough, U.W. (2001). Control of cell division by a retinoblastoma protein homolog in Chlamydomonas. Genes Dev. **15**: 1652–61.

Vandepoele, K., Raes, J., De Veylder, L., Rouzé, P., Rombauts, S., and Inzé, D. (2002). Genome-wide analysis of core cell cycle genes in Arabidopsis. Plant Cell **14**: 903–16.

De Veylder, L., Beeckman, T., and Inzé, D. (2007). The ins and outs of the plant cell cycle. Nat. Rev. Mol. Cell Biol. **8**: 655–65.

De Veylder, L., Larkin, J.C., and Schnittger, A. (2011). Molecular control and function of endoreplication in development and physiology. Trends Plant Sci. **16**: 624–34.

De Veylder, L., Segers, G., Glab, N., Casteels, P., Van Montagu, M., and Inzé, D. (1997). The Arabidopsis Cks1At protein binds the cyclin-dependent kinases Cdc2aAt and Cdc2bAt. FEBS Lett. **412**: 446–52.

Walker, J.D., Oppenheimer, D.G., Concienne, J., and Larkin, J.C. (2000). SIAMESE, a gene controlling the endoreduplication cell cycle in Arabidopsis thaliana trichomes. Development **127**: 3931–40.

Weinert, T. and Hartwell, L. (1988). The RAD9 gene controls the cell cycle response to DNA damage in Saccharomyces cerevisiae. Science (80-.). **241**: 317–22.

Weingartner, M. (2002). A plant cyclin B2 is degraded early in mitosis and its ectopic expression shortens G2-phase and alleviates the DNA-damage checkpoint. J. Cell Sci. **116**: 487–498.

Wiese, C. and Zheng, Y. (2006). Microtubule nucleation: gamma-tubulin and beyond. J. Cell Sci. **119**: 4143–53.

Winey, M., Goetsch, L., Baum, P., and Byers, B. (1991). MPS1 and MPS2: novel yeast genes defining distinct steps of spindle pole body duplication. J. Cell Biol. **114**: 745–54.

Witke, W. (2004). The role of profilin complexes in cell motility and other cellular processes. Trends Cell Biol. **14**: 461–9.

Wittenberg, C. and Reed, S.I. (2005). Cell cycle-dependent transcription in yeast: promoters, transcription factors, and transcriptomes. Oncogene **24**: 2746–55.

Wood, C.R., Wang, Z., Diener, D., Zones, J.M., Rosenbaum, J., and Umen, J.G. (2012). IFT proteins accumulate during cell division and localize to the cleavage furrow in Chlamydomonas. PLoS One **7**: e30729.

Yamagishi, Y., Yang, C.-H., Tanno, Y., and Watanabe, Y. (2012). MPS1/Mph1 phosphorylates the kinetochore protein KNL1/Spc7 to recruit SAC components. Nat. Cell Biol. **14**: 746–52.

Yamano, T. and Fukuzawa, H. (2009). Carbon-concentrating mechanism in a green alga, Chlamydomonas reinhardtii, revealed by transcriptome analyses. J. Basic Microbiol. **49**: 42–51.

Zhang, X., Wang, J., and Huang, J. (2012). Rare allele of OsPPKL1 associated with grain length causes extra-large grain and a significant yield increase in rice. Proc. Natl. Acad. Sci. U. S. A. **109**: 21534–21539.